Anatomy and physiology of bone perfusion in living and fossil birds as assessed by CT-scanning, microsphere distribution, vascular contrast imaging and foramen measurement

Qiaohui Hu

Presented for the degree of Doctor of Philosophy

School of Biological Sciences

University of Adelaide, South Australia, Australia

November 2020

CONTENTS

Publications arising from post-graduate work:

Hu, Q., Nelson, T. J. and Seymour, R. S. (2020). Bone foramen dimensions and blood flow calculation: best practices. *Journal of Anatomy* **236**, 357-369.

Hu, Q., Nelson, T. J., Snelling, E. P. and Seymour, R. S. (2018). Femoral bone perfusion through the nutrient foramen during growth and locomotor development of western grey kangaroos (*Macropus fuliginosus*). *Journal of Experimental Biology* **221**, 1-6.

Seymour, R. S., Bosiocic, V., Snelling, E. P., Chikezie, P. C., Hu, Q., Nelson, T. J., Zipfel, B. and Miller, C. V. (2019). Cerebral blood flow rates in recent great apes are greater than in Australopithecus species that had equal or larger brains. *Proceedings of the Royal Society B* **286**, 20192208.

Seymour, R. S., Hu, Q. and Snelling, E. P. (2020). Blood flow rate and wall shear stress in seven major cephalic arteries of humans. *Journal of Anatomy* **236**, 522-530.

Seymour, R. S., Hu, Q., Snelling, E. P. and White, C. R. (2019). Interspecific scaling of blood flow rates and arterial sizes in mammals. *Journal of Experimental Biology* **222**, jeb199554.

Snelling, E. P., Biewener, A. A., Hu, Q., Taggart, D. A., Fuller, A., Mitchell, D., Maloney, S. K. and Seymour, R. S. (2017). Scaling of the ankle extensor muscle-tendon units and the biomechanical implications for bipedal hopping locomotion in the post-pouch kangaroo *Macropus fuliginosus*. *Journal of Anatomy* **231**, 921-930.

Abstract

Artery sizes are determined by local blood flow rates, which are driven by local oxygen demand. Arteries that pass through bone foramina, leave the foramina as size representatives of the arteries. Therefore, measuring these foramina sizes without any presence of soft tissue can be a way to estimate blood flow rates. This 'foramen technique' can be a useful tool to estimate blood flow rates in ancient animals such as dinosaurs. However, the absolute blood flow passing though foramina needs to be calibrated at this stage, as the size relationship between the foramen and occupying vessel is unclear, especially in foramina with more than one vessel. The major aim of this thesis is to evaluate the foramen-artery size relationship, especially the relationship between the femoral nutrient foramen and nutrient artery, to improve the method of femoral bone blood flow estimation for further foramen studies. Chickens are chosen as the experimental animals. Studying blood flow in birds gives us an opportunity to get insight into blood flow rates in dinosaur bones, as birds are living dinosaurs. The thesis chapters involve several methods to measure foramen sizes or estimate regional bone blood flow rates. Microphotography is chosen to be the most practical foramen measurement method compared to micro-CT and impression material approaches. Chicken femoral bone blood flow rates estimated from infusion of fluorescent microspheres and vascular contrast imaging give similar results. Foramen-artery size relationships are evaluated in chicken femur bones, revealing that the morphologies of femoral nutrient arteries and nutrient foramina can vary among femora. The 'foramen technique' is used to estimate femoral bone blood flow in fossil cursorial birds.

Author declaration

I, Qiaohui Hu, certify that this work contains no material which has been accepted for the award of any other degree or diploma in my name in any university or other tertiary institution and, to the best of my knowledge and belief, contains no material previously published or written by another person, except where due reference has been made in the text.

I give permission for the digital version of my thesis to be made available in the University Library, the Library Search and also through web search engines, unless permission has been granted by the University to restrict access for a period of time.

I acknowledge that copyright of the published work involved in this thesis (as listed below*) resides with the copyright holder(s) of the work.

* **Hu, Q., Nelson, T. J. and Seymour, R. S.** (2019). Bone foramen dimensions and blood flow calculation: best practices. *Journal of Anatomy* **236**, 357-369.

Qiaohui Hu

November 2020

Acknowledgements

Chapter One: Introduction

The cardiovascular system transports nutrients, hormones, and most importantly, oxygen, all over the body to maintain homeostasis and satisfy metabolic demands. Endotherms in particular require more oxygen than ectotherms. Regional blood flows represent local energy requirements of the body (Wolff, 2008). Studying animal regional blood flow rates can thus improve our understanding of animal physiological processes and metabolic demands in relation to how animals interact with their environment. There have been previous studies that investigated regional blood flow rates through bone foramina by simply measuring foramen sizes (Allan et al., 2014; Boyer and Harrington, 2018; Boyer and Harrington, 2019; Hu et al., 2018; Seymour et al., 2015; Seymour et al., 2016; Seymour et al., 2012). There have been questions about whether this recent technique is capable of accurately estimating regional blood flow rates, as the estimated blood flows were rarely compared with measured blood flow rates in animals. The research in this thesis was conducted to improve this 'foramen technique' and to explore the relationships among regional blood flow rates, estimated foramen blood flow rates and foramen sizes. This introductory chapter describes the general information about cardiovascular system, bone blood flow, the foramen technique and a comparison of the techniques used in the study for estimating bone blood flow. Additionally, this chapter outlines the specific aims of the thesis.

The cardiovascular system of endotherms

Cardiovascular systems in animals have been studied for centuries. Before the third century, people had no idea which direction the blood goes inside the bodies, and some thought that the vessels contained air or blood that was continuously being consumed and later refilled by ingested nutrients. As an ancient Greek scientist, Galen realized that there were differences between arterial and venous blood, but he believed that there were pores in the interventricular septum to act as the passage of arterial and venous blood. In the early 1600s, William Harvey discovered the systemic circulation. He realized that blood was pumped to the brain and the rest of the body from the heart, and he also discovered the presence of one-way valves in veins (Aird, 2011). Harvey's work nearly 400 years ago began the study of blood flow and a completely new chapter of physiology.

The circulatory system is continuously responsible for transporting materials such as oxygen, hormones and nutrients throughout the body. As endotherms, both mammals and birds require large amounts of energy to maintain their body temperature and organ functions. In order to distribute oxygen efficiently, they both have a four-chambered heart to separate pulmonary and systemic circulation. Birds are more active than mammals, and they require more oxygen during flight. Their cardiovascular system thus evolved to match their high oxygen demand. For example, the heart mass of birds is about two times heavier than mammals of similar body mass, although heart mass among species in different environments is variable (Pees and Krautwald-Junghanns, 2009). Heart mass of Pekin ducks rapidly increases during a short period of time between external pipping to the first hour after hatching (Sirsat et al., 2016). In addition, birds have higher cardiac outputs and stroke volumes than mammals (Pees and Krautwald-Junghanns, 2009). The rapid oxygen transportation and energy distribution of birds are benefited by their smaller cardiac muscle fibres (Pees and Krautwald-Junghanns, 2009). These examples show that studying the structure and function of animal cardiovascular systems reveals how behaviour, metabolic rate and oxygen demands are dynamically related to blood flow rate and vessel dimensions.

Correlations among metabolic rate, blood flow rate and vessel size
Despite a century of research on the morphology of the circulatory trees, even today the relationships among arterial size, blood flow rate and metabolic rate of the supplied tissues remain obscure. There were many studies focusing on modelling the structures of the circulatory trees, and the models are based on a theory that a space-filling network should minimize energy cost to transport oxygen (Brummer et al., 2017; Hunt and Savage, 2016; Huo and Kassab, 2012; Huo and Kassab, 2016; Kassab, 2006; Newberry et al., 2015). One well-known theoretical model is called Murray's Law, which suggests the cube of the radius of a parent artery equals the sum of the cubes of the radii of two child arteries (Murray, 1926). Another similar empirical relationship named daVinci's rule originated even earlier in the 1600s, and it suggested that the square of the radius of a parent artery equals the sum of the squares of the radii of two child arteries (Richter, 1970). Although these models were proposed to investigate the morphologies of artery trees, they do not consider the correlations among metabolic rates, blood flow rates and vessel sizes. This is

important, because the structure of the circulatory system has often been considered to determine metabolic rate (Newberry et al., 2015). However, we believe the opposite, namely that the metabolic rate determines the artery size. It is clear that oxygen demands (i.e. metabolism) of local tissues determine local blood flow rates (Wolff 2008), and a number of studies demonstrate that the changes of blood flow rate result in the changes of artery sizes. For example, external carotid artery diameter decreased by 21% within two weeks of carotid ligation in rabbits (Langille and O'Donnell, 1986). Juvenile rats with flow-restricted carotid arteries developed smaller arteries compared to the controls (Guyton and Hartley, 1985). On the contrary, increasing blood flow rates result in increasing vessel sizes. For example, increasing flow rate by constructing an arteriovenous fistula (AVF) resulted in increased artery sizes in rabbits (Tronc et al., 2000). A collateral artery increased in size to bypass a stenotic artery and to adapt the elevated blood flow rate (Semenza, 2007). Overall, artery size change is determined by blood flow change, which is the result of change in metabolic demand.

Different mechanisms are involved in blood vessel remodelling. The way an artery forms and remodels involves three processes including vasculogenesis, angiogenesis and arteriogenesis (Carmeliet, 2003). Vasculogensis refers to blood vessel formation in embryos, and it occurs by differentiating angioblasts from mesoderm and a *de novo* formation of blood vessel (Risau and Flamme, 1995). Angiogensis refers to new blood vessel formation from existing blood vessels, and arteriogenesis refers to a change in artery lumen diameter and wall thickness in response to a change in blood flow rate (Heil et al., 2006). Both angiogenesis and arteriogensis occur as a result of increased local metabolism in growing organs (Heil et al., 2006). The change of blood flow changes the mechanical forces that the blood acting on the vessel inner walls. As blood flows through a vessel, it creates a tangential force called shear stress, and blood pressure creates a perpendicular force called circumferential stretch to the vessel wall (Jones et al., 2006). The mechanical forces created by blood flow demand determine blood vessel structure and maintain physiological functions of the arteries (Lu and Kassab, 2011). Wall shear stress increases after blood flow rate increases, and the artery increases size in order to bring the wall shear stress value back to the baseline value (Tronc et al., 2000; Tronc et al., 1996). An elevated blood flow triggers

endothelium cells to produce nitric oxide, metalloproteinases (MMPs) and angiogenic cytokines such as vascular endothelial growth factor (VEGF), which triggers vascular remodelling (Lehoux et al., 2002).

Bone blood flow

As living organs, bones also require constant blood supply, and they are constantly absorbed and renewed throughout a lifetime. Generally, about 10% of bone material is remodelled annually (Cohen, 2006). Bones are fully vascularized. Apart from the major blood vessels in the bone marrow, cortical bones also contain millions of blood vessels. Clopton Havers in 1691 first discovered small canals on cortical bones, which were later well described as the "Haversian canals". And in 1754, Albinus discovered that these canals contain blood vessels that supply the bone tissue (Brookes and Revell, 1998). Generally, the main physiological processes in bones can be osteogenesis, bone modelling and Haversian remodelling, and all processes require rich blood supply. Two main types of cells are responsible for bone tissue change processes. Osteoclast cells absorb bone matrix while osteoblast cells lay down new bone tissue (Rucci, 2008).

Osteogenesis only occurs during early life stage when bones are formed. Embryonic tissues are replaced by bone tissue during bone formation. Bone modelling changes bone size and shape to adapt loading change by adding or removing bone tissue on existing bone surfaces (Currey, 2002; Lieberman et al., 2003). When bones undergo the modelling process, osteoclasts and osteoblasts target different locations on endosteal or periosteal surfaces (Currey, 2002). Bone modelling and Haversian remodelling occur throughout the entire lifetime, but modelling mainly occurs before maturity (Kobayashi et al., 2003; Lieberman et al., 2003). Bones undergo Haversian remodelling to repair microfractures that occur on bones due to daily activity (Lieberman et al., 2003). Apart from these three major bone physiological processes, there is another process that is worth mentioning in bones of birds: calcium homeostasis. Birds lay eggs to reproduce, therefore they need to export extra calcium to form eggshell. Using domestic chickens as an example, in order to maintain calcium balance in bones, about 20 – 40 % of the eggshell calcium passes through bone for daily egg production (Bar, 2009). The calcium loss in bones can be regained the next day when layers consume calcium from their diet. The intense calcium

turnover in birds is benefited by a special bone type called medullary bone, which can only be found in birds and crocodiles (Whitehead, 2004). Medullary bone can be absorbed and renewed rapidly, as it is able to metabolize at a higher rate than cortical bone (Hurwitz, 1965).

Regional oxygen demand determines local blood flow rate in bone as it does in other tissues (Wolff, 2008). Using the femur bone as an example, microfractures occur in the bone as it experiences loading and dynamic stresses during locomotion. Bone remodelling intensity increases as bone micro-damage increases. Femur bone metabolism and bone blood flow increase from rest to exercise (Heinonen et al., 2013). In contrast, blood flow rapidly decreases if loading is removed from the hind limb (Colleran et al., 2000). If we can measure bone blood flow, we are able to correlate it with local bone metabolism in association with the physiological processes described above.

Foramen technique: blood flow estimation from foramen sizes
There have been many techniques developed to measure regional bone blood flow. Seymour et al. (2012) was the first to use foramina in bones to estimate regional blood flow rates that pass through the foramina. This recent technique involves an assumption that the foramen size is proportional to the occupying vessel size, which is driven by the required blood flow rate. A larger foramen size represents a larger occupying blood vessel in relation to a higher blood flow rate. There have been studies that estimated blood flow rates through femoral nutrient foramina and carotid foramina in numerous species. By measuring femoral nutrient foramen sizes in relation to body mass in adult mammalian, avian and reptilian species, the blood flow index, derived from nutrient foramen size, scaled with body size in parallel with maximal aerobic metabolic rate during treadmill exercise (Allan et al., 2014; Seymour et al., 2012). The relationship between maximum metabolic rates and femoral nutrient foramina size was tested on house mice artificially selected for greater voluntary running activity which developed relatively larger foramen sizes than normal house mice (Schwartz et al., 2018). Likewise, when applying the foramen technique to carotid foramina, relatively larger carotid foramen sizes are associated with higher internal carotid artery blood flow rates, which are determined by higher metabolic demands of the brains (Boyer and Harrington, 2018; Boyer and Harrington, 2019;

Seymour et al., 2015; Seymour et al., 2016). Higher demand for blood during rapid growth in juvenile mammals was demonstrated by Hu et al. (2018), who found that young kangaroos require higher blood flow to supply femur growth as they have massively larger nutrient foramen sizes than adult diprotodont marsupials with similar body mass.

All above-described results are valid if three assumptions are true. Firstly, foramen size is proportional to the occupying vessel size. Secondly, the size relationship between the foramen and the occupying vessel remains constant among species. Thirdly, the size relationship between the foramen and the occupying vessel is remains constant ontogenetically. To test these assumptions, both vessel and foramen sizes are required. The major advantage of the foramen technique is that it only requires measurement of foramen sizes without working on living specimens, or even without blood vessels. However, the size relationship between the occupying vessel and the foramen needs to be further investigated. Without knowing this size relationship, the foramen size can only produce relative blood flow indices rather than absolute blood flow rates.

Blood flow rate ($\dot{Q}$, cm^3 s^{-1}) can be estimated from artery lumen radius (r_i, cm) using theoretical and empirical approaches. There were two theoretical equations involved in the previous foramen studies. One is a blood flow index equation ($Q_i = r_o{}^4/L$) (Seymour et al., 2012), where Q_i is the blood flow index (arbitrary units presumed proportional to flow rate), r_o is foramen radius (cm) and L is femur length (cm). This equation is derived from the Poiseuille-Hagen equation ($\dot{Q} = \pi \Delta P r_i{}^4/8\eta l$), which calculates absolute blood flow rate ($\dot{Q}$) based on blood pressure difference (ΔP; dyn cm^{-2}) between two points along a vessel with certain length (l; cm), vessel lumen radius (r_i; cm) and blood viscosity (η; dyn s cm^{-2}). ΔP and η are assumed independent of body mass. Another theoretical approach is through Poiseuille's "shear stress equation": $\dot{Q} = (\tau \pi r_i{}^3)/(4\,\eta)$, where τ (dyn cm^{-1}) is wall shear stress and η is blood viscosity (dyn s cm^{-2}) (Lehoux and Tedgui, 2003). Blood flow index equation can only estimate relative blood flow rate, whereas the shear stress equation can estimate absolute blood flow rates if vessel size, shear stress and viscosity values are known. Recently, an empirical equation ($\log \dot{Q} = -0.20\,(\log r_i)^2 + 1.91 \log r_i + 1.82$) was

determined by comparing simultaneously measured artery lumen radii and blood flow rates in 22 named arteries in nine mammalian species (Seymour et al., 2019b). This empirical equation can estimate blood flow rates based only on vessel radius, and it can also apply to the foramen studies with known vessel lumen-foramen size relationship. Among these 22 named arteries, another equation ($\dot{Q} = 155\ r_i^{2.49}$) describes the relationships between lumen radius and blood flow rate for cephalic arteries only. Figure 1 shows a comparison of three equations. Black data points on the graph represent actual lumen radius and blood flow data of the 22 named arteries (Seymour et al., 2019b). If shear stress is constant in all arteries, the blood flow index (Poiseuille-Hagen equation) and shear stress equations are allometrically equivalent. In this case, the empirical equations can better represent the lumen size-blood flow relationship than the shear stress equation. Wall shear stress seems to decrease with body mass in named arteries (Greve et al., 2006; Seymour et al., 2019b; Weinberg and Ethier, 2007), and the relationship is well determined in internal carotid internal carotid artery (Seymour et al., 2015) and the vertebral artery (Boyer and Harrington, 2018; Boyer and Harrington, 2019). The relationship remains unclear in smaller arteries. The shear stress equation may also capable of well describing the lumen size-blood flow relationship with known wall shear stress in varied sized arteries.
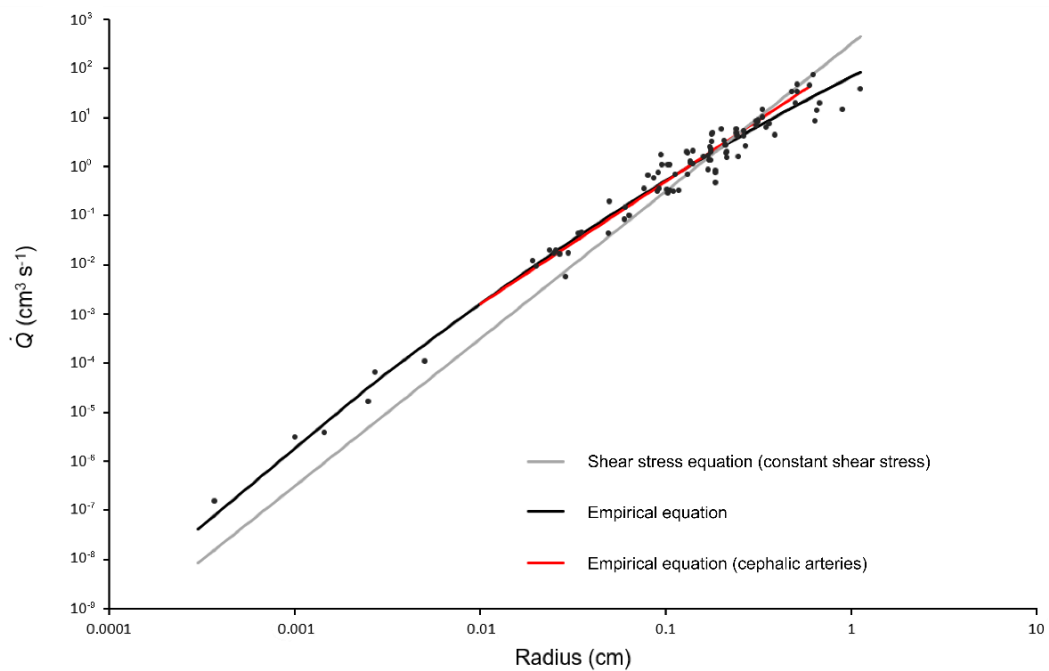
Figure 1. Comparison of three equations (grey line: $\dot{Q} = (\tau \pi r_i^3)/(4\ \eta)$; black line: log $\dot{Q} = -0.20\ (\log r_i)^2 + 1.91 \log r_i + 1.82$; red line: $\dot{Q} = 155\ r_i^{2.49}$;) to estimate blood

flow from artery lumen radius. Data points represent artery lumen radii coupled with blood flow rates in 22 named arteries varying in radius from 3.65 μm to 1.12 cm in nine mammalian species.

Foramen size measurement methods

A range of methods including direct size measurements using calipers or rulers, microphotography, digital camera, digital microscope and micro-Computerized Tomographic (micro-CT) scanning, have been used to measure foramen sizes in previous foramen studies. Microphotography, digital camera and digital microscopes all use optical instruments to measure sizes. Micro-CT scanning uses X-rays to detect materials with different densities. Different methods have specific advantages such as ease of use or high resolution, and disadvantages such as being time consuming or expensive. Moreover, methodological errors exist among the various methods. Back in the 20th century, a study measured human skull foramen sizes using both digital calipers and CT scanning, and the researchers observed a good correlation between the two methods, if the foramen opening was at a right angle to the scanline (Berlis et al., 1992). However, the resolution of this study was very low (1000 μm), and they measured foramen openings only on the bone surface. Cross-sectional area along a foramen passage is not constant, and the smallest cross-sectional area is probably better correlated with the vessel size than the area of the opening. Therefore, a better understanding of the anatomy of foramina is needed to further explore whether microphotographic and micro-CT methods can provide comparable data on foramen size.

The foramen technique attracts more and more attention in the field of comparative physiology, as it can be a useful tool to investigate blood flow in fossil bones without preservation of any soft tissues. If we can measure bone blood flow of ancient animals, we might be able to solve questions such as whether extinct dinosaurs were ectotherms or endotherms, or what their metabolic rates might have been. Future studies involving the foramen technique will require a relatively simple method that can accurately measure foramen size. Apart from using different imaging methods, the approaches to define foramen radius also vary among studies. Foramen cross-sections are often not circular, and previous foramen studies either used foramen area

or foramen minor diameter to calculate foramen radius. However, blood flow estimated from foramen sizes is very sensitive to radius, as the two theoretical equations involved in the calculations of the previous foramen studies both have large exponents (3 or 4) on the radius factor (Seymour et al., 2015; Seymour et al., 2012). A standardized approach to measure foramen radii is thus required.

Other blood flow measurement methods
Although the foramen technique seems capable of estimating regional blood flow rates through bones, the estimated blood flow from the foramen sizes have not been validated with absolute blood flow rates, except for the work on carotid foramina in humans, rats and mice (Seymour et al., 2015). Few studies have measured animal femoral bone blood flow rates (Anetzberger et al., 2004a; Barbee et al., 1992; Boelkins et al., 1973; Brubaker and Mueller, 1971) and none have related blood flow to the nutrient foramen sizes. If the foramen technique needs to be validated for femoral bone blood flow, other techniques used for estimating absolute blood flow rates are required.

Apart from the foramen technique, there have been many other techniques and approaches created and developed to measure or estimate regional blood flow rates. One of the most commonly used is a microsphere infusion technique, which requires injection of microspheres into the animal's left ventricle or atrium from which they are distributed throughout the body and lodge in tissues. The number of recovered microspheres in a region indicates the blood flow proportion in this region (Anetzberger and Birkenmaier, 2016). Absolute blood flow can be calculated using the microsphere technique by withdrawing blood from the animal at a known rate during microsphere injection. The withdrawal rate and captured microspheres can be used to calculate the blood flow rates to other regions (Anetzberger and Birkenmaier, 2016). Another method is vascular contrast imaging, which requires infusion of contrast media into the animal's vascular system. Vascular beds can then be visualized once the blood vessels with contrast media are CT scanned. If the imaging is done when arteries are filled under physiological pressures, it is then possible to estimate flow rates from arterial lumen size with the empirical equation that relates lumen size and absolute blood flow rate (Seymour et al., 2019b). Using both vascular

contrast imaging and microsphere infusion techniques simultaneously, we can compare and validate them.

Size relationship between femoral nutrient foramen and occupying nutrient artery
The foramen technique measures foramen sizes, which are not necessarily the same as artery sizes, particularly if veins accompany the arteries. However, the artery sizes might be estimated if the size relationship between the foramen and the artery is known and constant. This size relationship is relatively simple in foramina passing only one vessel, as the artery nearly fill the entire cross-section of the foramen, and the relationship between wall thickness and the blood vessel lumen radius can be obtained easily. According to the Law of Laplace, vessel wall tension is directly proportional to vessel radius and pressure, and inversely proportional to wall thickness (Westerhof et al., 2010). Therefore, to maintain wall tension, vessel wall thickness increases as blood pressure or blood vessel radius increases. A previous foramen study on human carotid foramina proposed that the ratio of wall thickness:lumen radius was 0.4, which was estimated from only two published records (Seymour et al., 2015). The ratio was later proposed to be 0.3 according to 14 studies (Hu et al., 2020; Seymour et al., 2020). It means the artery wall thickness is 30 % of the artery lumen radius. Assuming that the artery fully fills the foramen, the artery lumen radius equals the foramen radius divided by 1.3. By using this ratio, human internal carotid artery blood flow rates were estimated and compared with the *in vivo* blood flow data, and the results show a high consistency of the two values.

The size relationship in foramina with more than one vessel becomes more complex. According to the literature, a femoral nutrient foramen contains both an artery and a vein (Singh et al., 1991). However, there is a lack of knowledge about how these two vessels occupy the foramen. In addition, no studies have ever looked into femoral nutrient artery sizes or femoral nutrient artery blood flow rates. Previous femoral bone blood flow estimated from the foramen sizes only represent blood flow indices rather than absolute blood flow rates. The blood flow indices can be related to absolute blood flow rates, if the size relationship between the vessel and the foramen becomes clear and consistent.

Thesis and chapter objectives

The major aim of this thesis is to evaluate the relationship between nutrient foramen size and blood flow rate, specifically to improve the method of femoral bone blood flow estimation for further foramen studies. The following chapters also investigate the relationships among femoral nutrient foramen sizes, femoral nutrient artery sizes and femoral bone blood flows in domestic chickens. Chickens are chosen as the experimental animals, as they are common laboratory animals, they are large enough for cardiovascular surgery, and few studies have considered blood flow rates in birds. More importantly, studying bone blood flow in chickens gives us an opportunity to get insight into the role of bones as calcium reserves for eggshell formation. It also leads to estimation of blood flow rates in dinosaur bones, as birds are living dinosaurs.

Chapter two: *Detailed description and comparison of three foramen measurement methods, including microphotography, micro-computerized tomographic scanning and impression material approach.* This chapter investigates the specific benefits and limitations of each method, using femoral nutrient foramina and carotid foramina in Western grey kangaroos (*Macropus fuliginosus*), carotid foramina in humans and artificial foramina drilled in long bone. In addition, a sensitivity analysis is conducted to investigate how the estimated blood flow from foramen sizes relates to shear stress, vessel size and blood viscosity.

Chapter three: *Absolute blood flow estimated using a fluorescent microsphere method in femoral bone of three chicken groups including non-laying hens, laying hens and roosters with similar body mass.* Blood flow distribution and rates are compared among three chicken groups in relation to differences in gender and age. The absolute rates of blood flow in the femoral bone of chickens are compared with values estimated from the foramen sizes, to get insight into the relationship between the two, and this is later used for estimating absolute perfusion rate of femoral bone in other cursorial birds.

Chapter four: *Sizes and morphologies of femoral nutrient foramina and nutrient arteries in chickens.* Vascular contrast medium is infused into chicken vascular systems and imaged using a micro-CT scanner. Another three chicken groups including non-laying hens, laying hens and roosters are used. Absolute nutrient artery

blood flow rates are estimated from nutrient artery lumen sizes and compared with the blood flow rates estimated from the fluorescent microsphere method. Micro-CT images of nutrient foramina and artery lumina, along with histological sectioning of nutrient foramen passages containing vessels, provide information about foramen morphologies and artery size and location inside a foramen.

Chapter five: *Femoral bone blood flow in extant and extinct cursorial birds*

To investigate femoral bone blood flow in extinct cursorial birds, and to examine whether the 'foramen technique' can be applied to fossil bones, femoral nutrient foramen sizes of 19 extinct cursorial birds were measured. To compare femoral bone blood flow values between extant and extinct cursorial birds, the estimated femoral bone blood flow indices of these extinct birds were combined with values of eight extinct cursorial birds reported by a previous study (Allan et al., 2014) and compared to 13 extinct cursorial bird species.

Chapter Two: Bone foramen dimensions and blood flow calculation: best practices

Statement of Authorship

Title of Paper	Bone foramen dimensions and blood flow calculation: best practices
Publication Status	Published
Publication Details	**Hu, Q., Nelson, T. J. and Seymour, R. S.** (2020). Bone foramen dimensions and blood flow calculation: best practices. *Journal of Anatomy* **236**, 357-369.

Principal Author

Name of Principal Author (Candidate)	Qiaohui Hu		
Contribution to the Paper	Conducted experiments, data analysis, performed sensitivity analysis, wrote the initial manuscript draft, and reviewed and edited subsequent drafts.		
Overall percentage (%)	65%		
Certification:	This paper reports on original research I conducted during the period of my Higher Degree by Research candidature and is not subject to any obligations or contractual agreements with a third party that would constrain its inclusion in this thesis. I am the primary author of this paper.		
Signature		Date	1/11/2020

Co-Author Contributions

By signing the Statement of Authorship, each author certifies that:

i. the candidate's stated contribution to the publication is accurate (as detailed above);

ii. permission is granted for the candidate in include the publication in the thesis; and

iii. the sum of all co-author contributions is equal to 100% less the candidate's stated contribution.

Name of Co-Author	Thomas J. Nelson		
Contribution to the Paper 15%	Assisted in the experiments, helped with data collection and literature research, reviewed and edited manuscript drafts.		
Signature		Date	9/11/2020

Name of Co-Author	Roger S. Seymour		
Contribution to the Paper 20%	Provided advice and assisted the experiments, helped with data analysis, reviewed and edited manuscript drafts.		
Signature		Date	20/11/2020

2.1. Abstract

Some blood vessels enter bones through foramina, leaving the size of the foramen as a gauge for estimating the rate of blood flow and hence the metabolic rate of the supplied tissues. Foramen dimensions have been measured using varied methods in previous foramen studies, to relate regional blood flows with associated physiological processes. With the increasing interests in this 'foramen technique', standard methods with minimized measurement errors are therefore required. This study provides details of microphotographic and micro-computerized tomographic methods, and introduces a new alternative method, which uses impression material to measure foramen dimensions. The three methods are compared and the results indicate that all of them are capable of obtaining precise and accurate foramen dimension values, although they all have limitations. A microphotograph of the external opening is suggested to be the standard method because of its ease of use, but the alternative methods provide more detailed information on foramen shape. If the foramen is mainly occupied by one artery, blood flow rates can be estimated from foramen size and artery wall-lumen ratio, which is evaluated from the literature survey in this study. If veins or nerves also penetrate the foramen, a relative index of blood flow rate is nevertheless possible for comparative purposes

2.2. Introduction

Generally, the metabolic rate of an organ determines its oxygen requirement and perfusion rate (Wolff, 2008). Therefore, studying regional blood flow helps investigate an organ's metabolism with associated physiological processes. Some blood vessels pass through holes in bones to supply tissues on the other side or the bones themselves. The opening is called a foramen (window) and the passage is called a canal by some anatomists, but here we call the whole passage a foramen for simplicity. A technique to estimate regional blood flow relies upon measurement of foramen sizes to estimate the amount of blood flow passing across that foramen, because foramen size correlates with blood vessel size, which is related to the blood flow rate (Seymour et al., 2015; Seymour et al., 2019b; Seymour et al., 2012). This 'foramen technique' has been successfully applied to estimate animal femoral bone perfusion via femoral nutrient foramina, and brain perfusion via carotid foramina. The results indicated that femoral bone blood flow in adult mammals and reptiles may associate with bone remodelling and thus matches the maximum metabolic rate during locomotion of the animal, providing a way to assess metabolic and locomotor status of extinct dinosaurs (Seymour et al., 2012). This hypothesis was further supported by a following foramen study, which discovered that femoral bone blood flow in cursorial birds is two times higher than in quadruped mammals of similar body mass (Allan et al., 2014). High aerobic capacity house mice, which were artificially bred, have larger nutrient foramen cross-sectional areas than the normal house mice (Schwartz et al., 2018). Ontogenetically, femoral nutrient foramina appeared to be larger in developing kangaroos than in adult diprotodont marsupials of similar body mass, which indicates extraordinarily high rates of blood flow during bone growth (Hu et al., 2018). Blood flow through the carotid foramina can illustrate the evolution of brain perfusion among primates (Boyer and Harrington, 2018; Boyer and Harrington, 2019; Boyer et al., 2016; Seymour et al., 2015), fossil hominins (Seymour et al., 2016; Seymour et al., 2017) and humans during ontogenetic growth (Harrington et al., 2019).

There are two types of bone foramina that pass vessels. Type I foramina may pass a combination of arteries, veins and nerves, and Type II foramina pass essentially only one artery. For example, femoral nutrient foramina pass both a nutrient artery and a vein (Singh et al., 1991), but the carotid canal in the skull mainly passes the internal

carotid artery with negligibly sized arterial vessels, venous plexus and sympathetic nerves (Overbeeke et al., 1991; Paullus et al., 1977). Two blood flow calculation equations have been involved to estimate blood flow through foramina.

In foramina that pass more than just an artery (Type I), a blood flow index equation can be applied to estimate relative blood flow in femoral nutrient foramina (Seymour et al., 2012):

$$Q_i = r_o{}^4/L \tag{1}$$

where Q_i is the blood flow index (arbitrary units), r_o is foramen radius (cm) and L is femur length (cm).

Equation (1) is derived from the Poiseuille-Hagen equation ($\dot{Q} = \pi \Delta P r_i{}^4/8\eta l$), which calculates absolute blood flow rate ($\dot{Q}$; cm^3 s^{-1}) based on blood pressure difference (ΔP; dyn cm^{-2}) between two points along a vessel with certain length (l; cm), vessel lumen radius (r_i; cm) and blood viscosity (η; dyn s cm^{-2}). The pressure drop across a certain blood vessel length is practically impossible to measure. In addition, there are no studies on size relationships between the femoral nutrient foramina and the occupying vessels. However, any linear measurement of geometrically similar shapes, scales with mass or volume to the 0.33 power. Equation 1 thus assumes femur length and foramen radius to be substitutes for vessel length and vessel radius (Allan et al., 2014; Seymour et al., 2012). Furthermore, blood pressure and blood viscosity are independent of body mass in adult terrestrial species, except for very large animals (White and Seymour, 2014; Windberger et al., 2003), therefore these two parameters are not included in Eq. 1.

In cases where an artery passes through a foramen alone (Type II), a derivation of Poiseuille's Law, called the shear stress equation, has been used to calculate absolute internal carotid artery perfusion:

$$\dot{Q} = \tau \pi r_i{}^3/4\eta \tag{2}$$

where $\dot{Q}$ is absolute blood flow rate, r_i is vessel internal radius, τ is wall shear stress (dyn cm^{-2}), and η is blood viscosity. The latter is often considered to be a constant in the arterial system (Glagov et al., 1988; Ku, 1997). However, it appears that wall shear stress in named arteries decreases with body mass (Greve et al., 2006; Seymour et al., 2019b; Weinberg and Ethier, 2007). Good estimates of the relationship between wall shear stress and body mass have been determined for the internal carotid artery (Seymour et al., 2015) and the vertebral artery (Boyer and Harrington, 2018; Boyer and Harrington, 2019), which permit calculation of brain perfusion.

A new empirical approach to measuring absolute blood flow rate ($\dot{Q}$) in relation to artery lumen radius (r_i) is based on recent imaging studies of flow in 20 named arteries in nine mammalian species (Seymour et al., 2019b). One equation describes flow rate in all 92 arteries with ri between 0.00037 and 1.12 cm:

$$\log \dot{Q} = -0.20 \log r_i^2 + 1.91 \log r_i + 1.82 \tag{3}$$

Another describes flow in 57 data for cephalic arteries only:

$$\dot{Q} = 155\ r_i^{2.49} \tag{4}$$

These equations are useful because they do not involve adherence to theory or knowledge of wall shear stress, but are comparable to results calculated from Eq. (2) (Seymour et al., 2019b).

Equations (2)–(4) apply to type II foramina and result in absolute blood flow rate if the relationship between artery radius and wall thickness is known. Because blood pressures are nearly the same in major arteries, the ratio of wall thickness and lumen radius is nearly constant, according to the Law of Laplace, and larger arteries consequently have proportionately thicker walls (Wolinsky and Glagov, 1967). Previously, vessel wall thickness of internal carotid artery was estimated from only two studies (Orsi et al., 2006; Skilton et al., 2011), which was a weakness (Seymour et al., 2015). Better information on wall thickness is necessary, so this study collects meta-data from 14 investigations to evaluate the wall–lumen ratio.

Blood flow values calculated from the equations are very sensitive to radius because of the large exponents, so accurate foramen radius measurement is required. Previous

foramen studies measured foramen dimensions using different methods, including calipers, digital cameras or microscopic photography, and computerized tomographic (CT) imaging. This study also introduces an alternative method, which uses dental impression material to mold and measure the foramen dimensions. Different methods applied to different types of bone specimens have various methodological errors and limitations. In addition, two approaches were used to calculate foramen radius. Either foramen minor diameter or foramen area has been used to calculate a single value of foramen radius. To achieve consistency and comparability between studies, and to provide recommendations for future work by functional morphologists with access to limited equipment, this study compares the results from different methods applied to the same specimens and indicates the advantages and disadvantages of each approach. In addition, a sensitivity analysis is performed to illustrate the impacts of different factors in shear stress equation on calculated blood flow.

2.3. Foramen measurement methods

Three methods can be applied to measure foramen dimensions under different situations (summary shown in supplementary material Figure S1). The microphotographic method is best suited to measure foramina on dry bones. We describe the microphotographic method as taking photos of foramina using any optical instruments such as stereomicroscopes, digital cameras and digital microscopes. The micro-CT method is applicable to bones surrounded by wet tissues and to complex foramen shapes. Impression casts are applied on dry bones to obtain a physical record of the foramen.

2.3.1 Microphotography

In many cases, microphotography is the simplest, cheapest and altogether most straightforward method for obtaining foramen dimension values. To measure foramen areas microphotographically, we used a 5MP digital imager (#44422, Celestron, USA), which was attached to both a stereomicroscope (SZ40 Microscope with SZ-PT Photo tube, Olympus, Japan) and a computer to take microphotographs of foramina. A dual fiberoptic light (Volpi Intralux 150H, United States) was aimed into the foramen to help investigate the foramen pathway inside the bone. We then positioned the bone so that the foramen passage was parallel to the view of the microscope and adjusted it to achieve the minimum cross-sectional area along the foramen.

Magnification was increased to enlarge the image and reduce measurement errors. A stand with a clamp is helpful for adjusting the position of long bones under the microscope, whereas a box full of millet seed or plastic spheres may be more suitable for adjusting positions of skulls. Three methods can be used for scale: (1) a calibrated ocular micrometer in the microscope, (2) a reference scale in the view next to the foramen at the same distance and (3) a separate photograph of a scale under the same magnification and the same focal plane of the microscope. The depth of field at high magnifications generally is very shallow. By moving the foramina or scale into this shallow plane of focus, it is possible to ensure that the fields resolved in different photographs are consistent. Based on the reference scale and the foramen photos, foramen area were measured using FIJI (Open Source, www.fiji.sc) by outlining the areas with the best-fit ellipses. A best-fit ellipse is the maximum-sized ellipse that best describes the outline of the foramen, which is the junction between illuminated bone and the shadow within the opening. Where the junction is uneven, the ellipse is adjusted to match the areas between the ellipse and the shadow junction inside and outside of the ellipse. Foramen radius is obtained from the area value by assuming the elliptical area of a foramen opening is the area of a perfect circle.

In some cases, due to foramen positioning or large-sized specimens, a digital microscope or even a smart phone camera can replace the stereomicroscope to take photos of foramen dimensions with a known scale at the same distance.

2.3.1.1 Microscope depth of field determination

In many cases, a scale and a foramen cannot be placed next to each other under a microscope. In addition, the minimum cross-sectional area is often located slightly within the foramen passage rather than on the bone surface. Since blood flow calculations are sensitive to radius, the focal plane of the microscope needs to be relatively shallow to obtain reliable foramen area measurements. To determine the depth of field of our microscope set up, a scale with known distance (e.g. 1 mm) was placed under the microscope. Microphotographs were taken serially by moving the stand in 1-mm increments on both sides of the focal plane of the microscope. Scale images were subjectively classified as either 'clear' or 'unclear'. Three microscope magnifications were chosen ($13.4\times$, $20\times$ and $80\times$) in this study. The number of 'clear' photos under each magnification was used to determine the depth of field range of the

current set up. Scale length was measured using FIJI on each 'clear' image and compared with the known scale distance (i.e. 1 mm).

The shallow depth of field can 'slice' along the foramen outer region by changing the distance between the lens and the foramen. Since the smallest cross-sectional area of the foramen is usually located at a certain depth from the foramen opening, having a deep depth of field may lead to underestimation of the foramen area. In addition, in situations when photos of a reference scale need to be taken separately from the foramen, a shallow depth of field is also vital for obtaining precise reference scale length.

It is difficult to measure the depth of field of a microscope because classification of whether an image is 'clear' or not is somewhat subjective. Nevertheless, we clearly observed that depth of field becomes much shallower as the magnification increases (Table 1), and thus increases the precision of our foramen measurements at higher magnifications. Fuzziness of a microphotograph leads to a less precise estimate of the scale length. Clear images taken using a high magnification microscope with a shallow depth of field are therefore recommended (Table 1).

Table 1. Relationship between microscope magnification and depth of field. The depth of field is a range of focus with subjectively defined boundaries. The actual length of the scale is 1 mm.

Magnification of microscope	Depth of field (mm)	Actual length of the scale (mm)	Measured scale length range within depth of field (mm)
13.4×	5	1	0.989-1.018
20×	3	1	0.996-1.004
80×	<1	1	1

2.3.1.2 Effects of viewing angle

Foramina often enter bones at an angle, and some of them curve severely inside bones. The pathway of the foramen reflects the pathway of the occupying vessels. To find and measure the cross-sectional area accurately, the foramen opening should be perpendicular to the view of a microscope or a camera. Inaccurate viewing angle can

lead to severe measurement errors. As an example, photos of a human carotid foramen at different viewing angles under a microscope are shown in Figure 1. One previous foramen study suggested orientating bones until a round foramen can be viewed, in an effort to minimize measurement errors (Allan et al., 2014). However, finding a round cross-section can introduce measurement errors, as most foramen cross-sections have an elliptical shape. If a foramen cross-sectional area is elliptical, a more 'round' foramen in the view indicates the view is not perpendicular to the foramen passage. For example, a more 'round' human carotid foramen can be viewed in photo A compared with B, even though the photos were taken of the same foramen (Figure 1). Foramen area measured in photo A is almost half of that measured size in photo B. Because of an oblique viewing angle, bone overhangs the foramen in image A and alters the cross-sectional area. The smallest cross-sectional area of the same foramen collected using the micro-CT method (photo C) illustrates that the shape of the area is similar to the area in photo B. Therefore, the area in photo B is more representative of the actual cross-sectional area of the foramen. Careful observation of a foramen pathway before a photo is taken is therefore necessary to minimize measurement errors while using the microphotographic method.
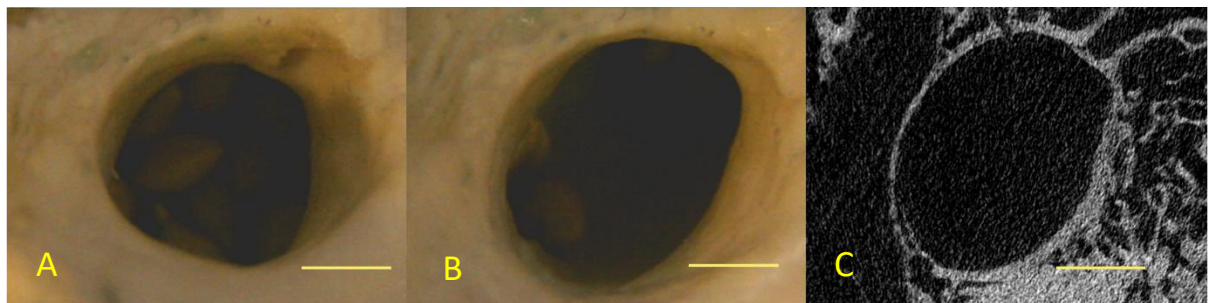
Figure 1. Microphotographs of a human carotid foramen with different viewing angles under the microscope. (A) The foramen from an oblique viewing angle. (B) The same foramen with view perpendicular to the opening. (C) Smallest cross-sectional area collected by a micro-CT method of the same foramen. Scale bars: 2 mm.

Here we evaluate the errors involved in differences in changes in viewing angle and changes in viewing distance. When a circular foramen is considered, changing the viewing angle with respect to the foramen opening, changes both the observed foramen area and observed foramen minor diameter on a microphotograph. Minor diameter of the viewing area decreases as viewing angle increases, but major diameter

does not change (Figure 2). In reality, because of perspective, distortion occurs when observing any object from a distance in a three-dimensional space. Therefore, apart from the viewing angle, distance between the viewing point to the centre of the opening is another factor that affects the observed minor diameter and area. When viewing distance approaches infinity, the observed length approaches a constant (Figure 2). If we arbitrarily set a circular foramen to have a radius of 1 mm, the 'observed minor diameter' of the opening at different viewing angles and viewing distances can be calculated based on trigonometry (Figure 2). Assuming the areas of the foramen 'observed' at different angle are ellipses, the areas are calculated from the changing minor diameter and the unchanged major diameter (2 mm) [area of an ellipse = π (minor diameter $\times$ unchanged major diameter/4]. Viewing distance was set to be 2-, 4-, and infinite-times of the circle radius. A sensitivity analysis was performed to investigate the calculated minor diameter changes in relation to the foramen area changes at viewing angle ranging from 0° to 90°. Radius of the foramen was calculated either from the observed areas by assuming the area is a perfect circle, or from observed minor diameters (Figure 3).
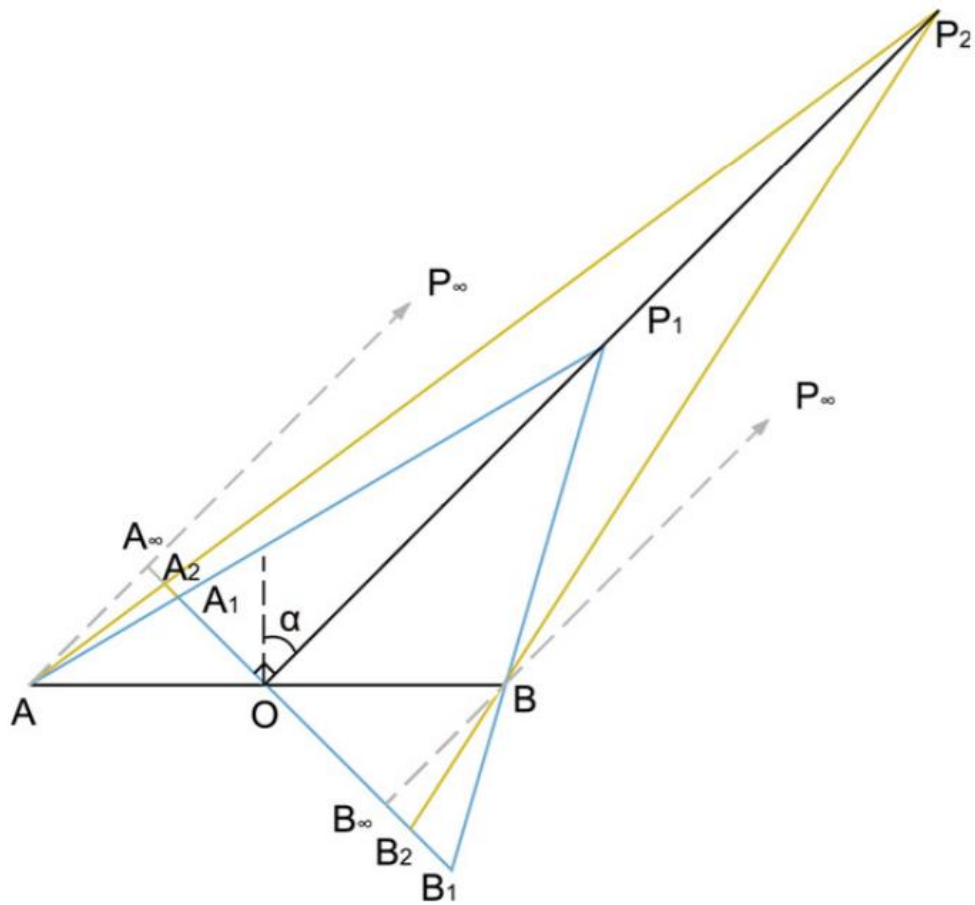
Figure 2. Schematic diagram of distance impacts on observed opening minor diameter. AB: Actual foramen diameter, which is the same as the unchanged major diameter. O: Center of the opening. P_1, P_2 & P_∞: Viewing point 1, 2 and viewing point at an infinite distance. A_1B_1, A_2B_2 & $A_\infty B_\infty$: Observed minor diameter at P_1, P_2 and P_∞ viewing point, respectively. $A_\infty P_\infty$ and $B_\infty P_\infty$ can be considered to be parallel to OP_∞. α is viewing angle.
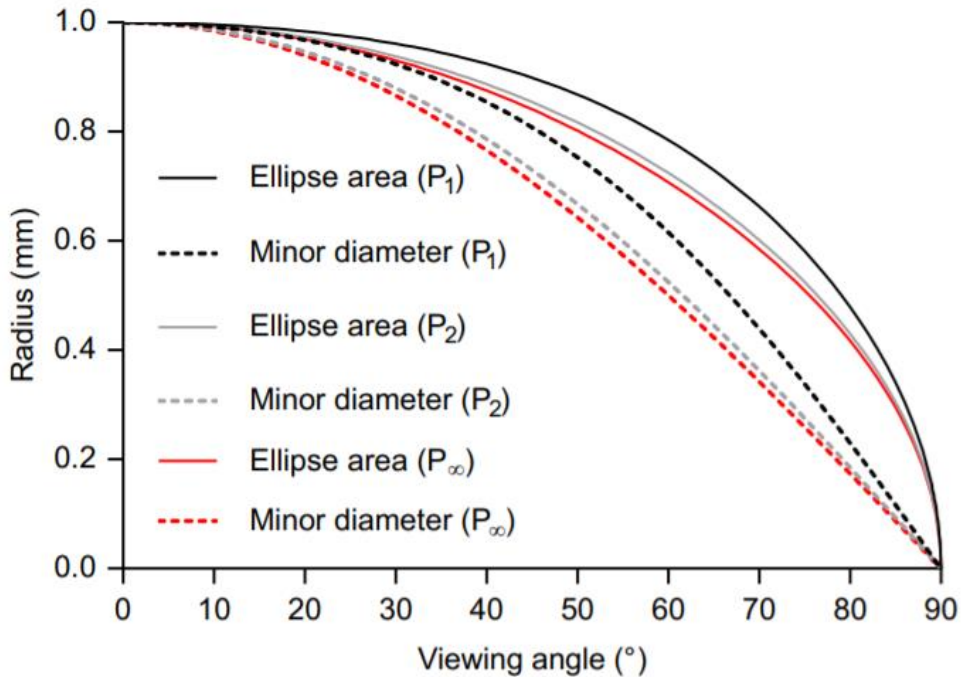
Figure 3. Opening radius calculated from either observed ellipse area or observed opening minor diameter at different viewing distance. P1, P2 & P∞: At a viewing distance of 2, 4 and infinite times of the opening radius, respectively. There is little difference between the methods if viewing angle is changed $< 20°$.

Radius calculated from the area at $10°$ and $20°$ with an infinite viewing distance is 0.99 and 0.97 mm, respectively. At the same viewing angles, radius calculated from the minor diameter is 0.98 and 0.94 mm, respectively. In practice, the foramen opening is required to be perpendicular to the view (i.e. viewing angle $= 0°$). A viewing angle larger than $20°$ should be avoided. With or without considering impacts of viewing distance, variation in radius calculated from the area is smaller than the variations calculated from the minor diameter (Figure 3). This is not surprising, because the ellipse area is calculated from two diameters and the major diameter does not vary with the viewing angle. The effects of viewing distance on calculated radii seem to be small if the distance is more than four times the opening radius (Figure 3). In reality, the viewing distance is always set to be much greater than four times the opening radius because the whole opening cannot appear in the view if the viewing point is too close to the foramen centre. Therefore, the viewing distance is considered to have negligible impacts on calculated foramen radii in practice.

Most views of the opening show somewhat elliptical shapes, which change apparent dimensions depending on the orientation of the view and the distance of the camera. In practice, we suggest setting the viewing angle carefully so that the aimed minimum cross-sectional area is maximized in the view. In general, the maximum-sized minimum cross-sectional area is also perpendicular to the view. If a dramatically curved pathway can be observed outside of a foramen (e.g. human carotid foramen), we suggest locating the area carefully by eye prior to taking the photo.

2.3.1.3 Effects of light angle

Lighting may have an impact on the quality of the microphotographs and thus the accuracy of the data. Foramina do not have a sharp opening edge but often flare at the surface, so changing the light angle may lead to change in the appearance of the foramen area, and thus introduce errors. In theory, light angle should be kept constant for all measurements to reduce measurement errors. However, in practice this requirement proves almost impossible to achieve because of varied foramen and bone shapes among samples. To investigate the impact of different light angles on microphotographic foramen area measurements, two kangaroo femoral nutrient foramina (foramen 1 and 2) were examined under the microscope, one at a time. Light angle was varied from directly perpendicular (0°) to the foramen to directly parallel to it (90°). Microphotographs were taken each time by moving the light angle at 10° intervals (Figure 4). Foramen areas were measured using FIJI by replacing the areas with the best-fit ellipses (Figure 5). Each foramen area image was measured six times at a different light angle. The relationship between foramen area and light angle was then plotted onto a graph. Mean area of the six replicates and 95% confident intervals (CI) were plotted on the graph using PRISM 6.0 statistical software (GraphPad Software, La Jolla, CA, USA).
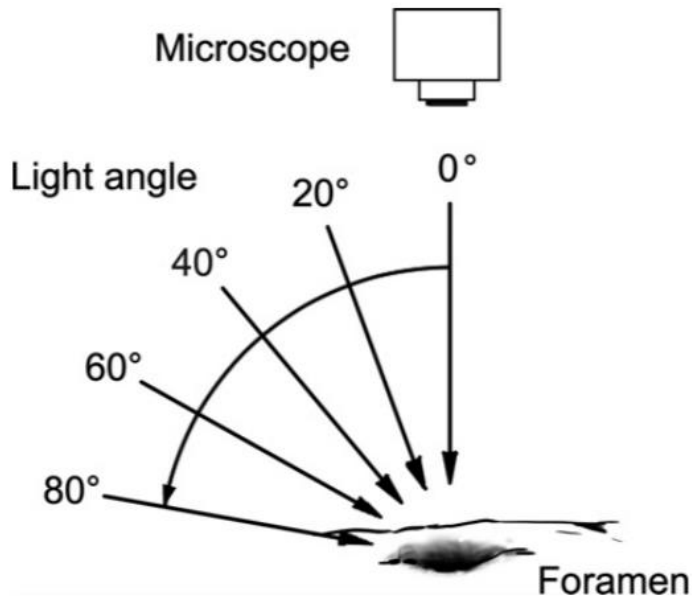
Figure 4. Schematic diagram of the light angle experiment. Microphotographs were taken at 10° intervals.
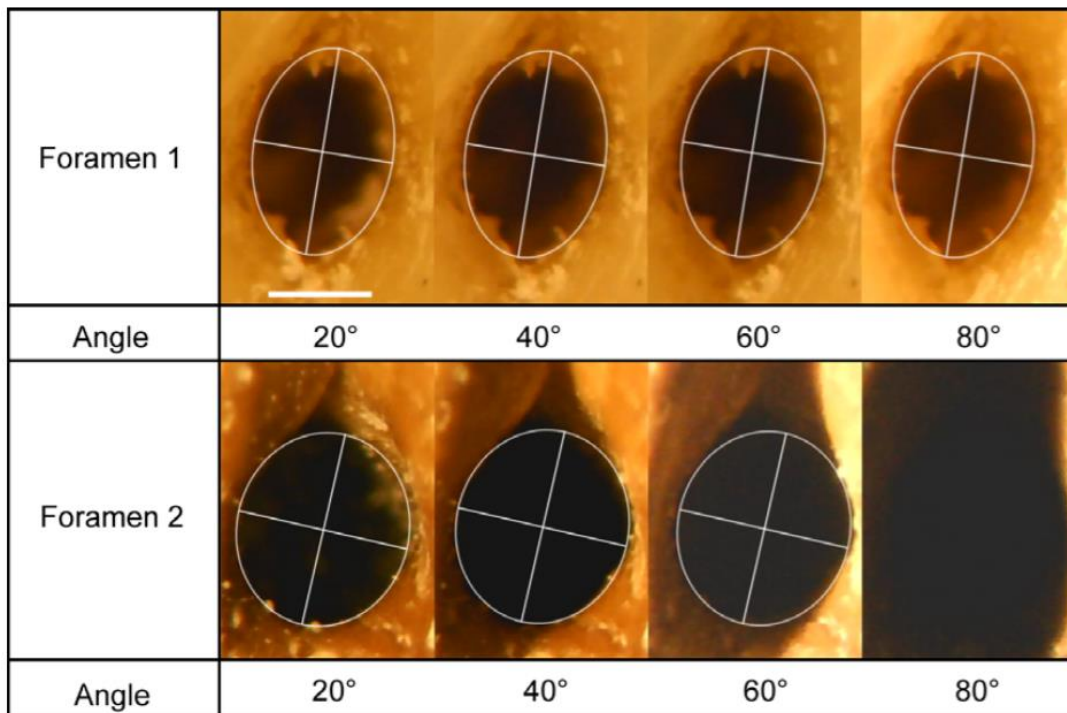
Figure 5. Microphotographs of foramen A and B at 20°, 40°, 60° and 80° light angle. The white ellipses are best-fit ellipses with minor and major diameters. All microphotographs have the same scale. Scale bar: 0.5 mm.

Because of the overexposure and underexposure, area measurements are invalid for the foramen 2 microphotographs with light angles of 10°, 80° and 90°. Mean and 95% CI of six measurement replicates at each light angle are shown in Figure 6A. Variations remain relatively minimal under different light angles. However, when the light angle approaches 0° or 90°, the microphotographs become either overexposed or underexposed. Thus light angle is recommended to range between 30° and 70°, where the data are constant. Although the area of the shadow differs at different light angle, the foramen edge can still be determined at the approximate same locations. The relationship of mean area calculated from the six replicates on light angle ranging from 30° to 70° is plotted in Figure 6B. The 95% CI for the relationship indicates that the measured foramen areas remain similar regardless of the light angle because the slopes for both foramina are not significantly different from 0 (Foramen 1: $F_{1,3} = 2.41$, $P = 0.22$; foramen 2: $F_{1,3} = 1.19$, $P = 0.35$). In practice, it is best to become familiar with the structure of the foramen and arrange the lighting in a consistent manner such that the images reveal a clear contrast between illuminated bone and the shadow.
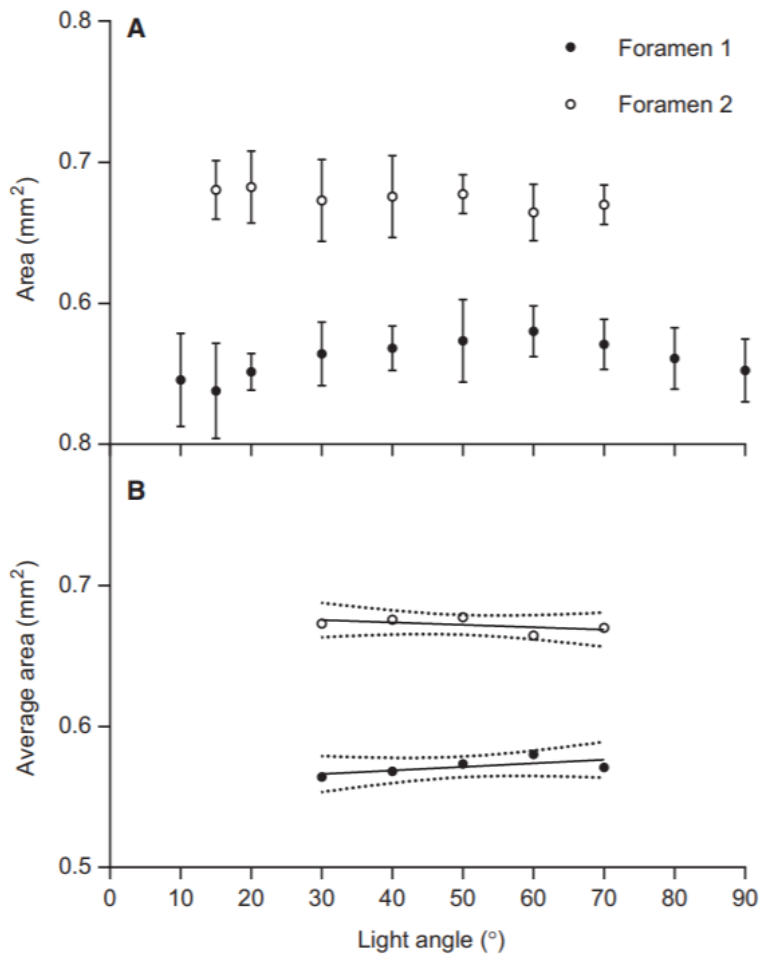
Figure 6. Relationship between light angle and measured foramen area using a microphotographic set up. (A) Mean and 95% confidence bands of six measurement replicates at each light angle. (B) Relationship between foramen areas averaged from six measurements and light angles ranging between 30° and 70°. The 95% confidence bands for the regressions indicate that the slopes are not significantly different from zero, and thus there is no significant effect of light angle between these limits.

2.3.2 Micro-CT scanning

When working on wet bone specimens within tissues, it is impossible to measure foramen dimensions via microphotography. Computerized tomographic (CT) scanners use energy (X-rays) to detect materials with different densities. Micro-CT can provide slice-by-slice high resolution images of a sample without disturbing the sample. To obtain foramen size measurements in this study, bone samples were scanned using a micro-CT scanner (in our case, SkyScan-1076 or -1276, SkyScan-Bruker, Kontich, Belgium). Polystyrene foam and tape were used to immobilize bones on the scanning

bed. If fresh bones with wet tissue attached were used, plastic wrap was used to prevent the specimen from drying out during the scan. Generally, the higher the resolution of a micro-CT image, the more precise the foramen size values that can be obtained. In reality the resolution chosen often depends on a balance of specimen size, desired image quality and scanning time required. Pixel size is recommended to be < 10% of foramen radius. A pilot study can be done to assess micro-CT image quality and determine the associated time required. In most cases, the whole bone sample with its foramina can be scanned completely in one scan. In circumstances when bone morphology data are required but the resolution does not need to be as high as necessary to image the foramen, it is feasible to perform a scan of the foramen separately from the rest of the specimen. In situations where bones are too large to fit in the scanner and when it is permissible to damage bone samples, a section containing the foramen can be excised from the bone and scanned separately.

After scanning, the raw topographic projection CT imagery data (TIFF file) collected from the micro-CT scanner was reconstructed to cross-sectional BMP images using NRECON 1.6.10.4 (Bruker microCT, Kontich, Belgium). Reconstruction and thresholding settings were optimized to maximize the image quality for each sample. Inaccurate thresholding will lead to inaccurate foramen sizes. Volume of interests (VOI) in DataViewer 1.5.2.4 (Bruker microCT) were used to include just the region of a foramen and to obtain a series of foramen cross-sectional images. Since a VOI is cuboidshaped, more than one VOI was drawn for saving cross-sections of a curved foramen. Each VOI should be drawn as parallel as possible to the foramen passage (Figure 7). The series of foramen cross-sectional images were then analysed using FIJI, and radii (r, mm) of the foramina were then calculated.
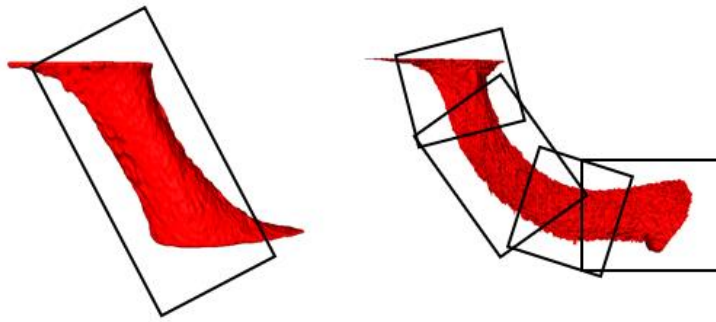
Figure 7. Two foramen virtual casts from CT scans. The left is a straight and the right is a curved foramen. The rectangles represent side view of volumes of interest along the foramen passages. More than one volume of interest is required for finding the minimum cross-sectional area along a foramen.

2.3.3 Impression material casting

Dental impression material can be used on dry bone specimens and has the advantage of allowing visualization of the foramen passage in a three-dimensional form without damaging the bone, like the micro-CT method. Test runs need to be done to find suitable products that can suitably produce foramen casts and do not stick to the bone. This study recommends CharmFlex Light LV impression material (Dentkist, South Korea) to mold foramina. Foramina should be cleaned to prevent any large particles remaining in the molding area. After mixing two components of the impression material, it is pressed or injected into a foramen to fill it to the walls. After the material is set, a suitable impression material can be pulled from the foramen easily without much deformation (Figure 8A). The time duration for the material to set depends upon the product, the foramen shape and the foramen size. The duration cannot be too short because the product will deform during extraction. The duration cannot be too long, especially for the relatively large-sized and markedly curved foramina (e.g. internal carotid foramina), because the pliability of the material will decrease and the material has a greater chance of breaking inside the foramen during extraction. The small cross-sectional region of the cast can be cut perpendicularly into thin slices. Microphotographs of the slices with a known scale are used to measure foramen areas using FIJI (Figure 8B).
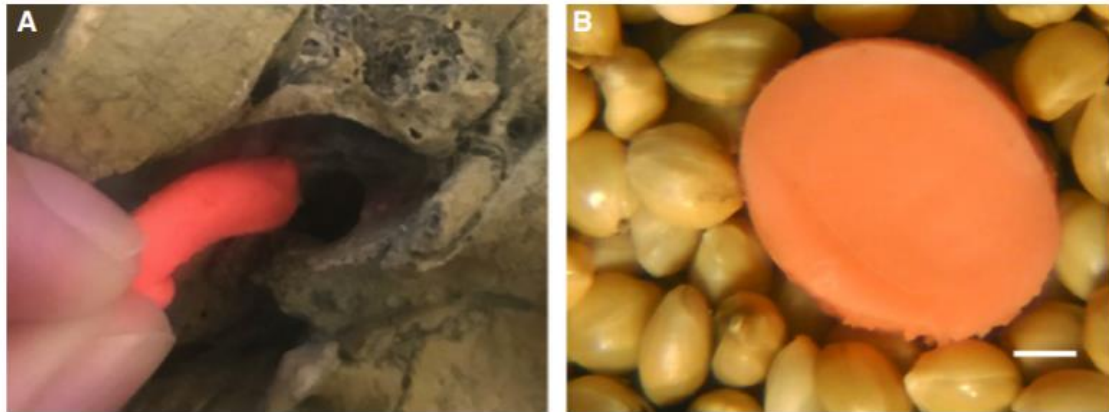
Figure 8. Photographs of the impression material casting method. (A) Pulling out of impression material from a human carotid foramen. (B) Cross-section of the cast resting in millet seed under a microscope.

2.4. Arterial wall thickness

Blood flow rate in arteries that pass through type II foramina can be calculated according to Eq. 2 if the relationship between foramen radius and vessel lumen radius is known. Because the arteries largely fill type II foramina, the difference in radii is the arterial wall thickness. Mean wall thickness is $30 \pm 5\%$ of the lumen radius, based on wall-lumen ratios collected from 14 human studies of common carotid and internal carotid arteries (individual studies are listed in supplementary material Table S2). Thus artery lumen radius can be calculated by dividing the foramen radius by 1.30. This ratio of wall thickness and artery radius is thought to be a constant, according to the law of Laplace (Burton, 1965; Caro et al., 2012; Wolinsky and Glagov, 1967). However, it might be slightly different in other type II foramina or even in other animals' carotid canals, but further studies are required to test this.

2.5. Comparative results and discussion

2.5.1 Comparison of microphotographic, micro-CT and impression material casting methods

To compare the differences among microphotographic, micro-CT and impression material casting methods, three sets of real foramina and one set of artificial foramina were measured using these three methods. Two sets of real foramina came from western grey kangaroos (*Macropus fuliginosus*) with body masses ranging from 5.8 to

70.5 kg. One set consisted of 22 femoral nutrient foramina from 10 femur pairs, and the other of 20 lateral vertebral foramina from 10 C1 vertebrae. The third set of real foramina are six carotid foramina in human temporal bones from six individuals with unknown body mass. The set of nine artificial foramina were produced by drilling through segments of bone sourced from western grey kangaroo femora. Drill bits of known diameters (1, 1.5 and 2 mm) were drilled through small pieces of cortical bone, either at a right angle or at a shallow angle. The areas of these drill holes and foramina were measured with all three methods. Vertebral foramina were not scanned using the micro-CT method but were instead scanned using a Philips Ingenuity Core 128 scanner with lower image resolutions (pixel size ranging from 200 to 300 µm). Data from two nutrient foramina with areas smaller than 0.4 mm^2 were excluded while performing the impression material casting method because our product cannot be injected or pressed properly into these small foramina. Minimum cross-sectional areas (mm^2) and radii (mm) were measured using FIJI. The area or radius measurements among different methods were then plotted against each other on a graph. A line of identity (Y = X) was drawn on the graph to show the measurement difference between the two methods. 95% confidence intervals were plotted on the graphs using the GraphPad Software.

The area and radius comparisons among the three methods show good concordance and consistency (supplementary material Fig. S2–S5). The 95% CI of the area and radius measurements among three method comparisons show slopes mostly not significantly different from 1, except for a few comparisons (supplementary material Table S1). The 95% CI of the slope of femoral nutrient foramen area collected between micro-CT and dental impression material is slightly lower than 1 (0.85 ± 0.13), but the 95% CI of the slope of the radius comparison between these two methods is not significantly different from 1.0 (0.85 ± 0.15). The 95% CI of the slopes of carotid foramen area and radius comparison between microphotographic and micro-CT are slightly different from 1 (area comparison: 1.1 ± 0.06; radius comparison: 1.1 ± 0.06), but there is no significant difference between microphotographic and dental impression casting methods, or between micro-CT and dental impression casting methods. The biggest percentage difference of the carotid foramen radius between any two methods is only about 3%. For the drill holes, the 95% CI of slope of microphotographic area on micro-CT area is slightly different

from 1 (0.93 ± 0.06), whereas the 95% CI of slope of radius is not significantly different from 1 (0.94 ± 0.06). In general, most measurement data lie close to the line of identity, and the 95% CI bands are very narrow in each graph (supplementary material Figs S2–S5, Table S1); thus it is valid to suggest the three methods are comparable and are able to obtain similar foramen dimension values. The few significant differences in slopes are all very close to the slope of 1, which may be due to random measurement errors, possibly due to failure to find the same location of cross-sectional areas along the foramen passage.

The three methods are subject to biases specific to each one. The micro-CT method is able to observe the overall interior shape of a foramen passage and is potentially the most accurate method. Microscopes can only observe the foramen opening and the most external regions of the canal. The dental impression material casting method can represent part of the internal pathway of a foramen. The micro-CT and dental impression material casting methods can both 'cut through' a foramen so that a series of foramen cross-sectional images are obtained. Since a foramen passage is usually curved, it is impossible for all cross-sectional images to be perfectly aligned perpendicular to the passage. The micro-CT and dental impression material approaches tend to overestimate the foramen area slightly, as each cross-section area is theoretically either the same or larger than the actual foramen area at the same point along the foramen passage. In addition, some of the interior micro-CT cross-sectional areas observed in this study are neither elliptical nor circular due to extra groove structures present on the interior of the foramen passage (Figure 9). Thus, measuring the entire areas on the inside of a foramen using micro-CT or impression material methods may also lead to overestimation of the area. Foramen minimum cross-sectional areas often occur inside the foramen rather than on the bone surface. We initially believed that the microphotographic method would tend to overestimate the foramen areas compared with the other two methods, but our results reveal that the microphotographic method is more likely to underestimate the foramen area. The major reason is the difficulty in aligning a view down into a foramen passage if the foramen is obstructed by overhanging bone protuberances (refer to section on Effects of viewing angle). The microphotographic method generally does not measure areas at the bone surface because foramina flare at the surface and do not have a definite edge; however, light penetrates the foramen and creates a shadow where the flare

34

narrows. Additionally, some bone samples in this study have grease on the bone surface and inside the foramina as a result of the maceration process used to prepare the specimens. Other dried specimens have remains of the lining of the canal and the vessels. These substances have relatively light density compared with bone and thus seem to be more of less radiolucent and hence are hardly visualized on a micro-CT image. The presence of grease or dried tissue lining the foramen results in underestimation of the foramen area with microscopic or impression materials. With all the limitations considered, there are systematic errors among the three methods.
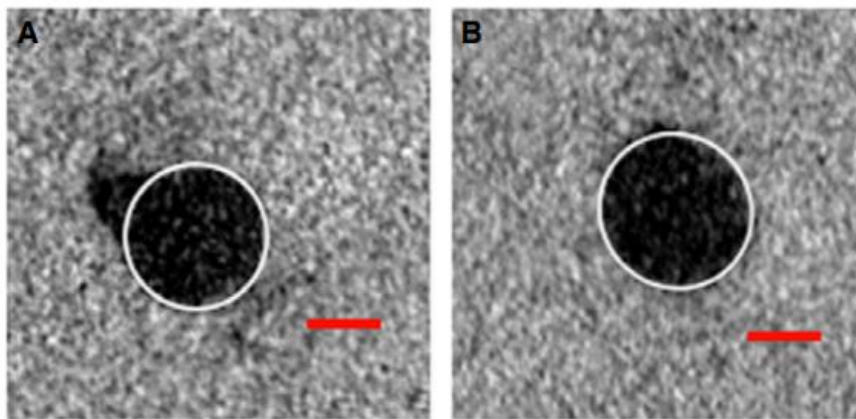
Figure 9. Cross-section micro-CT images of kangaroo femoral nutrient foramina. (A) A foramen with a groove has a larger area than the best-fit ellipse. (B) A round foramen with a close-fitting ellipse. Scale bars: 0.5 mm.

Fortunately, there are three means to minimize and correct the systematic errors. First, foramina should be properly cleaned prior to area measurement to avoid underestimating the foramen area in microphotographs or from impression material casts. Degreasing foramina can be simply done by carefully cleaning the foramina using plastic toothpicks and toothbrushes. Tools made of hard materials such as metals should be avoided during the cleaning process to prevent damaging the foramina. Secondly, foramen passages need to be carefully adjusted perpendicular to the view. Our study observed that most foramen passages do not enter bones at a right angle. It is important to find the right viewing angle so that the camera looks directly into the foramen, rather than simply at the surface of the foramen. Thirdly, to

maintain measurement consistency among the three methods, the foramen area is best determined by measuring the area of a foramen using the best-fit ellipse.

**2.5.2 Foramen radius calculated from foramen diameter or area**

The blood flow calculation equations for determining blood flow depend upon a value of radius (r) rather than a value of area. Previous foramen studies calculated foramen radius from either minor diameter (Allan et al., 2014; Seymour et al., 2012) or foramen area converted to a circle (Hu et al., 2018; Seymour et al., 2015; Seymour et al., 2016). These two approaches produce the same radius only if the foramen is circular. However, in reality, perfect circular foramina are rare, even for the type II foramina with circular artery cross-sections due to the high blood pressure inside. In addition, the size relationship between a type I foramen cross-section with an artery has not been studied, so the location and the area percentage of an artery inside a foramen is not clear. There are remaining questions that need to be solved in the future for this foramen type. For instance, is the size of an artery proportional to the size of a type I foramen that both an artery and a vein pass through? How does cross-sectional area of the vein affect the shape of the foramen? Future studies are required to investigate the detailed anatomy before improving the foramen blood flow estimation method. At this stage, since we have not enough information about the size relationships between foramina and arteries, foramen morphology values including minor diameter, major diameter and area are recommended to be recorded for each specimen. Fitting the best-fit ellipse into a foramen can directly provide all these values in FIJI. Until more is known, the relative blood flow index Qi can be calculated (Eq. 1) from type I foramina for comparative purposes.

The foramen pathway is more straightforward inside a type II foramen such as the carotid canal because it mainly passes the internal carotid artery. However, the cross-section of the foramen often changes shape, size and even angle in bone. To investigate the effects of these changes, we examined cross-sectional area shape and size change along six human carotid canals by creating 3D canal models in AVIZO 9.0.0 (FEI SAS, Hillsboro, OR, USA). Cross-sectional areas were obtained using DataViewer at five locations along each carotid canal (Figure 10). The areas were measured by fitting the best-fit ellipses using FIJI. Radii were measured from the area value by assuming the elliptical area of a foramen opening is the area of a perfect

circle. Minor diameter, major diameter and circularity ($4\pi \times$ (area/perimeter^2)) of the ellipse at each location were recorded. The area is more circular as the circularity approaches 1 and less as it approaches 0. Among these six 3D models, five carotid canals bend into almost 90° after they run into the skull for approximately 1 cm. One carotid canal in this study has an approximate 140° bend, which is much larger than the maximum internal carotid artery angle (110°) at the bend reported by Vijaywargiya et al. (2017). The five locations with associated area, radius and circularity show some variability (Figure 11). Generally, the external region of the canals has larger and more circular cross-sectional areas compared with the areas at the bend, and the areas become larger and more circular again as the foramina run towards the foramen lacerum.
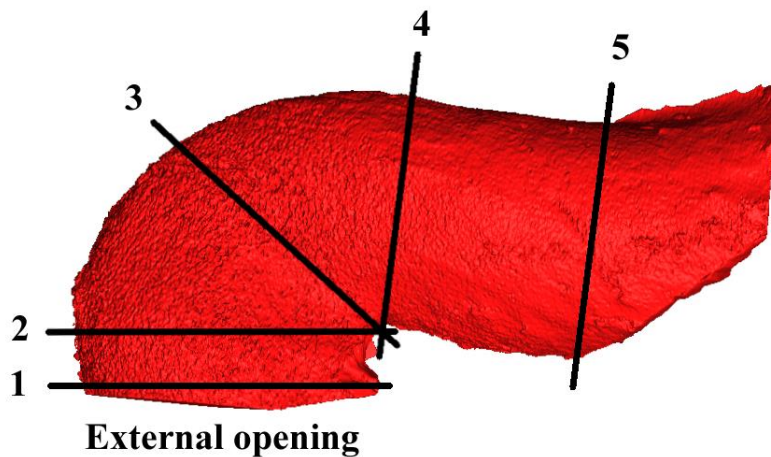
Figure 10. Five cross-sectional area locations of a virtual cast of a human carotid canal. Cross-sectional area #1 is at the foramen external opening; #2 is parallel to 1 at the bend; #3 is at the mid-section of the bend; #4 is perpendicular to the back section of the canal at the bend; #5 is parallel to 4 at the internal end for the carotid canal (i.e. the foramen lacerum).
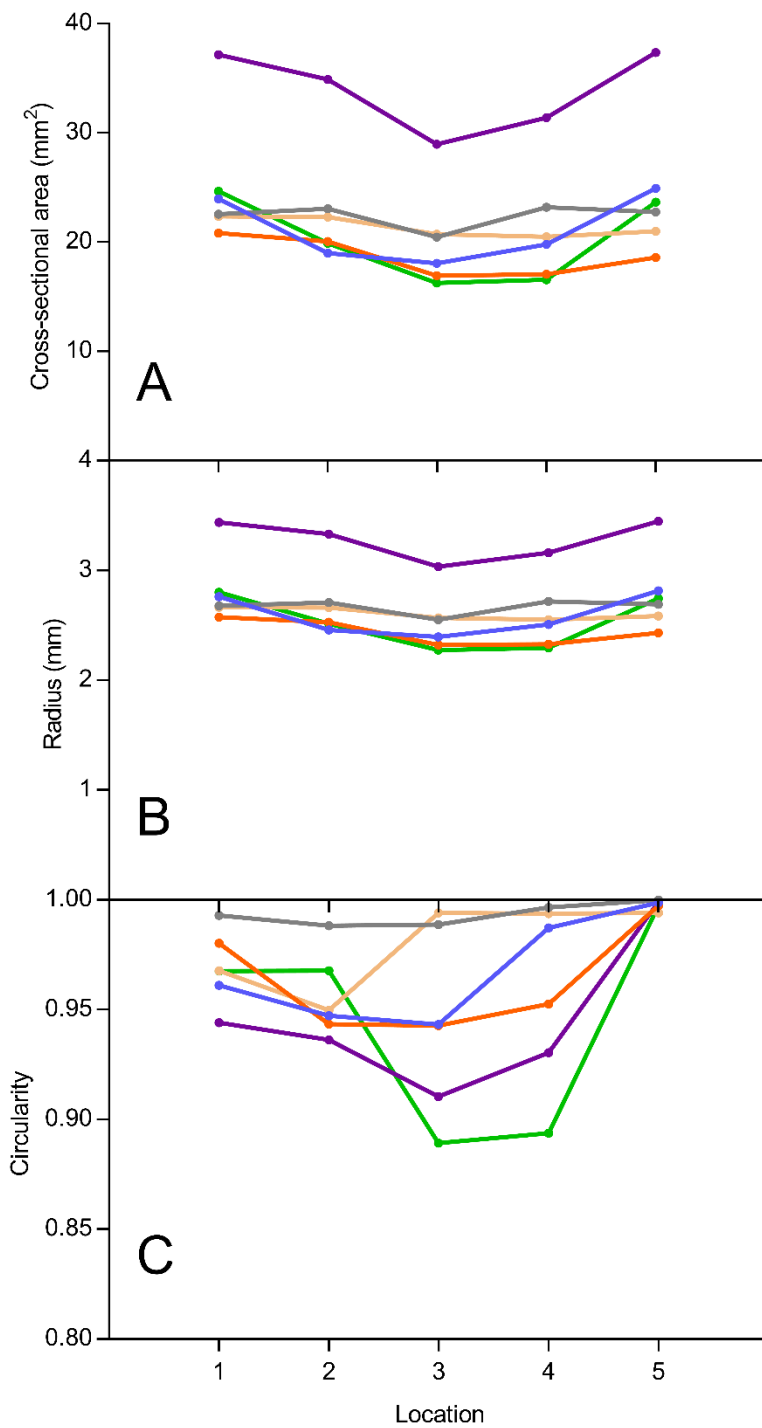
Figure 11. Cross-sectional area (A), radius (B) and circularity (C) at five locations corresponding to those marked in Figure 10 along six human carotid foramina. Radii were measured from the area value by assuming the elliptical area of a foramen opening is the area of a perfect circle. Six colours represent six carotid canals.

The circularity of the foramina in some canals dropped to approximately 0.95 at the bend (Figure 11C), which results in a 1.45-times longer major foramen diameter than minor diameter. However, with this decreasing circularity, the radii calculated from the foramen areas remain similar among the five locations along the canals (Figure 11B). But if the radii are estimated from minor diameters instead, the variations increase and both the foramen and artery size may be severely underestimated. The internal carotid artery is firmly enclosed by the canal at the entrance, but it does not completely fill the internal end of the canal because the artery appeared to be 'loose' in this region (Overbeeke et al., 1991; Vijaywargiya et al., 2017). With the current knowledge about human internal carotid artery and the canal, the optimal foramen area to measure is at the vertical section of the canal. In this study, all three foramen measurement methods were intended to find the smallest crosssectional area along a foramen passage because of two reasons. One reason is that the smallest area may be more representative of the artery size. The second reason is to standardize three methods, as it is difficult to locate the same cross-sectional area using different methods. The smallest cross-sectional areas of human carotid canals obtained from micro-CT and dental impression material casting methods are often found at the region between locations 2 and 3. With the microphotographic method this region can also be observed by adjusting the temporal bone position under the microscope.

2.5.3 Sensitivity analysis of different parameters in the shear stress equation

Once foramen radius and wall thickness are quantified for a type II foramen, blood flow rate can be estimated absolutely from internal arterial radius with the shear stress equation (Eq. 2) or empirical equations (Eqs 3, 4). A sensitivity analysis of Eq. 2 was conducted to investigate the impacts of four parameters (i.e. vessel wall thickness, vessel lumen radius, shear stress and blood viscosity), using human internal carotid artery as an example. Standard parameter conditions are used as a starting point. Blood viscosity is considered to be 0.04 dyn s cm^{-2} (Amin and Sirs, 1985; Schmid-Schönbein et al., 1969). Mean human internal carotid artery lumen radius (0.24 cm) and estimated wall shear stress (16.1 dyn cm^{-2}) values were averaged from 13 studies in the literature (Seymour et al., 2019b). Human internal carotid artery wall thickness (0.086 cm) is averaged from 10 internal carotid artery or carotid foramen studies (Table S2). Based on these values, and assuming the carotid foramen size is constant, the blood flow rate in one internal carotid artery is 4.3 cm^3 s^{-1}, which is considered to

be 100% on a graph to show the sensitivity of flow rate in relation to each of the factors in the shear stress equation (Figure 12). One at a time, the four parameters were changed within a range between 50 and 150% while the other parameters were held constant. In reality, the ranges of the three parameters are much narrower than 50–150%. Therefore, values from the literature were used to evaluate the real variation within the different parameters.
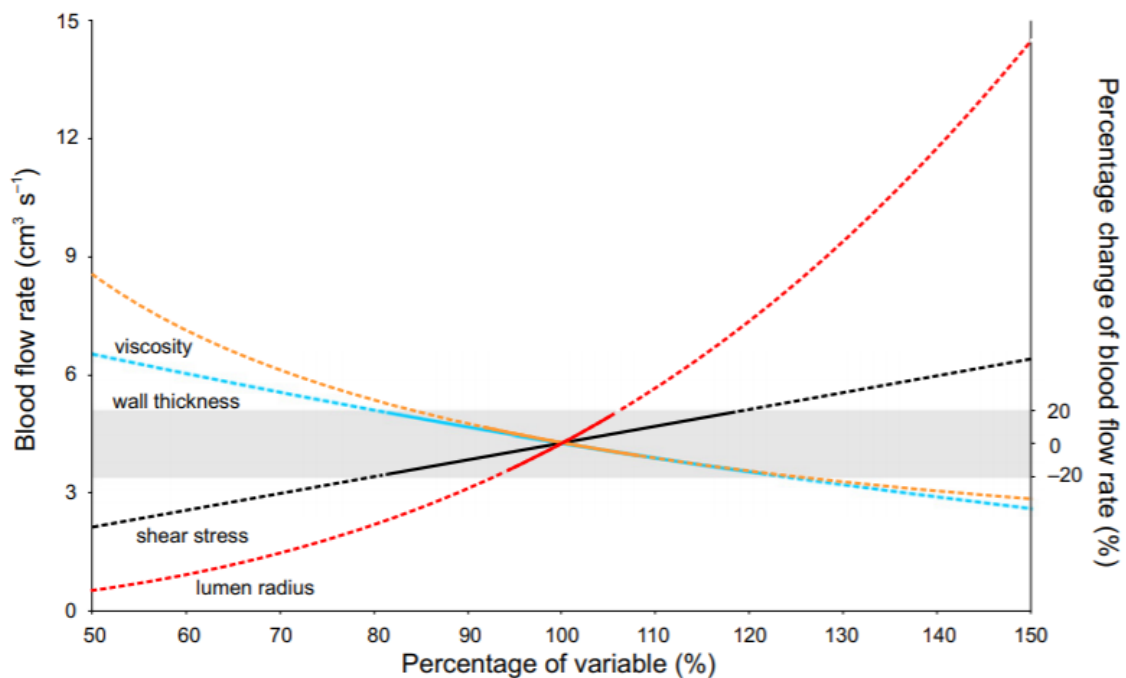
Figure 12. Sensitivity analysis of lumen radius, viscosity, shear stress and wall thickness on calculated blood flow rate based on the shear stress equation (Eq. 2). The intersection of the four lines at 100% is the average human internal carotid perfusion rate of 4.3 cm^3 s^{-1}. The curves represent changes in only one factor in the equation at a time, keeping all other factors constant. The solid lines represent the variability in the literature, bound by values at the upper and lower limits of the 95% CI of the published means. The dashed lines are extensions beyond these limits. The grey shaded area represents ± 20% change of calculated blood flow; the literature data produce blood flow rates within this range.

Blood flow rate is directly proportional to shear stress, inversely proportional to blood viscosity and proportional to radius cubed (Eq. 2). Among the three parameters, radius has the largest impact on the calculated blood flow shown by the steepest slope (Figure 12). Lumen radius data collected from 13 studies of human internal carotid artery reveal a mean of 0.24 cm (Seymour et al., 2019b). The 95% CI ranges from 0.22 to 0.25 cm, which can increase blood flow rate by 20% or decrease it by 18% (Figure 12). Human internal carotid artery wall thickness averages 0.086 cm, with a 95% CI ranging from 0.069 to 0.10 cm (Table S2), resulting in 19% more or 17% less calculated blood flow. Blood viscosity variation is narrow at high shear rate (Amin and Sirs, 1985), suggesting blood viscosity remains constant in major arteries. However, Windberger et al. (2003) recorded whole blood viscosity at high shear rates in 10 mammalian species, revealing a mean of 0.05 dyn s cm^{-2} with 95% CI of $\pm$ 0.004 dyn s cm^{-2}. This can result in a change of approximately $\pm$ 9% in calculated blood flow. Measurements from 13 studies of human internal carotid arteries give a mean shear stress of 16.1 dyn cm^{-2} and a 95% CI of $\pm$ 3.0 dyn cm^{-2} (Seymour et al., 2019b). This variation introduces a $\pm$ 19% change in calculated blood flow rate.

By considering all variations within each parameter of the shear stress equation, the calculated blood flow has a narrow variation range, with a maximum range of approximately $\pm$ 20% (Figure 12). The variation of each individual parameter thus has little impact on calculated blood flow. Although the variations can be combined and the impacts can add up, the current knowledge on blood flow cannot further improve the precision of the measurements.

In summary, microphotographic, micro-CT and dental impression material casting methods can obtain foramen size values that are relatively accurate, as no significant differences in foramen area and radius measurements were found among these three methods. Although micro-CT has the fewest disadvantages of the methods, it has a higher cost and involves a greater investment of time. More importantly, the micro-CT method may not be readily available in many situations. Similar to the micro-CT method, dental impression material can mold the foramen and it is relatively cheap and easy to use. Although it can be very useful tool in some situations, risks exist, as it may break inside foramina, stick in gaps between bones or fail to enter small foramina. The microphotographic method is thus recommended in general to measure

foramen sizes due to its lack of contact, high speed and low expense. However, measurement errors can be easily introduced if participants are not familiar with the technique. Major factors including depth of field, viewing angle and light angle of the microphotographic set-up need to be considered prior to taking photos. In situations where foramen openings cannot be properly viewed using the microphotographic method, the micro-CT method or impression material are alternative solutions.

2.6. Acknowledgements

2.7. Supplementary material

```
                    ┌──────────────────────────────┐
                    │      Examine the bone type    │
                    └──────────────────────────────┘
                       │                          │
                       ▼                          ▼
           ┌───────────────────┐        ┌──────────────────────┐
           │ Dry bone (e.g. fossils) │   │ Wet bone (e.g. bones   │
           └───────────────────┘        │ with tissues attached  │
                  │                      └──────────────────────┘
                  ▼                                  │
      ┌────────────────────────────┐                │
      │ Examine whether is possible to │   ┌─────┐   │
      │ cut and accurately measure the │──▶│ Yes │   │
      │ foramen under a microscope     │   └─────┘   │
      └────────────────────────────┘               │
                  │                                  │
                  ▼                                  │
              ┌──────┐                               │
              │  No  │                               │
              └──────┘                               │
                  │                                  │
                  ▼                                  │
      ┌───────────────────────┐                     │
      │ Is it feasible to excise │   ┌─────┐         │
      │ foramen region from the  │──▶│ Yes │         │
      │ bone                     │   └─────┘         │
      └───────────────────────┘        │            │
                  │                     ▼            │
              ┌──────┐        ┌──────────────────┐   │
              │  No  │        │ Excise foramen   │   │
              └──────┘        │ region           │   │
                  │           └──────────────────┘   │
                  ▼                     │            ▼
```
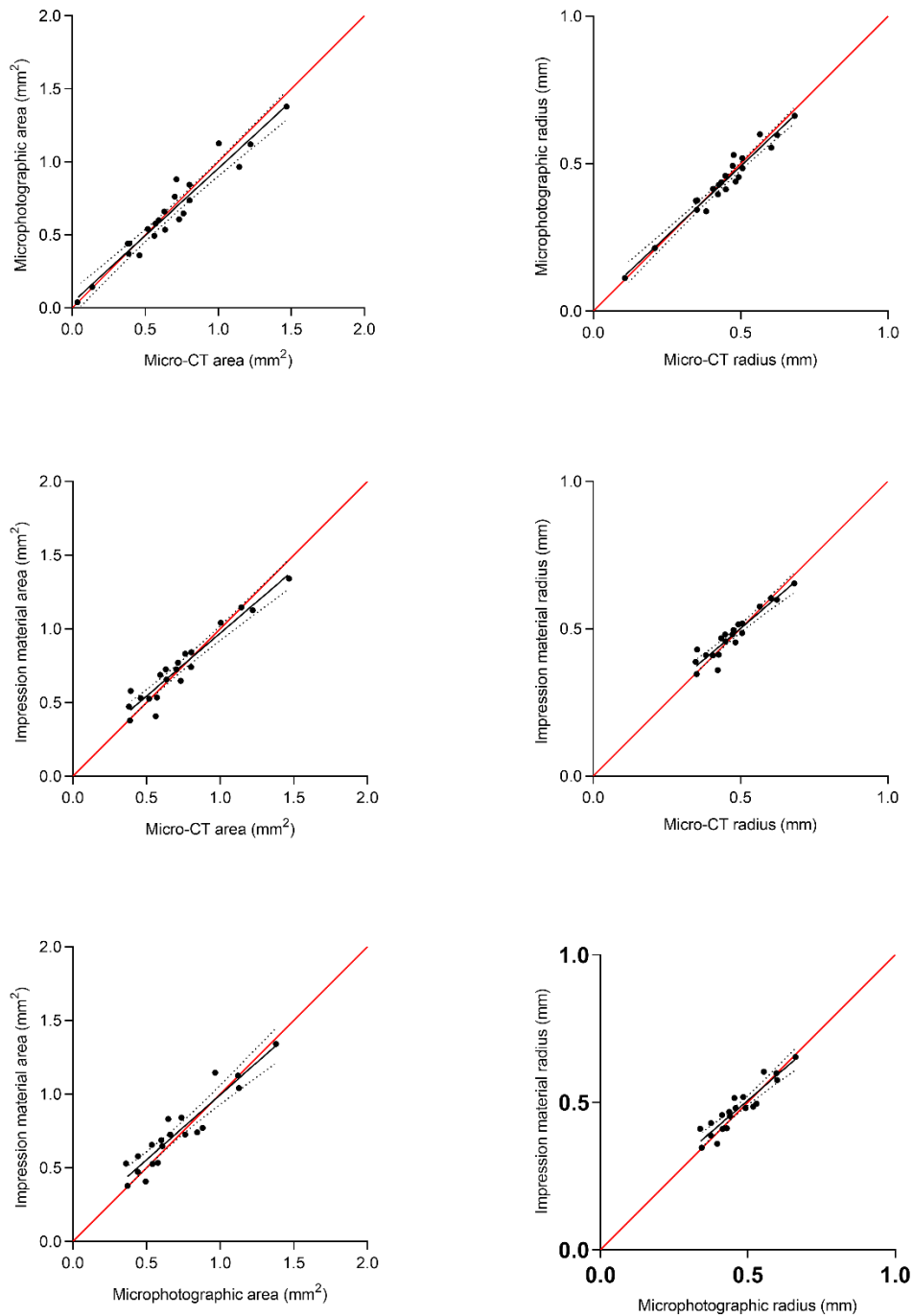
Examine the bone type

Dry bone (e.g. fossils)

Wet bone (e.g. bones with tissues attached

Examine whether is possible to cut and accurately measure the foramen under a microscope

Yes

No

Is it feasible to excise foramen region from the bone

Yes

No

Excise foramen region

Foramen photos taken by a digital camera or a digital microscope

(Alternative option: impression material casting method)

Foramen photos taken by a microscope

(Alternative option: impression material casting method)

Micro-CT method
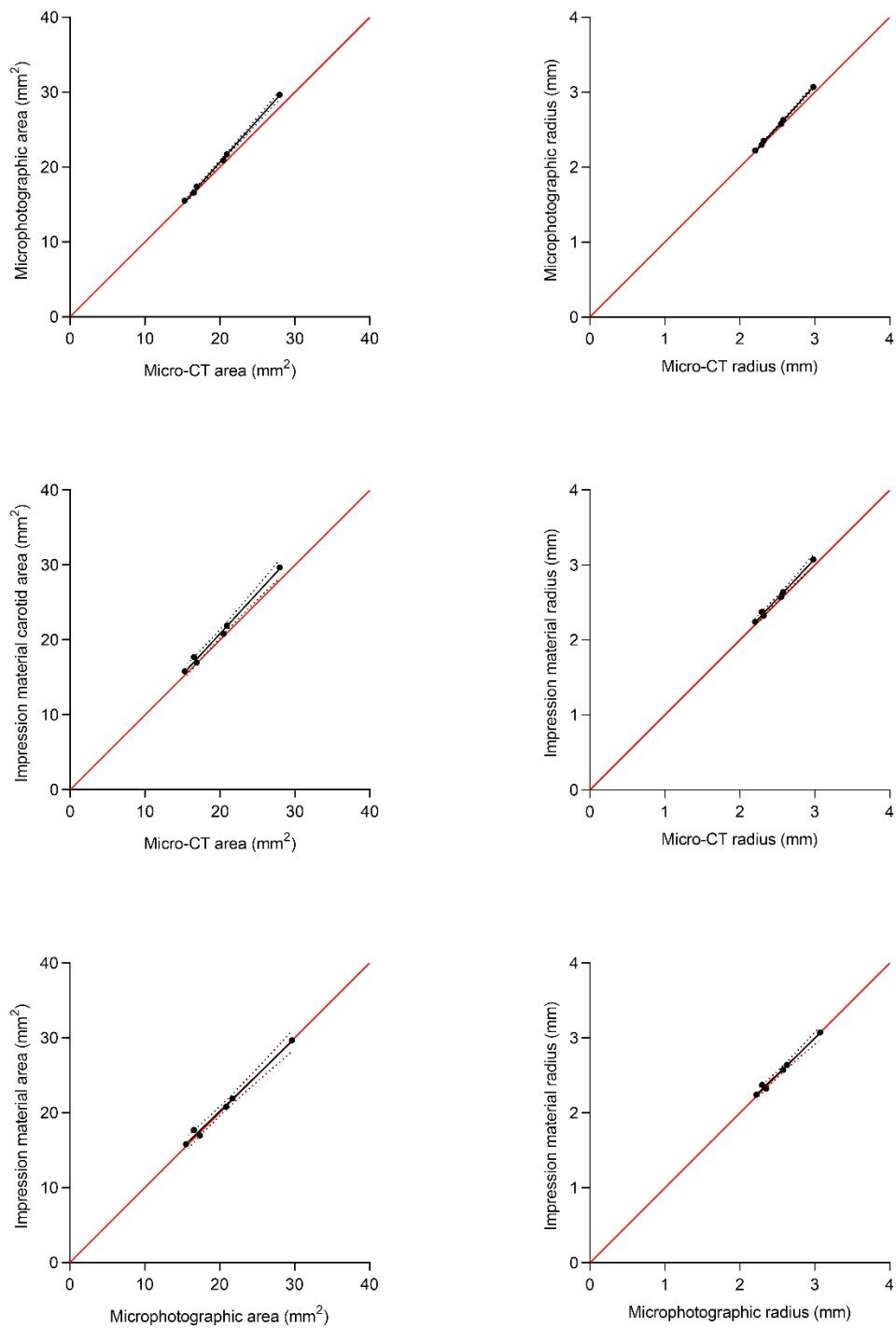
Nutrient foramen (kangaroos)

Figure S2. Comparisons of kangaroo nutrient foramen areas and radii measured with the three techniques of this study.
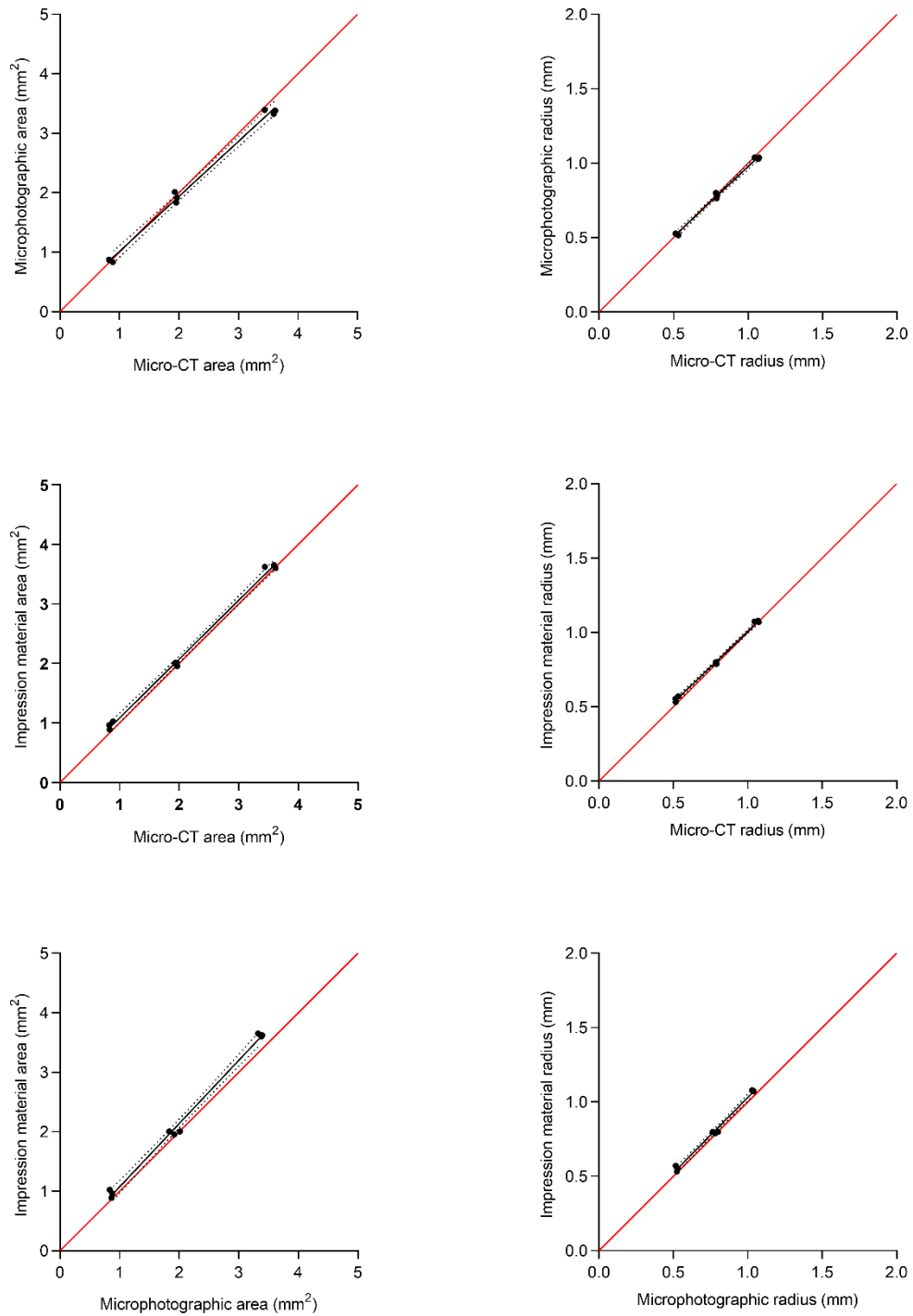
Vertebral foramen (kangaroos)
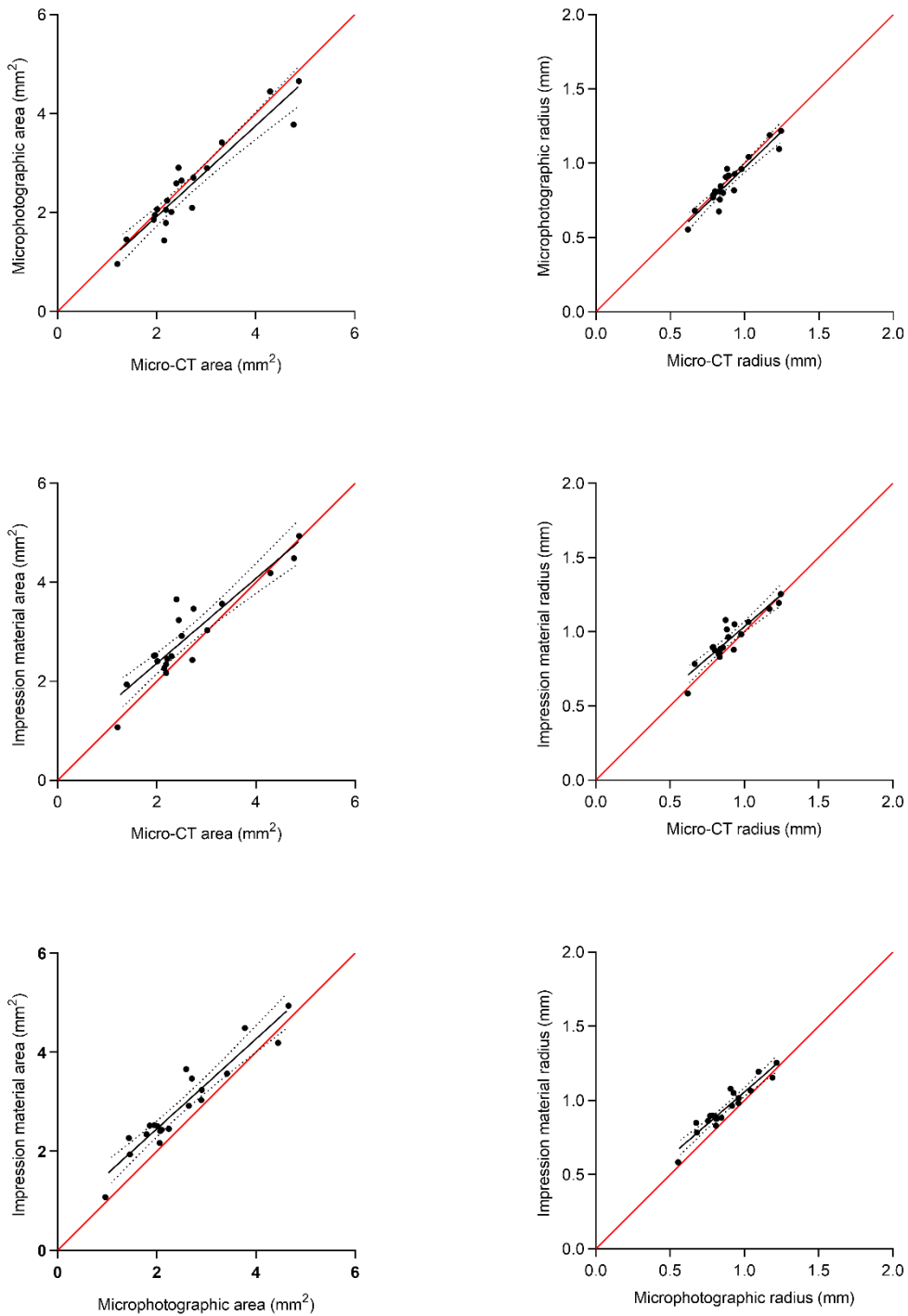
Figure S3. Comparisons of kangaroo vertebral foramen areas and radii measured with the three techniques of this study.

Carotid foramen (human)

Figure S4. Comparisons of human carotid foramen areas and radii measured with the three techniques of this study.

Drill hole

Figure S5. Comparisons of drill hole areas and radii measured with the three techniques of this study.

Table S1. Comparisons of three methods of measuring foramen area and radius. Results from two methods are plotted against each other and ordinary least squares regressions calculated. Mean slope ± 95% CI are presented. Asterisks denote comparisons with 95% CI of slope significantly different from 1.

	Area slope ± 95% CI	Radius slope ± 95% CI
Nutrient foramen (Kangaroo)		
Microphotography vs. Micro-CT	0.91±0.12	0.92±0.10
Impression material vs. Micro-CT	0.85±0.13*	0.85±0.15
Impression material vs. Microphotography	0.88±0.16	0.86±0.17
Vertebral foramen (Kangaroo)		
Microphotography vs. Micro-CT	0.92±0.16	0.96±0.18
Impression material vs. Micro-CT	0.86±0.18	0.86±0.19
Impression material vs. Microphotography	0.91±0.15	0.87±0.14
Carotid foramen (human)		
Microphotography vs. Micro-CT	1.1±0.06*	1.1±0.06*
Impression material vs. Micro-CT	1.1±0.13	1.1±0.14
Impression material vs. Microphotography	0.97±0.13	0.96±0.15
Drill hole		
Microphotography vs. Micro-CT	0.93±0.06*	0.94±0.06
Impression material vs. Micro-CT	0.99±0.05	0.96±0.05
Impression material vs. Microphotography	1.06±0.07	1.02±0.08

Table S2. Studies involving measurements of radius and wall thickness of internal carotid arteries (ICA), common carotid arteries (CCA) or carotid canals (CC).

Study	Method	Artery/canal	Outer radius (mm)	Lumen radius (mm)	Wall thickness (mm)	Wall-lumen ratio (%)
Sommer et al. 2009	In Vitro	ICA	3.17	2.56	0.61	24
Watase et al. 2018	MRI	ICA	4.30	3.40	0.90	26
Saam et al. 2009	MRI	ICA	3.98	3.33	0.64	19
Cibis et al. 2016	MRI	ICA	4.52	3.23	1.29	40
Qiao et al. 2016	MRI	ICA	4.82	3.81	1.01	26
Somesh et al. 2014	Caliper	CC	3.60	2.39[a]	1.21	51
Çalgüner et al. 1997	Caliper	CC	2.79	2.39[a]	0.40	17
Naidoo et al. 2017	Caliper	CC	3.23	2.39[a]	0.84	35
Berlis et al. 1992	Caliper	CC	3.38	2.39[a]	0.99	41
Aoun et al. 2013	Caliper	CC	3.10	2.39[a]	0.71	30
Saba et al. 2013	MDCTA	CCA	4.55	3.29[b]	1.26	38
Saba et al. 2008	MDCTA	CCA	4.11	3.29[b]	0.82	25
Saba et al. 2010	MDCTA	CCA	4.20	3.29[b]	0.91	28
Boussel et al. 2007	MRI	CCA	3.91	3.24	0.67	21

[a]Mean internal carotid artery lumen radius averaged from 13 studies (Seymour et al. 2019)

[b]Mean common carotid artery lumen radius averaged from 6 studies (Seymour et al. 2019)

Methods:

In Vitro: Blood vessels removed from cadavers and measured *in vitro* photogrammetrically

Caliper: Carotid canal of skulls measured using calipers

MRI: Magnetic resonance imaging

MDCTA: Multidetector Computed Tomographic Angiography

Chapter Three: Regional femoral bone blood flow rates in laying and non-laying chickens estimated with fluorescent microspheres

Statement of Authorship

Title of Paper	Regional femoral bone blood flow rates in laying and non-laying chickens estimated with fluorescent microspheres
Publication Status	Unpublished and Unsubmitted work written in manuscript style
Publication Details	

Principal Author

Name of Principal Author (Candidate)	Qiaohui Hu		
Contribution to the Paper	Conducted experiments, analysed data, wrote the initial manuscript draft, and reviewed and edited subsequent drafts.		
Overall percentage (%)	60%		
Certification:	This paper reports on original research I conducted during the period of my Higher Degree by Research candidature and is not subject to any obligations or contractual agreements with a third party that would constrain its inclusion in this thesis. I am the primary author of this paper.		
Signature		Date	1/11/2020

Co-Author Contributions

By signing the Statement of Authorship, each author certifies that:

i. the candidate's stated contribution to the publication is accurate (as detailed above);

ii. permission is granted for the candidate in include the publication in the thesis; and

iii. the sum of all co-author contributions is equal to 100% less the candidate's stated contribution.

Name of Co-Author	Thomas J. Nelson		
Contribution to the Paper 25%	Assisted in the experiments, helped with data collection and literature research, reviewed manuscript drafts.		
Signature		Date	9/11/2020

Name of Co-Author	Roger S. Seymour		
Contribution to the Paper 15%	Provided advice, helped with experiment set ups, assisted the experiments, helped with data analysis, reviewed and edited manuscript drafts.		
Signature		Date	20/11/2020

3.1. Abstract

Regional blood flow rates reflect local tissue oxygen requirements. Femoral bone blood flow rates estimated from femoral nutrient foramina in vertebrates may be associated with bone metabolism. In this study, a fluorescent microsphere infusion technique was used to investigate regional femoral bone blood flow in young non-laying hens, laying hens and roosters. Overall, mean cardiac output of anaesthetised chickens was 338 ± 38 ml min^{-1} kg^{-1}, and the two femora received 0.63 ± 0.10 % of this. Laying hens had higher bone-mass-specific femoral blood flow rates (0.23 ± 0.09 ml min^{-1} g^{-1}) than the non-laying hens (0.12 ± 0.06 ml min^{-1} g^{-1}) and roosters (0.14 ± 0.04 ml min^{-1} g^{-1}), presumably associated with bone calcium mobilization during eggshell production. Based on mean perfusion rate, the estimated metabolic rate of femoral bone was 0.019 ml O$_2$ min^{-1} g^{-1}. Absolute rates of blood flow to the femoral bone in this study were not significantly correlated with nutrient foramen sizes in chickens. Including our data, femoral bone blood flow rates in cursorial birds scale with body mass to the 0.90 ± 0.29 power, which is not significantly different from maximum metabolic rate of running birds.

3.2. Introduction

Physiological processes such as regional bone blood flow are poorly studied and understood in birds, compared to mammals. As living organs, bones continuously undergo processes that result in a change in bone mass, which are vital for bone health. Bones are fully vascularized. In addition to the major blood vessels in the bone marrow, cortical bone also contains millions of blood vessels. Bone mass change processes such as modelling (growth) and remodelling (repair) are all supported by the blood supply. Two main types of cells are responsible for bone tissue change processes. Osteoclast cells absorb bone matrix while osteoblast cells lay down new bone tissue (Rucci, 2008). Apart from cortical and trabecular bones, birds develop medullary bone, particularly in leg bones, to act as a labile calcium source for eggshell formation around the onset of sexual maturity (Whitehead, 2004). Commercial layer chickens require a lot of calcium for intense egg production, and about 10% of their total body calcium is cycled into the shell of every egg produced (Bar, 2009). Blood carries calcium as well as oxygen, hormones and nutrients to bones to satisfy varied metabolic demands. Studying regional blood flow rates improves the understanding of physiological processes that occur in different organs, because the oxygen demands of an organ determines the blood supplies to it (Wolff, 2008). Studying chicken femoral bone blood flow can thus provide insight into chicken femur metabolic demand associated with their physiological processes.

Measuring regional perfusion is challenging, but techniques such as Doppler ultrasound and microsphere infusion have been developed over the last century. Microsphere infusion has been particularly useful to quantify regional blood flow and blood flow distribution. This technique requires injection of microspheres into left ventricle or atrium of an animal, and it relies on a principle that the microspheres are distributed evenly within the blood stream after the injection and lodge in the microcirculation, because they are larger than the capillaries. The amount of microspheres that are trapped in tissue capillaries is proportional to the regional perfusion rates (Anetzberger and Birkenmaier, 2016). Early studies on regional perfusion using the microsphere infusion technique only estimated relative blood flows to different tissues, however, absolute regional blood flow rates can be measured after the invention of the arterial reference sampling technique, which uses a pump as an artificial organ to withdraw arterial blood with a constant, known rate

from the same experimental animal during microsphere injection (Kaihara et al., 1968; Makowski et al., 1968; Neutze et al., 1968).

Radioactive microspheres, which were introduced by Rudolph and Heymann in 1967 were commonly used for investigating regional blood flow rates in many cardiovascular studies (Barbee et al., 1992; Ferrell et al., 1990; Grundnes and Reikeras, 1991). However, since radioactive microspheres have many disadvantages such as potential health risks, disposal issues and high cost, colored or fluorescent microspheres were then introduced into cardiovascular research (Anetzberger and Birkenmaier, 2016). Blood flow estimated by florescent microspheres was shown to have similar accuracy to the blood flow measured by radioactive microspheres (Anetzberger et al., 2004c; Chien et al., 1995; Deveci and Egginton, 1999; Glenny et al., 1993; Van Oosterhout et al., 1995). Subsequently, fluorescent microspheres have been successfully used in numerous studies to quantify blood flow in bones (Anetzberger et al., 2004b; Aref et al., 2017; Serrat, 2009).

Another method to estimate regional blood flow rate is to measure the sizes of foramina that contain blood vessels in bones. This 'foramen technique' relies on a theory that the foramen sizes are proportional to the sizes of the occupying vessels. This technique has been developed to evaluate the blood supply to femora through nutrient foramina (Allan et al., 2014; Hu et al., 2018; Schwartz et al., 2018; Seymour et al., 2012) and to brains through carotid foramina (Boyer and Harrington, 2018; Boyer and Harrington, 2019; Seymour et al., 2015; Seymour et al., 2016; Seymour et al., 2019a). Blood flow rates estimated from human carotid foramina match direct blood flow measurements (Seymour et al., 2015), suggesting this technique can provide accurate regional perfusion values in some cases by simply measuring the sizes of foramina. However, no nutrient foramen studies have ever related the femoral nutrient foramen size with absolute blood flow of femoral bone because the nutrient artery does not completely fill the nutrient foramen. Therefore, the femoral bone blood flow rates estimated from the previous foramen studies represent relative blood flow indices only, rather than absolute blood flow rates.

The present study has two objectives. The first is to correlate absolute blood flow rates through femoral nutrient foramina and blood flow index estimated from foramen

size, by comparing the microsphere infusion technique and foramen technique. The second objective was to evaluate femoral bone perfusion in chickens with both techniques. Three chicken groups (i.e. non-laying hens, laying hens and roosters) with similar ages were chosen as experimental animals as only few studies have looked into bird femoral bone blood flow (Boelkins et al., 1973). We hypothesized that laying hens might reveal higher rates than non-laying hens due to the role of medullary bone in eggshell formation (Whitehead, 2004).

3.3. Methods
3.3.1 Animal preparation
Crossbreed ISA brown hens and roosters aged from 4 to 7 months old were used in this study. Animals were obtained under Animal Ethics Committee approval (S-2017-058). Chickens were divided into three groups: non-laying hens, laying hens and roosters. Each group has six replicates. Chickens were kept in a constant temperature room (25 °C) with a 16 h day and 8 h night cycle before operations. Hens that were sexually immature and had not developed any eggs in their reproductive organs were selected as non-laying hens, and usually they were not older than 19 weeks in our study. Hens that laid eggs regularly were selected as laying hens. All chickens had free access to water and calcium-rich food (layer's pellets).

3.3.2 Microsphere standard curve
Polystyrene, green fluorescent (excitation wavelength: 450 nm; emission wavelength: 480 nm), 15 μm microspheres (FluoSpheres, Thermo Fisher Scientific, Victoria, Australia) were used for determination of absolute cardiac output and femoral bone blood flow rate. Before using each microsphere vial for injections, six replicates of 10 μl and 100 μl of microsphere suspension were withdrawn from the vial using a precision 10 μl syringe (10R-RAX, P/N 002090, SGE Analytical Science Pty Ltd, New South Wales, Australia) and a 100 μl syringe (100F-GT, P/N 005200, SGE). 10 μl and 100 μl microsphere suspensions were then added into vials with 3.99 ml and 19.90 ml cellosolve acetate (2-Ethoxyethyl acetate, 98%, Sigma, cat. No. 109967-1L), respectively, in order to dissolve the microspheres and prepare standard solutions A and B for spectroscopy. Microsphere concentrations of solution A and B were 2500 ml^{-1} and 5000 ml^{-1}, respectively.

Standard solutions were then vortexed well and placed in darkness for 2 h. To produce fluorescence standard curves, five different volumes of solutions were withdrawn using pipettes from each standard solution vial A or B into individual 3-ml glass cuvettes, and cellosolve acetate was added into each cuvette to make up 3-ml solutions for fluorescence intensity analysis. Fluorescence intensities were analysed using a Cary Eclipse Fluorescence Spectrophotometer (Varian Australia Pty Ltd, Victoria, Australia) with an excitation wavelength of 450 nm and a slit width of 10 nm. Volumes withdrawn from solutions A and B are summarised in table 1. Producing microsphere fluorescence standard curves can, not only illustrate the relationship between the microsphere concentration and fluorescence intensity in a solution, but also test whether the relationship is linear, as a curvilinear relationship will be present if fluorescence intensity is too high (Serrat, 2009).

Table 1. Five withdrawal solution volumes obtained from solution A and B for producing fluorescence standard curve. The volume of added cellosolve acetate was based on the obtained volume from either solution A or B to make up a 3 ml solution in the cuvette for fluorescent analysis.

Volume from solution A (μl)	Volume from solution B (μl)	Volume of added cellosolve acetate (ml) (Solution A)	Volume of added cellosolve acetate (ml) (Solution B)	Estimated dissolved microspheres in the cuvette	Estimated concentration of microspheres in the cuvette (number of microspheres per ml)
0	0	3.00	3.00	0	0
40	20	2.96	2.98	100	33
100	50	2.90	2.95	250	83
200	100	2.80	2.90	500	167
300	150	2.70	2.85	750	250
350	175	2.65	2.825	875	292

Linear relationships were shown between fluorescent microsphere concentrations and fluorescence intensities, as all R^2 values are 0.99. Six standard curves of one of the microsphere vials are shown in Figure 1.
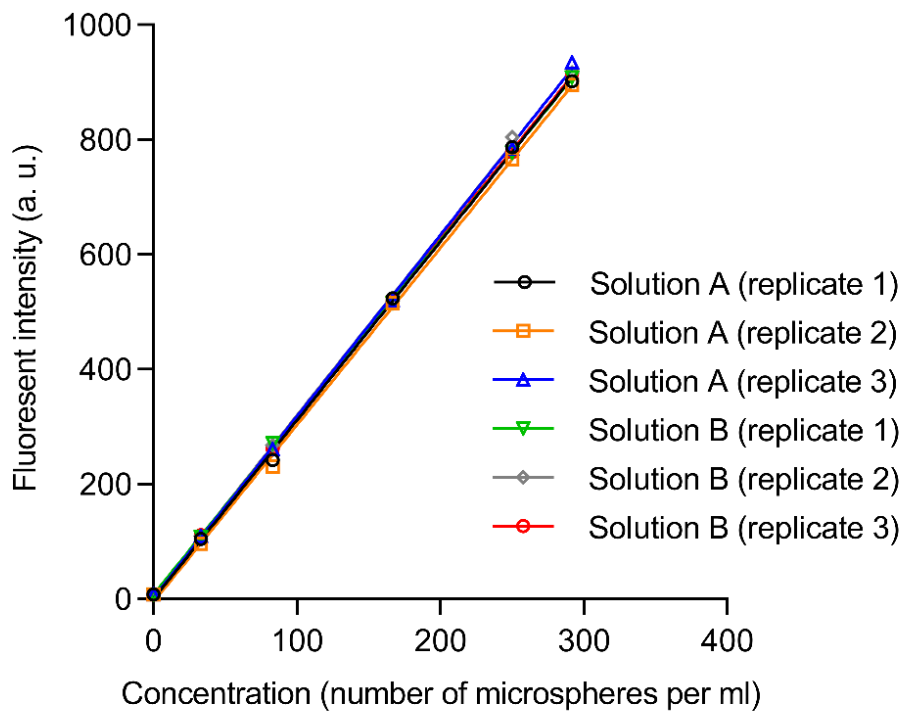
Figure 1. Relationship between microsphere concentrations and fluorescence intensities. Six lines represent six standard curves of one of the microsphere vials. Standard relationship averaged from six replicates is: Fluorescence intensity = $3.11 \times$ concentration + 2.51. (a. u.: arbitrary unit).

3.3.3 Procedures

A single use 2 ml plastic syringe with a cut-off 25 ga needle was prepared for microsphere injection. This syringe and the needle were weighed separately to 0.0001 g. A 2 ml glass syringe was filled with 1 ml heparinized saline (125 i.u. ml^{-1}) and placed on a syringe pump (Harvard Universal Infusion Pump, Harvard Apparatus, Holliston, Massachusetts, USA), modified to withdraw reference blood during the microsphere injection.

Before each operation, chickens were weighed to 1 g. Chickens were anesthetized with a combination of ketamine (40 mg kg^{-1}) and xylazine (4 mg kg^{-1}). Under anaesthesia, they were placed on their right side and were stabilized on a dissection table using a wooden frame with Velcro. Feathers at the left humerus (i.e. upper wing) region were plucked to expose the skin. Skin next to the wing brachial vein was removed. A scalpel was used to separate biceps and triceps next to the brachial vein to

expose the brachial artery underneath the muscles. The brachial artery was then isolated and blocked at the proximal region with a temporary ligature. The brachial artery was cannulated and sutured distal to the ligature and toward the heart using heparinized clear vinyl tubing (Cat. No. SV. 31, Dural Plastics & Engineering, NSW, AUS) (internal diameter: 0.5 mm; outer diameter: 0.8 mm) with a heparinized 25 ga needle connected to the end.

Right after the artery cannulation, a microsphere vial was vortexed for 10 s and sonicated for 4 min in an ultrasonic cleaner (Bransonic B-221, Branson Cleaning Equipment Company, Shelton, USA). During the sonication, feathers on the left chest region were plucked. The first three chest ribs were exposed by cutting into the left pectoralis major muscle. A self-retaining Weitlaner retractor was used to open the gap between second and third ribs to expose the pericardium. A heparinized 20 ga Venocan Pencil style IV catheter (Cat. No. 121931, Kruuse, Denmark) was inserted into the left ventricle and connected to a pressure transducer (P23Dc, Statham Instruments, Hato Rey, Puerto Rico) and amplifiers (Model 79D EEG, Grass Instruments, Quincy, Massachusetts, USA). The output of the equipment was recorded to computer with an analog-digital converter (DI-145) and software (WinDaq version 3.98) from DATAQ Instruments, Akron, Ohio, USA. As the catheter needle tip reached the left ventricle, blood pressure increased, and a typical left ventricular tracing wave was observed. Blood in the needle could be seen as bright red. Flow in the brachial artery was then restored at the proximal region by removing the ligature. More heparinized saline was injected into the brachial artery if blood did not flow out to the cannulated vinyl tubing because of blood blockage. The other end of the tubing with the 25 ga needle was then connected to the 2 ml glass syringe on the syringe pump. Blood was continuously withdrawn from the brachial artery from 30 s before microsphere injection until 2 min after it. The withdrawal rate was set at either 0.28 or 0.46 ml min^{-1}, depending on the size of the chicken. These rates were previously calibrated by weighing water drawn into the syringes in a given time. The microsphere suspension was removed from the sonicator, vortexed for 10 s, and 1.5 ml (~1.5×10^6 microspheres) was withdrawn into the preweighed 2 ml syringe. The syringe was weighed again to 0.0001 g, and the needle was removed for later weighing. The catheter needle was removed from the catheter inside the left ventricle, and 1.5 ml microsphere suspension was slowly injected into the heart in 15

s. The catheter was left in the heart to act as a plug. Chickens were sacrificed by injecting excessive anesthetic into the left ventricle through the catheter. To account for uninjected microspheres, the 2 ml plastic syringe were rinsed out with 2% Tween 80 into a 40 ml glass vial. Plastic syringes can cause microsphere loss due to attraction of the plastic microspheres and the plastic syringe. After injection, a visible microsphere rim can be observed on the plastic syringe wall. This number of microsphere loss is very small compared to the total injected number. Nevertheless, we still cut off the syringe tip with the rim and placed it into this vial. The needle with microspheres was weighed again and placed into another 4 ml glass vial to account for uninjected microspheres. The total injected microsphere number for each sample equals the number in the 1.5 ml suspension minus the uninjected numbers in both the plastic syringe and the needle.

3.3.4 Sample processing

Some of our processes referred to a recent protocol, which describes in detail a method to measure relative bone blood supply in mice with fluorescent microspheres (Serrat, 2009).

Reference withdrawal blood in the glass syringe was poured into a 100 ml glass bottle. The glass syringe was rinsed three times using about 20 ml 2% Tween 80, and all rinse liquid was poured into the 100 ml glass bottle. A further 2 ml of heparinized saline was added into the bottle to prevent blood from clotting. These samples were retained in the dark for fluorescence analysis.

Femora were harvested and muscles were removed. Spleen and kidneys of five laying hens were harvested and weighed to determine organ blood flows for comparisons with the literature. Nutrient foramen microphotographs were taken using a microscope set up. Fiji (Open Source, www.fiji.sc) was used to measure the foramen areas to calculate foramen radii. Methods that measure foramen size microphotographically were described in detail elsewhere (Hu et al., 2020). Femur lengths were measured with rulers to 1 mm. Because nutrient arteries mainly support femur shaft regions, nutrient foramen sizes may be more related to flow to the shaft region rather than the whole femur. Femora were therefore sectioned into three parts (Figure 2), with two ends and one shaft, as previously illustrated (Aref et al., 2017;

Colleran et al., 2000). We defined the lengths of the proximal and distal ends to be 25 % and 33 % of the total femur length. Bone marrow was retained in all sections. Each bone section was weighed to 0.001g and then placed into Cal-Ex decalcifying solution in the dark for 4–5 days, depending on the tissue size. After decalcification, bones were rinsed three times with phosphate buffered saline (PBS) and placed into 100 ml bottles. Freshly prepared 100 ml quantities of 2M ethanolic KOH with 2% Tween 80 was added into the bottles that contained reference withdrawal blood or decalcified tissues for tissue digestion. The bottles were placed on a swirling shaker (No. 436, Penetron Mark III, Sunkay Laboratories, Inc., Tokyo, Japan) in the dark for 2–3 days, depending on the tissue size. The tissue digestion process was complete when there were no large bone particles remaining in the bottles.
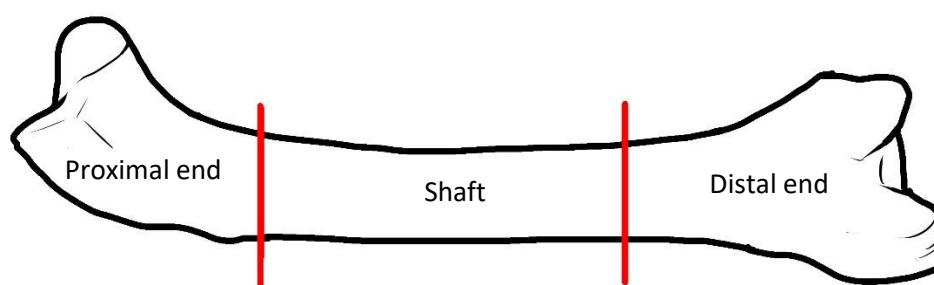
Figure 2. Three sections of a femur (proximal end, shaft and distal end).

3.3.5 Tissue and blood filtration and fluorescence intensity analysis
Digested tissues and blood were filtered using a glass vacuum filtration apparatus with glass microfiber 1.2 μm filter paper (Grade 333, 47 mm DIA, Filtech, NSW, AUS). During filtration, 2% Tween 80 was used to rinse the sample bottles three times and at least 100 ml potassium phosphate buffer rinse solution was used for the final rinse of the filtration unit and to adjust pH. After filtration, filter papers were moved into 70 ml, flat bottom vials (Diameter: 44; height: 57 mm). Polyethylene plungers were used to push the filter papers to the bottom of the vials and the plungers remained inside the vials. The vials were placed in dark before fluorescence intensity analysis. On the day of analysis, 12 ml cellosolve acetate was added into each vial to dissolve the microspheres and release fluorescent dye. Vials were vortexed well and placed in dark for 2–4 h before analysis. Three replicates of 3 ml solutions from each sample vial were pipetted into glass cuvettes for analysis. If the fluorescence intensity

was higher than the upper record limit of the spectrophotometer, the samples were quantitatively diluted with cellosolve acetate in the cuvette to make up 3 ml solutions. Uninjected microspheres in the injection syringe and needle were also dissolved and quantified using the spectrophotometer. Injected microspheres were calculated by subtracting the uninjected microspheres from the total number in 1.5 ml microsphere suspension.

3.3.6 Microsphere analysis

Standard relationships between microsphere concentrations and fluorescence intensities of each vial of microsphere suspensions were plotted on Figure 1 and linear equations $Y = ax + b$ were used to represent the relationships. R^2 was used to determine whether the relationships were linear. Since each microsphere vial produced six standard lines, the final standard curve of each vial had an intercept and a slope that were averaged from the six linear equations. We used 5 microspheres vials during the experiment and the 5 final standard curves are very similar to each other.

A pilot study was conducted to investigate whether our experimental setups would cause severe microsphere loss. Known numbers of microspheres were placed in different glass vials with either Cal-Ex or 2M ethanolic KOH solutions for 2–4 days, and the microspheres filtered and dissolved in cellosolve acetate solutions. The number of recovered microspheres were quantified. We found that almost all microspheres ($> 95\,\%$) can be successfully recovered. Based on the mean fluorescence standard curve, fluorescence intensities detected in different tissue samples and in reference withdrawal blood were converted to numbers of microspheres. Numbers of injected microspheres for each chicken were calculated and calibrated based on microsphere suspension density, the weight difference between the syringe and needle with and without microspheres and uninjected microspheres in the injection syringes and needles. Cardiac output form the left ventricle ($\dot{Q}_{lv}$, ml min^{-1}) of each chicken was calculated as: $\dot{Q}_{lv} = (\dot{V}_{with} \times N_{inj}) / N_{blood}$, where $\dot{V}_{with}$ is pump withdrawal rate (ml min^{-1}), N_{inj} is number of injected microspheres, and N_{blood} is the number of microspheres in the reference blood sample. Absolute blood flows ($\dot{Q}$, ml min^{-1}) to different tissues were calculated by the equation: $\dot{Q} = (V_{with} \times N_{tis}) / N_{blood}$, where N_{tis} is the number of microspheres recovered

from the target tissue. Femoral bone blood flows were averaged from both left and right femora for each individual chicken.

3.4. Statistical analysis

All error statistics refer to 95% confidence intervals (CI) calculated in Graphpad (Prism 6.0; GraphPad Software, La Jolla, CA, US).

Body masses of three chicken groups were compared using ANOVA, and Tukey's multiple comparisons test was used for comparing means between any two groups. Mass-specific cardiac output (ml min^{-1} kg^{-1}) and tissue blood flow rates (ml min^{-1} g^{-1}) were calculated by dividing the absolute blood flows by body mass (kg) and individual tissue mass (g), respectively. Mass-specific cardiac output and blood flow values are commonly used in literature. However, most biological factors scale with body mass in non-linear ways. Body mass should be considered as a biological factor in this study, as the chickens have a 2.5-fold body mass range. In this study, absolute blood flow to femoral bone scales with body mass (g) has a scaling exponent of 1.3 ± 0.93. (Figure S1). Therefore, to remove the influence of body mass and produce mass-independent data, cardiac output and blood flow values were calculated by dividing absolute blood flow rates by body mass (kg) to the 1.3 power. ANOVA with Tukey's multiple comparisons test was used to test whether there are significant differences in cardiac output and regional blood flow rates among three chicken groups. Percentages of blood flow that supply three femur regions were calculated compared to the whole femur. ROUT or Grubbs' method in Graphpad was used to detect any outliers.

3.4.1 Nutrient foramen size

Femoral bone blood flow index (Qi, mm^3) was previously calculated using an equation derived from Poiseuille's Law: $Qi = r^4/L$, where r (mm) is the foramen radius and L (mm) is an arbitrary length, measured as femur length (Allan et al., 2014; Hu et al., 2018; Seymour et al., 2012). It was assumed that Qi is proportional to blood flow rate. Qi in the femoral bone of cursorial birds scales with body mass to the 0.89 power (Allan et al., 2014). Any lengths in objects scale with their volumes (or masses) to the 0.33 power, if the shapes of the objects are the same. Assuming that Q_i is proportional to body mass to the 0.89 power, L to the 0.33 power, foramen radius should scale with body mass to the 0.305 power, and area to the (0.305 x 2 = 0.61).

The raw data were thus converted to mass-independent areas (mm^2 $kg^{-0.61}$) and radii (mm $kg^{-0.305}$) for analysis. To compare foramen sizes among three groups, mass-independent foramen areas (mm^2 $kg^{-0.61}$) and radii (mm $kg^{-0.305}$) were calculated and compared using ANOVA. If ANOVA showed a significant difference among groups, Tukey's multiple comparisons test was used for comparing means between two groups. To compare Qi between chickens and other cursorial birds interspecifically, nutrient foramen sizes of adult chickens were required. However, some of our chickens were not mature enough to be considered as adults, especially non-laying hens. To compare Qi more precisely, average Qi of chickens were calculated only from laying hens and roosters, as they could be considered as adults.

No studies have used mass-independent cardiac output or blood flow values, and we need to compare our data with literature values. To present and compare our data clearly, and to avoid confusion, only mass-specific cardiac output and blood flow values are presented in the results and discussion sections. However, mass-independent foramen size values remain in the results and discussion, as no comparisons of the size of the nutrient foramen in chickens are available from literature. Information on mass-independent cardiac and blood flow values are presented in the supplementary information.

3.5. Results

Fluorescent microsphere concentrations had a linear relationship with fluorescence intensities, as $R^2 = 0.99$ for all replicates. Fluorescence intensities of all tissues and blood samples analysed in this study were within the fluorescence intensity range of the standard curves presented in Figure 1.

A total of 18 chickens were used successfully for the fluorescent microsphere experiment. Body mass of the chickens ranged from 1.1 to 2.7 kg, and the mean body mass was 1.7 ± 0.22 kg. Body mass was significantly different among three groups (P = 0.0036) with non-laying hen body mass (1.2 ± 0.11 kg) being significantly lower than laying hens (1.8 ± 0.20 kg) (P = 0.026) and roosters (2.0 ± 0.54 kg) (P = 0.0035). The mean and 95% confidence intervals of body-mass-specific cardiac output of three chicken groups was 338 ± 38 ml min^{-1} kg^{-1}. ANOVA showed no significant differences in mass-specific cardiac output among three groups (P = 0.90). All mass-

specific rates of blood flow (ml min^{-1} g^{-1}) were calculated by dividing the absolute rates by individual tissue mass (g). Average spleen and kidney masses of five laying hens were 1.8 ± 0.4 and 10.7 ± 2.9 g, respectively. Data collected incidentally showed that the spleen of laying hens received 1.6 ± 1.0 % of cardiac output and required 5.6 ± 5.3 ml min^{-1} g^{-1} of mass-specific blood flow. The kidneys received 4.2 ± 1.0 % of cardiac output and required 2.4 ± 1.4 ml min^{-1} g^{-1} of mass-specific blood flow.

Laying hens had significantly higher mass-specific blood flows in femoral bone and higher mass-specific blood flows in shaft bone than the non-laying hens (P = 0.024 and P = 0.0053, respectively) (Figure 3A & B). Femoral and regional femoral bone blood flows between the non-laying hens and roosters were not significantly different from each other (Table 1). Mass-independent cardiac output, femoral bone blood flow and shaft blood flow rate values compared among three chicken showed results similar to the mass-specific value comparisons (supplementary information).

One extra laying hen was measured in this study, as the femur blood flow datum of one of the original six laying hens was identified as an extreme outlier. All of the data analysed above did not include the outlier value. Estimated mass-specific blood flow rates in the femoral bone of this chicken was 1.3 ml min^{-1} g^{-1}. This value is 5.7-fold higher than the mean of 0.23 ml min^{-1} g^{-1} for layers (Table 1). There were no significant differences in regional bone blood flows between both legs of this sample. Despite the extremely high femoral bone blood flow, values of foramen sizes, femur mass, femur length and cardiac output of this chicken were not significantly different from other specimens. The unusual high blood flow values may have been due to unknown experimental error, and it is very unlikely that these values are the actual blood flow rates of a laying hen.
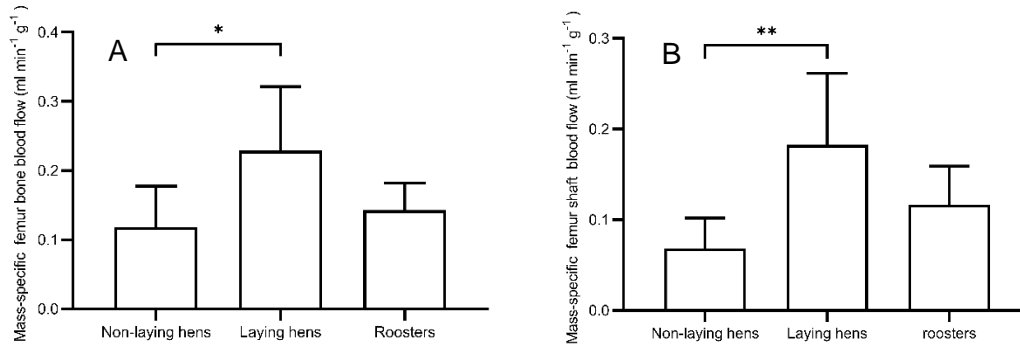
Figure 3. Mass-specific blood flow rates to the entire femur (A) and to the femur shaft (B) among non-laying hens, laying hens and roosters. Error bars represent 95% confidence interval of the means of 6 replicates. (*: P ≤ 0.05; **: P ≤ 0.01).

Table 1. Mean and 95% confidence intervals of femoral bone blood flow rates and regional femoral bone blood flow of non-laying hens, laying hens and roosters. Mass-specific blood flow rate is the blood flow rate per gram of the bone tissue. All data are averaged from both left and right femora from 6 chickens.

	Tissue wet weight (g)	Absolute blood flow rate (ml min^{-1})	Mass-specific blood flow rate (ml min^{-1} g^{-1})	Proportion of cardiac output (%)
Non-laying hens				
Average femur	8.76 ± 0.66	1.05 ± 0.55	0.12 ± 0.06	0.26 ± 0.13
Femur proximal end	2.78 ± 0.25	0.38 ± 0.20	0.13 ± 0.07	0.09 ± 0.05
Femur shaft	2.28 ± 0.22	0.16 ± 0.08	0.07 ± 0.03	0.04 ± 0.02
Femur distal end	3.69 ± 0.25	0.51 ± 0.28	0.14 ± 0.07	0.13 ± 0.07
Laying hens				
Average femur	10.07 ± 0.74	2.29 ± 0.93	0.23 ± 0.09	0.39 ± 0.07
Femur proximal end	3.24 ± 0.29	0.70 ± 0.31	0.22 ± 0.10	0.12 ± 0.03
Femur shaft	2.61 ± 0.24	0.47 ± 0.20	0.18 ± 0.08	0.08 ± 0.02
Femur distal end	4.22 ± 0.33	1.11 ± 0.46	0.27 ± 0.11	0.19 ± 0.04
Roosters				
Average femur	13.89 ± 3.34	1.91 ± 0.35	0.14 ± 0.04	0.30 ± 0.06
Femur proximal end	4.42 ± 1.12	0.61 ± 0.13	0.14 ± 0.04	0.10 ± 0.03
Femur shaft	3.61 ± 0.84	0.41 ± 0.14	0.12 ± 0.04	0.06 ± 0.01
Femur distal end	5.87 ± 1.47	0.90 ± 0.21	0.16 ± 0.04	0.14 ± 0.03

On average, the two femora received 0.63 ± 0.10 % cardiac output of all chickens. Within the average femur of six young chickens, the proximal end received 35.7 ± 1.6 %, the shaft $15.7 \pm 2.7\%$ and the distal end 48.6 ± 3.2 % of total blood flow. Laying hens received $30.5 \pm 4.8\%$, 20.9 ± 3.4 % and $48.6\% \pm 5.5\%$, respectively and roosters received $31.7 \pm 4.6\%$, $21.1\% \pm 5.8\%$ and $47.1 \pm 6.4\%$ respectively (Figure 4).

Non-laying hens	35.7%	15.7%	48.6%
Laying hens	30.5%	20.9%	48.6%
Roosters	31.7%	21.1%	47.1%
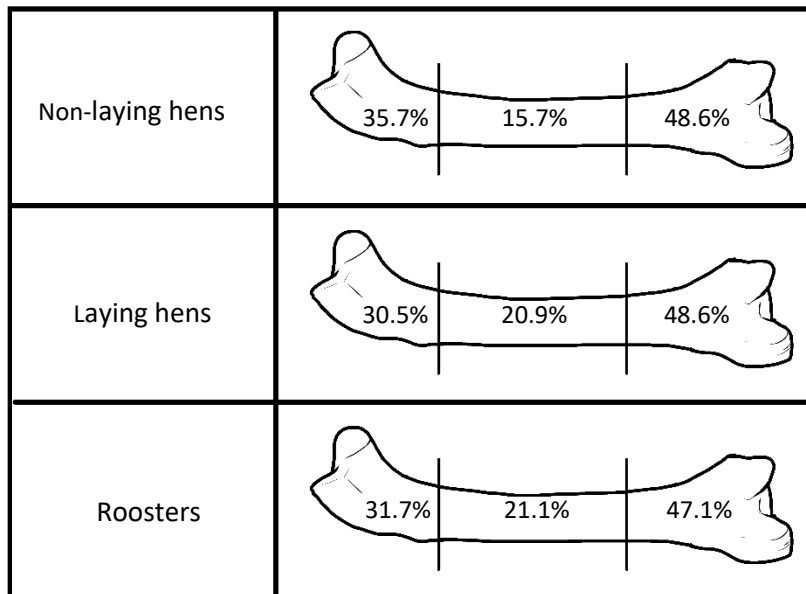
Figure 4. Distribution of fluorescent microspheres captured within femora among non-laying hens, laying hens and roosters. The three sections from the left to the right are femur proximal end, shaft and distal end. All data were averaged from left and right femora of 6 replicates.

Mean foramen radius was 0.33 mm, and foramen area was 0.36 mm^2 in 12 adult chickens (laying hens and roosters). Average femoral bone blood flow index of adult chickens was 1.50×10^{-4} mm^3. Mean foramen area of non-laying hens, laying hens and roosters was 0.36 ± 0.09, 0.27 ± 0.07 and 0.45 ± 0.08 mm^2, respectively. Mean foramen radius of all three groups was 0.34 ± 0.04, 0.29 ± 0.04 and 0.38 ± 0.03 mm, respectively. Laying hens had significantly smaller nutrient foramen sizes than the roosters (Area: $P = 0.003$; Radius: $P = 0.003$), but foramen sizes were not significantly different between laying hens and non-laying hens (Area: $P = 0.13$; Radius: $P = 0.10$) or between non-laying hens and roosters (Area: $P = 0.16$; Radius: $P = 0.20$). (Figure 5A & B).
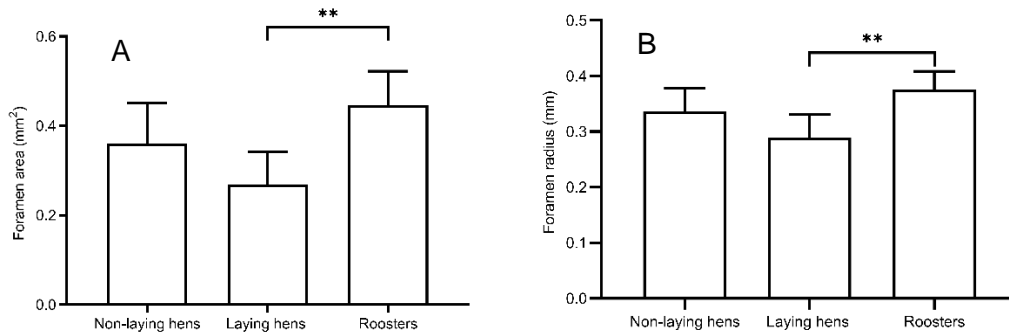
Figure 5. Nutrient foramen areas (A) and radii (B) of non-laying hens, laying hens and roosters. Error bars represent 95% confidence interval of the means of 6 replicates. (**: P ≤ 0.01).

Laying hens had significantly smaller mass-independent areas and radii of nutrient foramina than the non-laying hens (Area: P = 0.0058; Radius: P = 0.0039) and roosters (Area: P = 0.014; Radius: P = 0.0081), while no significant differences in mass-independent foramen area or radius were observed between the non-laying hens and roosters (Figure 6A & B).
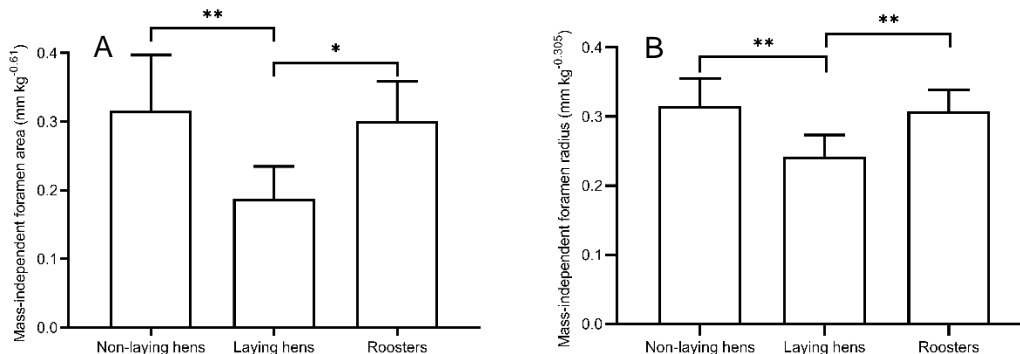
Figure 6. Mass-independent nutrient foramen areas (A) and radii (B) of non-laying hens, laying hens and roosters. Error bars represent 95% confidence interval of the means of 6 replicates.

3.6. Discussion

3.6.1 Relating nutrient foramen size with femoral bone blood flow

Despite the microsphere experiment showing that laying hens have higher blood flow rates of femoral bone and higher blood flow rates of femur shaft than the non-laying hens, laying hens have relatively smaller mass-independent foramen sizes than the non-laying hens (Fig. 6). No significant differences in foramen sizes occur between non-laying hens and roosters. We expected that the higher femoral bone blood flows in laying hens would correlate with larger, rather than smaller foramen sizes. There is no correlation between nutrient foramen radius and femoral bone blood flow, as the slope is not significantly different from zero (slope = -1.17 ± 1.66) (Figure 7).
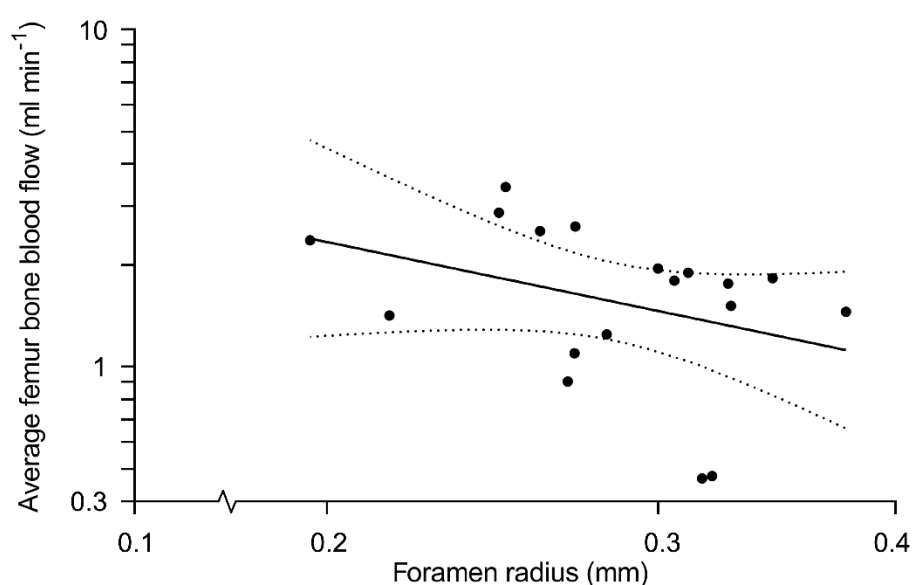

Figure 7. Relationship between femoral nutrient artery radius (mm) and femoral bone blood flow (ml min^{-1}) in 18 chickens. Femoral bone blood flow = 0.36 × nutrient foramen radius$^{-1.2 \pm 1.7}$. The dotted lines represent 95% confidence interval for regression mean. Data are plotted on logarithmic scales.

All previous foramen studies are based on an assumption that the foramen size is proportional to the occupying artery size, which represents the amount of supplying blood flow. The mass-independent foramen radius of laying hens is smaller than the non-laying hens, which results in a lower estimated blood flow index (*Qi*). Previous foramen studies also assumed the size ratio between the foramen and artery remains constant interspecifically and intraspecifically. It could be possible that the size ratio

between the foramen and occupying vessels may differ at different life stages across growth. Moreover, the 18 chicken samples in this study cover a body mass range of 1.1–2.7 kg. This is only a 2.5-fold range and is likely the main reason why we cannot find a correlation between the foramen sizes and femoral bone blood flow rates, because allometric studies generally require body mass ranges of 100-fold or more. For example, Q_i of 100 species of adult birds varied over 10-fold at any given body mass, and required a body mass range of over 10-fold to reveal a significant positive relationship (Allan et al., 2014).

Chicken femoral bone Q_i was estimated based on both laying hens and roosters, and the mean value is 1.50×10^{-4} mm^3. Laying hens and roosters are nominally classified as "adults" in order to estimate Q_i in this study for data comparison. Non-laying hens are excluded because of their relatively higher growth rate and larger mass-independent foramen sizes (Figure 6). It should be pointed out that the "adults" in this study were actually still growing, therefore the chicken Q_i is higher than other species (Figure 8).
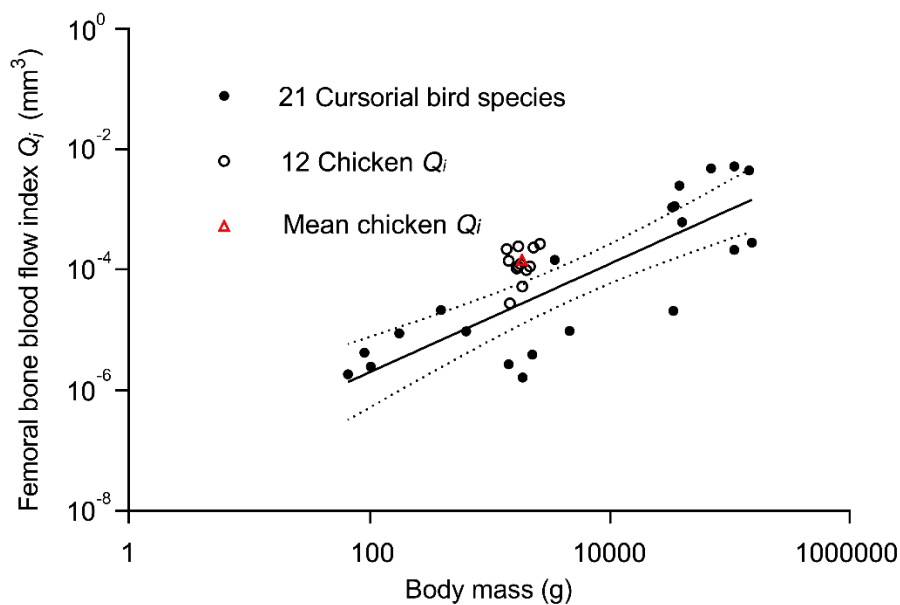
Figure 8. Scaling of femoral bone blood flow index (Q_i, mm^3) on body mass (M_b, g) of 22 cursorial birds including chickens. Solid circles represent mean Q_i values of 21 cursorial bird species. Open circles present individual Q_i value of 12 adult chickens in this study, and the red triangle represents the mean Q_i of these 12 data points. The equation of the regression is $Q_i = 3.2 \times 10^{-8} M_b^{0.90 \pm 0.29}$, and it includes the

single mean value for chickens (red triangle). The dotted lines represent 95% confidence interval for regression mean. Data other than chicken are collected from Allan et al. (2014).

The regression presented in Figure 8 includes the average mean of chicken Q_i, and the Q_i exponent (0.90 ± 0.29) is significantly higher than zero. Average absolute blood flow of femoral bone estimated from both laying hens and roosters is 2.1 ± 0.42 ml min^{-1}. At this stage, we only have this one femoral bone blood flow value from a cursorial bird. However, we can use this value to predict the absolute rate of blood flow in the femoral bone of other cursorial birds from femoral bone blood flow index values by using a simple ratio of absolute flow rate (ml min^{-1}) and Qi (mm^3), the units becoming ml min^{-1} mm^{-3}. This ratio is a constant number (13998 ml min^{-1} mm^{-3}), therefore the scaling of predicted absolute blood flow in the femoral bone of cursorial bird on body mass has the same exponent of 0.90 ± 0.29. The scaling of absolute blood flow in the femoral bone of cursorial bird matches their maximum metabolic rate measured during treadmill exercise, which relates to their locomotor activity levels (Allan et al., 2014). The absolute blood flows of cursorial birds are predicted only based on the relationship between chicken femoral bone blood flow and femoral bone Qi, and this prediction assumes that the conversion ratio is constant across species. However, this relationship may not be constant interspecifically or intraspecifically. Future studies are thus required to get insight into the blood flow and blood flow index relationship of other bird species. If the relationship becomes clear, it is possible to estimate absolute blood flow in the femoral bone of ancient species, such as dinosaurs and archosaurs.

3.6.2 Chicken cardiac output

Average cardiac output of three chicken groups is 337.8 ± 38.0 ml min^{-1} kg^{-1}. There were no significant differences in mass-specific cardiac output among three chicken groups. Cardiac output of our roosters (337.9 ± 39.7 ml min^{-1} kg^{-1}) is significantly higher than the 150.4 ± 28 ml min^{-1} kg^{-1} measured using radioactive microspheres in adult roosters under local anaesthesia (Merrill et al., 1981). Cardiac output of our laying hens (327.2 ± 104.7 ml min^{-1} kg^{-1}) is also significantly higher than the 177 ± 11 ml min^{-1} kg^{-1} and the 218 ml min^{-1} kg^{-1} reported by Boelkins et al. (1973) and Sapirstein and Hartman (1959) using an indicator dilution technique in adult laying

hens. However, Boelkins et al. (1973) used two different dyes to measure cardiac output, and the 277 ± 16 ml min^{-1} kg^{-1} measured using Evans Blue dye is not significantly different from our value. Therefore, methodological differences may cause a wide range of cardiac output values. Interspecifically, the scaling of cardiac output on bird body mass is $CO = 290.7M^{0.69}$, where CO is cardiac output (ml min^{-1}), and M is body mass (kg) (Grubb, 1983). Grubb's cardiac output values were collected by measuring arteriovenous oxygen content difference and oxygen consumption rate (Fick Principle) under local anaesthesia. According to the equation, chicken cardiac output is calculated to be 241.4 (ml min^{-1} kg^{-1}) using our average chicken body mass (1.82 kg). This estimated cardiac output value is significantly lower than our calculated cardiac output, and significantly higher than all the literature values of laying hens described above.

It is not clear why mass-specific cardiac output was somewhat high in this study, but it may be related to the fact that previous studies involve larger, older chickens in which cardiac output would be expected to be lower (Grubb, 1983). Body-mass-specific cardiac output of broilers was found to decrease as age increases from 4 to 6 weeks (Wideman, 1999). The experimental treatment may also be involved. Anesthetics can affect animal heart rates and cardiac output, although the impacts on birds are not fully understood. Ketamine alone can retain or increase heart rate in birds while Xylazine alone can reduce heart rate, respiration rate and may cause hypoxemia, hypercarbia and death in birds (Abou-Madi, 2001). Xylazine alone has been found to reduce respiration rate in chickens (Varner et al., 2004). Ketamine/xylazine combination has been widely used to anesthetize animals including birds, as xylazine well relaxes muscles along with ketamine (Abou-Madi, 2001). However, the ketamine/xylazine combination still has side effects. For example, lower doses of the combination (Ketamine: 15 mg kg^{-1}; Xylazine: 0.15 mg kg^{-1}) can reduce heart rate of great horned owl (Raffe et al., 1993).

3.6.3 Absolute rate of blood flow in the chicken femoral bone

The percentages of blood flow to three femoral regions in chickens (Fig. 4) are similar to the blood flow proportions in rats (Aref et al., 2017), with two ends receiving more blood flow than the shaft. Mass-specific blood flow in the femoral bone of laying hens is 0.23 ± 0.09 ml min^{-1} g^{-1}, which is much lower than the 0.77 ± 0.09 ml min^{-1} g^{-1}

measured using radioactive microspheres in laying hens (Boelkins et al., 1973). Despite this difference, spleen and kidneys of our laying hens received 5.6 ± 5.3 ml min^{-1} g^{-1} and 2.4 ± 1.4 ml min^{-1} g^{-1} of mass-specific blood flow, which are not significantly different from the 4.81 ± 0.95 ml min^{-1} g^{-1} and 2.48 ± 0.26 ml min^{-1} g^{-1} reported by Boelkins et al. (1973). Mass-specific blood flow rates in the femoral bone of non-laying hens (0.12 ± 0.06 ml min^{-1} g^{-1}) and roosters (0.14 ± 0.04 ml min^{-1} g^{-1}) are not significantly different from the 0.13–0.15 ml min^{-1} g^{-1} measured in rabbit femora using both radioactive and fluorescent microspheres (Anetzberger et al., 2004a). Mass-specific flow rates in proximal end, shaft and distal end of rabbit femora are approximately 0.16–0.17 ml min^{-1} g^{-1}, 0.15 ml min^{-1} g^{-1} and 0.11–0.12 ml min^{-1} g^{-1}, respectively (Anetzberger et al., 2004a), and are not significantly different from most of our regional femoral bone blood flow values in chickens, the shaft in non-laying hens and the distal ends in roosters, being exceptions (Table 1).

Blood flow rates can roughly estimate metabolic rates of the supplied tissues. The haemoglobin content of chicken blood is about 0.18 g ml^{-1} (Elagib and Ahmed, 2011). Assuming each gram of haemoglobin carries 1.34 ml of oxygen (Bunsen coefficient), and assuming half of oxygen is consumed by bone tissue, every milliliter of blood then supplies $(1.34 \times 0.18) / 2 = 0.12$ ml of oxygen to the bone tissue. Mean absolute femur bone blood flow rate is 1.75 ml min^{-1} and femur mass is 10.9 g. Therefore, the femur metabolic rate is estimated to be $(0.12 \times 1.75) / 10.9 = 0.019$ ml min^{-1} g^{-1}. This about twice the metabolic rate (0.0095 ml min^{-1} g^{-1}) of adult guinea pig calvarial bone (Schirrmacher et al., 1997), but is expected given that the chickens were measured *in vivo* at body temperature and the guinea pig bone measured *in vitro* at room temperature. We are unaware of any other estimates of avian bone metabolic rate.

Laying hens have significantly higher mass-specific femoral bone blood flow and femur shaft blood flow rates than the non-laying hens. Femoral bone blood flows of roosters are not significantly different from non-laying hens and laying hens, suggesting gender alone does not affect femoral bone blood flow in chickens around the onset of sexual maturity. However, egg production in laying hens may also affect bone perfusion. The mean mass-specific blood flow rate of femoral bone is approximately 1.9 times higher, and femur shaft blood flow rate is 2.7 times higher, in laying hens than in non-laying hens (Fig. 3). The major cause of this blood flow

difference may relate to calcium homeostasis. Laying hens may require extra blood flow to transport calcium from their bone reserves to form eggshells. As hens reach sexual maturity, osteoblasts in chicken leg bones start to form medullary bone, which is a special bone type that exists only in birds and crocodilians, and it acts as a labile calcium reserve for eggshell formation (Whitehead, 2004). During egg production, calcium can be removed and regained rapidly in medullary bones. To maintain calcium balance, laying hens need to consume a great amount of calcium from their diet. During the daytime when chickens are active, calcium from their diet is absorbed from intestines and used for eggshell formation and stored in bone. Almost no calcium is left in intestines 6 to 10 h after feeding (Bar, 2009). Eggshell formation of laying hens is high during the night, and therefore calcium is obtained from bone. The calcium loss in bones can then be regained the next day when layers absorb calcium from their food source (Bar, 2009). Laying hens need to use 2.2 g of calcium, which represents about 10% of total body calcium volume, for daily egg production (Bar, 2009; Bouvarel et al., 2011). Almost all this calcium goes into eggshell, as egg yolk only contains negligible amount of calcium (Etches, 1987). The 2.2 g eggshell calcium mostly comes directly from the food source, but 20–40% comes from bone (Bar, 2009). Therefore, laying hens need to export about 0.44–0.88 g calcium from their skeleton in every laying cycle. Medullary bones are capable of being absorbed and renewed rapidly (Bain et al., 2016), and is capable of metabolizing at a much higher rate than the cortical bones and femur ends (Hurwitz, 1965). Therefore, most bone-sourced eggshell calcium is from medullary bones. Hurwitz (1965) fed laying hens using Ca^{45}-labeled diet, and he found that calcium turnover rate of medullary bone is about 10 times higher than cortical bones. Moreover, he discovered that about 70% calcium in femur and tibia medullary segments were renewed within a 12-day period in laying hens. The high calcium turnover rate of medullary bone is associated with its structure, which is very different from cortical bone. Medullary bone has a lower mineral concentration, lower mineral crystallinity, and has thinner, shorter and less organized mineral particles (Kerschnitzki et al., 2014; Nys and Le Roy, 2018). Bone density and calcium content also change in pregnant and lactating human females. For example, bone mass density decreased by about 2 % in lumbar spine from prepregnancy to postpartum, and the decrease of bone mass density in total hip bones during this period was about 3.6 % (Black et al., 2000). 200 mg of calcium is delivered in the maternal milk during lactation, and the total loss of bone mass (5–

10 %) in women may result in increased risk of bone fracture (Salles, 2016). It may be possible to relate the change of bone blood flow to the change of bone metabolism and bone health during pregnancy and lactation in future studies, as no studies have investigated the relationships so far.

Femoral nutrient foramen sizes in relation to femoral bone blood flow were previously correlated with bone growth in growing animals. Intraspecifically, growing animals may require higher blood flow to supply their femora, as femoral nutrient foramen sizes of in-pouch kangaroo joeys are many-fold larger than the adult marsupial species of similar body mass (Hu et al., 2018). Long bones of younger mammals have higher relative blood flow rates than in older ones (Nakano et al., 1986; Pasternak et al., 1966; Whiteside et al., 1977), also revealing the long bones require more energy during growth. All chickens in our study were still growing to some extent, so they may have been influenced by elevated bone perfusion for growth. Younger non-laying hens tend to have relatively larger mass-independent foramen sizes than older laying hens (Figure 6). Although the chickens in this study were selected to have similar age around the onset of sexual maturity, in order to avoid bone growth differences among groups, the ages among three chicken groups were still slightly different and were all much younger than the chickens studied previously. Age and body mass differences still play a part in influencing the blood flow comparisons in this study.

Femora are responsible for absorbing stresses from weight-bearing and locomotion. The microfractures on bones caused by the stresses can be fixed by energy-driven Haversian remodelling (Lieberman et al., 2003). Femoral bone blood flow is therefore also related to locomotor activity levels in adult terrestrial vertebrates. Interspecifically, terrestrial vertebrates with higher maximum metabolic rates and higher activity levels tend to have relatively larger femoral nutrient foramen sizes (Allan et al., 2014; Seymour et al., 2012). The femoral bone perfusion rates between the non-laying hens and roosters are not significantly different. It probably suggests that they have no great difference in locomotion intensity, without considering the minor effects of calcium mobilization and growth rate differences between the two groups. The higher perfusion rates in chicken femur ends than the shaft may relate to higher oxygen demand in these regions. Femur ends include both metaphyses and

epiphyses, which are supplied by a great number of arteries. Some foramina at the ends are larger than the shaft nutrient foramen (Brookes and Revell, 1998), suggesting long bone ends contain larger arteries and thus require higher blood flow rates. The femur ends may require more energy for undergoing the remodelling process than the shaft, as they locate near the joints and experience more intense stress during daily activity. Additionally, as our chickens were still growing, and the femur ends may have higher growth rates than the shaft, as the secondary ossification centre locates at the ends of long bones (Brookes and Revell, 1998). The femoral bone perfusion rates of all three chicken groups may all relate to metabolic rate of bone growth and remodelling, and the extra cost of calcium mobilization may account for the increase in femoral bone perfusion and metabolic rate of laying hens.

In summary, laying hens have higher mass-specific blood flow rate to femoral bone shaft than the non-laying hens, probably associated with augmented calcium mobilization during eggshell production. Bone growth and remodelling may have impacts on chicken regional femoral bone flow rates. Femoral bone blood flows are similar in non-laying hens and roosters of similar age around the onset of sexual maturity. The current study is the first to get insight into the relationship between absolute femoral bone flow rates and blood flow index estimated from nutrient foramen sizes in birds. No relationship was found between blood flow rate to the femur bone shaft and nutrient foramen sizes in hens, despite significant differences in blood flow rate. Further research on relationships among absolute blood flow, foramen sizes and sizes of the occupying vessels are required in the future.

3.7. Acknowledgements

3.8. Supplementary material

Most blood flow studies present cardiac output and blood flow rates as mass-specific values. We calculated mass-specific cardiac output and mass-specific blood flow rates to compare our data with literature data. However, most biological factors are related to body size in non-linear ways and are rarely proportional. Therefore mass-specific values do not remove the correlation with body mass and they may not be very accurate to compare biological factors among species or within species (Packard and Boardman, 1999). Body mass of three chicken groups in this study ranges from 1.1 to 2.7 kg, which represents a 2.5-fold range in body mass. To make biological factors be more comparable among specimens, mass-independent values were also calculated in this study. Absolute blood flow in femoral bone scales with body mass has a scaling exponent of 1.3 ± 0.93. (Figure S1). Mass-independent cardiac output and blood flow values were calculated by dividing absolute blood flow rates by body mass to the 1.3 power. The mean and 95% confidence intervals of mass-independent cardiac output of three chicken groups is 294.8 ± 39.0 ml min^{-1} kg$^{-1.3}$. ANOVA shows no significant differences in mass-specific ($P = 0.90$) and mass-independent ($P = 0.48$) cardiac output among three groups. Mass-independent blood flow rates in femoral bone are not significantly different among three chicken groups ($P = 0.29$), but laying hens have significantly higher mass-independent blood flow rates in shaft bone than the non-laying hens ($P = 0.04$) (Figure S2A & B).
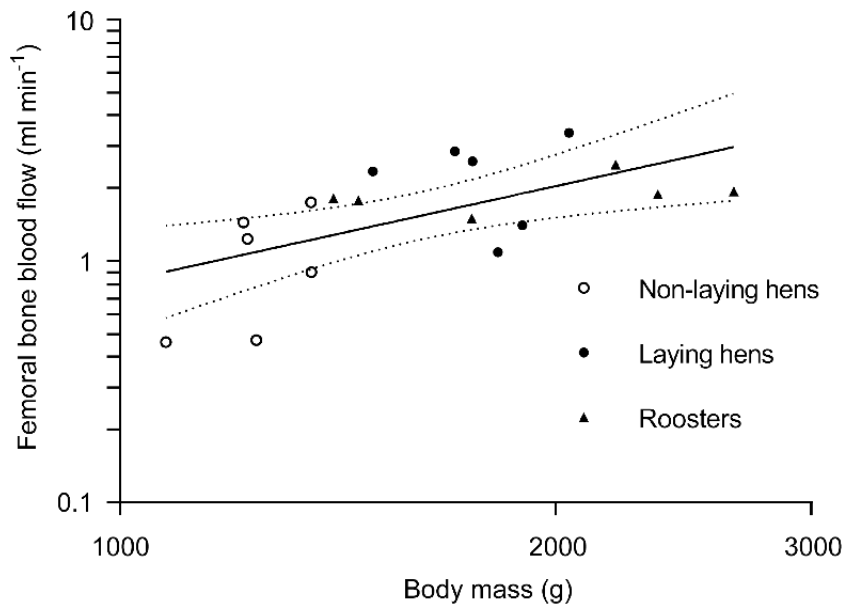
Figure S1. Relationship between log femoral bone blood flow rate ($\dot{Q}$, ml min⁻¹) and log chicken body mass (M_b, g). Three different symbols represent three different chicken groups. The equation set to all groups is $\dot{Q} = 9.1 \times 10^{-5} M_b^{1.3\pm0.93}$. Dashed lines represent the 95% confidence interval for the regression mean.
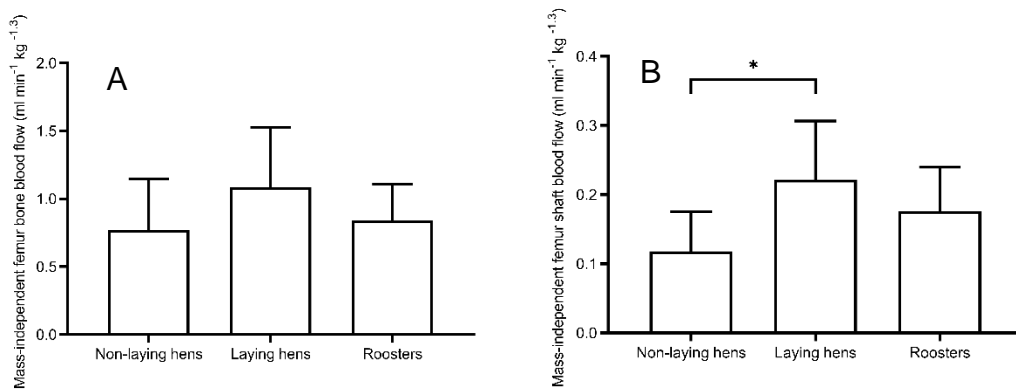
Figure S2. Mass-independent blood flows in femoral bone (A) and femur shaft (B) among non-laying hens, laying hens and roosters. Error bars represent 95% confidence interval of the means. (*: $P \leq 0.05$).

Mass-independent blood flow in femoral bone of laying hens is 1.08 ± 0.44 ml min⁻¹ g⁻¹·³. The mean mass-independent blood flow in femoral bone of laying hens is approximately 1.4 times higher than the non-laying hens, and the mean femur shaft

blood flow is 1.8 times higher. Mass-independent blood flow rates of each femur section among three chicken groups were calculated and summarized in Table S1.

Table S1. Average and 95% confidence intervals of mass-independent blood flows in femoral bone and regional femoral bone of non-laying hens, laying hens and roosters. All data are averaged from both left and right femora

	Mass-independent blood flow rate (ml min^{-1} kg$^{-1.3}$)
Non-laying hens	
Average femur	0.77 ± 0.38
Femur proximal end	0.28 ± 0.14
Femur shaft	0.12 ± 0.06
Femur distal end	0.38 ± 0.19
Laying hens	
Average femur	1.08 ± 0.44
Femur proximal end	0.33 ± 0.14
Femur shaft	0.22 ± 0.08
Femur distal end	0.53 ± 0.24
Roosters	
Average femur	0.84 ± 0.27
Femur proximal end	0.27 ± 0.12
Femur shaft	0.18 ± 0.06
Femur distal end	0.39 ± 0.11

Chapter Four: Chicken femoral nutrient foramen and artery morphologies in relation to nutrient artery blood flow rates

Statement of Authorship

Title of Paper	Chicken femoral nutrient foramen and artery morphologies in relation to nutrient artery blood flow rates
Publication Status	Unpublished and Unsubmitted work written in manuscript style
Publication Details	

Principal Author

Name of Principal Author (Candidate)	Qiaohui Hu		
Contribution to the Paper	Conducted experiments, analysed data, wrote the initial manuscript draft, and reviewed and edited subsequent drafts.		
Overall percentage (%)	60%		
Certification:	This paper reports on original research I conducted during the period of my Higher Degree by Research candidature and is not subject to any obligations or contractual agreements with a third party that would constrain its inclusion in this thesis. I am the primary author of this paper.		
Signature		Date	1/11/2020

Co-Author Contributions

By signing the Statement of Authorship, each author certifies that:

i. the candidate's stated contribution to the publication is accurate (as detailed above);

ii. permission is granted for the candidate in include the publication in the thesis; and

iii. the sum of all co-author contributions is equal to 100% less the candidate's stated contribution.

Name of Co-Author	Thomas J. Nelson		
Contribution to the Paper 25%	Assisted in the experiments, helped with data collection and literature research, reviewed manuscript drafts.		
Signature		Date	9/11/2020

Name of Co-Author	Roger S. Seymour		
Contribution to the Paper 15%	Provided advice, guidance on experiments, reviewed and edited manuscript drafts.		
Signature		Date	20/11/2020

4.1. Abstract

Femoral bone blood flow rates estimated from nutrient foramen sizes were previously not absolute, but only a blood flow index (Q_i), because the size relationship between the foramen and the occupying artery is unknown. Injected contrast medium has been used to reveal morphological structures of an animal's vascular network. The current study used vascular contrast and micro-computerized tomographic scanning to investigate femoral nutrient foramen and nutrient artery sizes in three groups of chickens (non-laying hens, laying hens and roosters). The results indicated that the nutrient artery lumen cross-section occupies approximately 23.0 ± 3.8 % of the nutrient foramen area. This ratio is about 20 ± 3.2 % for femora with only one foramen. Histological embedding and sectioning along with vascular contrast imaging were used to explore vessel locations inside nutrient foramina. Nutrient foramen morphologies and nutrient artery locations can be very different among femora with more than one nutrient foramen. Vascular contrast imaging is capable of estimating blood flow rates through nutrient arteries, because blood flow rates estimated from artery lumen casts are similar to flow rates measured by infusion of fluorescent labelled microspheres. Laying hens tend to have higher nutrient artery perfusion rates than the non-laying hens, probably due to extra calcium requirements for eggshell production, although the difference was not statistically significant.

4.2. Introduction

Mechanical forces created by blood flow demands determine blood vessel structure. As blood flows through a vessel, it creates a tangential force called shear stress, and blood pressure creates a perpendicular force called circumferential stretch to the vessel wall (Jones et al., 2006). The forces acting on vessel wall control artery sizes and maintain physiological functions of the arteries (Lu and Kassab, 2011). Blood vessel sizes thus reflect regional blood flow rates, which are determined by oxygen requirements of local organs (Wolff, 2008). Nutrient arteries contribute 50–70% blood flow to the long bones (Trueta, 1963), which are responsible for absorbing loading stresses from locomotion and for calcium balance. A nutrient artery enters a femur shaft through a hole called the nutrient foramen, usually along with a vein (Currey, 2002; Singh et al., 1991). Foramen sizes should correlate with blood vessel sizes. Femoral bone blood flow is related to locomotor activity levels in mature terrestrial vertebrates, as relatively larger nutrient foramina tend to occur in animals with higher metabolic rates during locomotion (Allan et al., 2014; Seymour et al., 2012). It is known that elevated stress and strain in bones during locomotion lead to more micro-damage and enhanced remodelling (Lieberman et al., 2003; Robling et al., 2006). Higher oxygen demands of bone cells result in higher blood flow rates, which are associated with larger vessels and foramina. This approach of using foramen sizes to evaluate regional blood flow rates is called the 'foramen technique'.

If the size relationship between the foramen and the occupying artery is known, then quantitative flow rate can be calculated from theoretical or empirical equations. For example, flow rates in the marsupial and primate internal carotid arteries have been estimated from foramen size, because the artery occupies the carotid foramen almost entirely (Boyer and Harrington, 2018; Boyer and Harrington, 2019; Seymour et al., 2015; Seymour et al., 2016; Seymour et al., 2019a). The foramen must be measured accurately, and the arterial wall thickness must be known to estimate arterial lumen size in foramina occupied by a single artery (Hu et al., 2020). However, the relationship between foramen and artery lumen size becomes much more complex when a foramen, such as the femoral nutrient foramen, also passes substantial veins. Previous research on femoral bone nutrient foramina resulted in a semi-quantitative blood flow index (Q_i) rather than absolute blood flow rates, because the

lumen/foramen ratio had not been determined. No studies have ever quantified how nutrient arteries occupy the nutrient foramina of long bones.

To improve the foramen technique on femoral bone blood flows, the size relationship between femoral nutrient arteries and nutrient foramina needs to be investigated. Vascular contrast techniques have been commonly used for studying vascular beds with associated tissues or organs in vertebrates. The technique requires inserting a radiopaque medium into the circulatory system, and the medium can then be detected by X-ray without tissue corrosion (Sedlmayr and Witmer, 2002). We used high resolution micro-computerized tomographic (Micro-CT) imaging to measure the relationship between nutrient foramen size and nutrient artery lumen size. To observe vessel locations inside a nutrient foramen, histological tissue embedding and sectioning were also used. Non-laying hens, laying hens and roosters of similar age were selected for examining the relationships among femoral bone blood flows, nutrient artery and nutrient foramen sizes. Commercial chickens were selected as experimental animals because bone blood flow rates of birds are poorly studied compared to mammals. Additionally, birds lay eggs to reproduce, so extra calcium is exported partly from the bones into eggshell during reproduction periods. Calcium turnover in commercial layers is much more intense to satisfy intense egg production. Birds develop medullary bones to act as a labile calcium source for eggshell production, and femora contain medullary bone (Whitehead, 2004). The foramen-artery size relationship in chickens may relate sizes to femoral bone blood flow rates associated with these physiological processes. We hypothesized that femoral nutrient foramen sizes correlate with nutrient artery sizes, which reflect nutrient artery blood flow rates and metabolic demands.

4.3. Methods

4.3.1 Vascular contrast imaging

Three groups of crossbreed ISA brown chickens (non-laying hens, laying hens and roosters) with age ranging from 4–7 months were obtained under Animal Ethics Committee approval (S-2017-058). Each group contained six chickens, which were kept in a constant temperature room at 25 °C before operations. The room was set to have a 16-h day time and 8-h night time cycle. All chickens had free access to food and water.

4.3.1.1 Surgical operation

Chickens were prepared for whole-body infusion of contrast medium under physiological pressure. They were first anaesthetized with a combination of ketamine (40 mg kg^{-1}) and xylazine (4 mg kg^{-1}) through intramuscular injection. On average, about 1 ml of the anaesthetic mixture was injected into each chicken. After 20 min, toe-pinch was performed by applying pressure on toes to check whether chickens responded. If they still responded, another 0.2 ml of the anaesthetic mixture was administered. Chickens were then placed on a dissection table on their right side. The left wing was spread and stabilized by grasping the radius and ulna. Feathers on the inside of the wing were plucked, and a scalpel was used to cut the skin open next to the brachial vein near the humerus. The vein was isolated gently from the muscle using a pair of surgical scissors and college tweezers. A heparinized 20 ga Venocan Pencil style IV catheter (Cat. No. 121931, Kruuse, Denmark) was inserted into the brachial vein towards the heart. When venous blood slowly flowed into the needle chamber, the catheter was further inserted into the brachial vein, and the needle was pulled out from the catheter, leaving the catheter inside the vein. To heparinize blood of the entire vasculature, 2 ml heparinized saline (125 i.u. ml^{-1}) was injected into the brachial vein though the catheter. Two minutes after the injection, chickens were euthanased by injecting excessive anaesthetic into the brachial vein. The catheter was then removed, and both sides of the brachial vein next to the injection point were sutured, in order to prevent any liquid from leaking out from the injection point during the following procedures.

Feathers were removed at the left chest region. A scalpel and a pair of surgical scissors were used to cut into the chest skin and muscles to expose the first three ribs. The cut was as small as possible to reduce any blood vessel damage. A self-retaining Weitlaner retractor was used to open the gap between the second and third ribs to expose the pericardium, which was removed using both a haemostat and a scalpel. A pair of microscissors was used to cut a small hole through the myocardium into the left ventricle. A clear vinyl tube (internal diameter: 1.4 mm; external diameter: 1.9 mm) was inserted into the left ventricle and was stabilized to the myocardium using cyanomethacrylate glue. The other end of the tube was connected to a needle. The chicken was then gently placed on its left side. The same procedure was performed on the right side to expose the heart. Tweezers were used to tear the right atrium open to

release blood and perfusate. Thus the whole body vasculature was perfused via the tubing into the left ventricle with saline from a reservoir bottle positioned at a vertical distance of 2.03 m above the chicken to produce approximately average systemic arterial blood pressure of 150 mm Hg. As chickens grow up, their blood pressure becomes stable at about 140 mm Hg when they reach 10 weeks old (Koike and Nomura, 1966). Adult roosters generally have a higher blood pressure than hens (Sturkie, 1986). Since all experimental chickens in this study were at the stage around sexual maturity, and there was not much difference in body mass between them, mean blood pressure of all chickens was assumed to be about 150 mm Hg in this study. The blood-flushing process lasted for about 15–20 min until little blood remained in the saline solution draining out from the right atrium.

4.3.1.2 Vascular contrast medium injection

BriteVu (Scarlet Imaging, Murray, Utah, United States) was selected as the contrast medium in this study. Right after the blood-flushing process, chicken legs were harvested by cutting across the ilium using a pair of secateurs. The femoral head and ilium remained intact and connected. During pilot studies, we observed that the chicken femoral nutrient arteries branch from the ischiatic arteries. Because the nutrient artery lumen cross sections were too small (less than 0.1 mm^2) to observe and cannulate, BriteVu was instead perfused into the ischiatic arteries near the femoral head (Figure 1). A scalpel was used to cut carefully into the muscles near the femoral head to expose ischiatic nerve, ischiatic vein and ischiatic artery. The ischiatic artery was isolated and cannulated using a pair of college tweezers, and a clear vinyl tubing (internal diameter: 0.5 mm; external diameter: 0.9 mm) with a 25 ga needle connecting to the end. A drop of cyanomethacrylate glue was applied at the joint to stabilize the tubing. Because the femoral nutrient arteries are much smaller than the ischiatic arteries, BriteVu sometimes bypassed the nutrient arteries and caused experimental failures. To compensate for this problem, we exposed and ligated the downstream ischiatic artery near the knee (Figure 1).
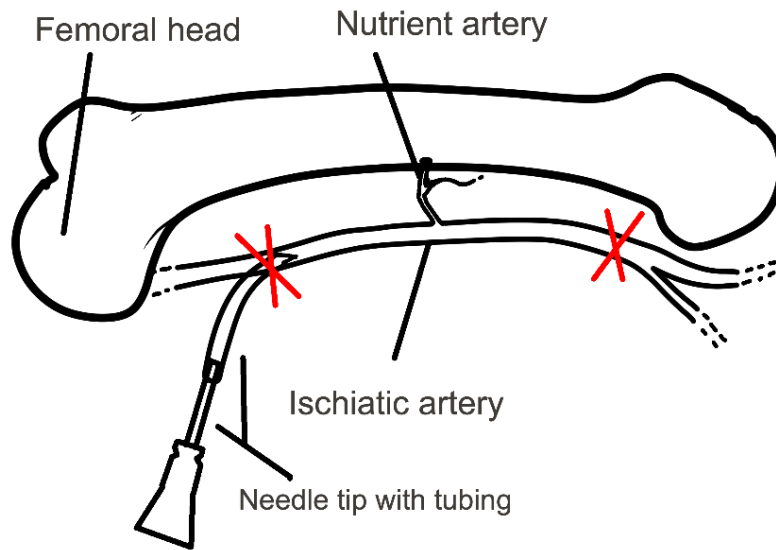
Figure 1. Schematic diagram of an ischiatic artery cannulation. Red crosses represent ligations with suture.

After cannulation, the leg was placed into a plastic bag, which was put into a warm water bath prior to BriteVu perfusion. One part of BriteVu, 3 parts of water and 1.5 % BriteVu enhancer (Scarlet Imaging, Murray, Utah, United States) were mixed continuously in a glass beaker with a stirring bar and a thermometer on a magnetic stirrer hotplate, heated to 70–80 °C. The mixture was kept at 70–80 °C for 10 min before infusing into the ischiatic artery via the needle and tubing under physiological pressure, using a reservoir bottle at a vertical distance of 1.87 m (i.e. 150 mm Hg) above the heart of the animal. BriteVu was perfused into the artery continuously until it cooled down and no more could be perfused into the leg. The leg was then placed back into the plastic bag in an ice bucket and placed into a refrigerator to speed up BriteVu solidification prior to micro-CT scanning.

In total, 27 legs from 6 non-laying hens, 6 laying hens and 7 roosters were successfully perfused with BriteVu under physiological pressure. Among these chicken samples, one leg of 2 non-laying hens and 2 laying hens was perfused with BriteVu manually under hand pressure via the ascending aorta, to explore blood vessel distribution surrounding a femur. One leg of an extra non-laying hen and a

rooster was also perfused with BriteVu manually under hand pressure. Therefore, 6 legs were infused with BriteVu by hand pressure in total.

4.3.1.3 Micro-CT scanning

Micro-CT scanning was used to measure both nutrient foramen sizes and nutrient arteries infused with BriteVu. Chicken femora with tissues were separated from the tibia and wrapped in plastic wrap. Tape was used to stabilize femora onto the CT scanner bed (Skyscan 1276, Bruker microCT, Kontich, Belgium). Since femora can have more than one nutrient foramen, femur shafts were first scanned using a lower resolution (20 µm) to observe foramen numbers and locations. Each nutrient foramen was then scanned using a higher resolution (10 µm). After scanning, NRecon 1.6.10.4 (Bruker microCT) was used for image reconstruction. The scanning parameters and reconstructing settings are shown in Table 1. Foramen areas and radii were collected and measured using both DataViewer 1.5.2.4 (Bruker microCT) and Fiji (www.fiji.sc). Methods to measure foramen size are well described in detail in Hu et al. (2020) (i.e. Chapter 2). Nutrient artery cross-sectional areas filled with BriteVu were measured separately from the foramina as sometimes the artery pathways do not perfectly align with the foramen pathways.

Table 1: Scan parameters and reconstruction settings of Skyscan-1276 scanner and NRecon for chicken femur shafts and femur foramina.

| Scan parameters	Image pixel size (µm)	Source voltage (kV)	Source current (µA)	Exposure (ms)	Filter	Rotation Step (°)	Frame Averaging
Femur shafts	20.5	95	200	715	Al+Cu*	0.4	OFF
Nutrient foramina	10.3	95	200	715	Al+Cu*	0.2	OFF
Reconstruction settings	Smoothing	Ring artifacts reduction	Beam-hardening correction	Contrast limits			
	2	10	30 %	0-0.04			

* Aluminium-Copper filter

4.3.2 Histology study

4.3.2.1 Femur shaft sectioning

Another three laying hens were used for histological sectioning of the femoral nutrient foramen. The same surgical operation procedures were performed on these chickens. Right after blood flushing under physiological pressure for 15–20 min, 10 % formalin was perfused for 15 min via the left ventricle into chicken circulatory system from a reservoir bottle at a different vertical distance of 1.87 meters (i.e. 150 mm Hg) above the heart of the animal. All procedures involving fixative were performed in a room or in a fume hood with proper ventilation. After formalin perfusion, most feathers were removed, and chickens were then placed in buckets filled with 10 % formalin for 2 weeks. After whole body fixation, chicken femora were harvested. Most attached tissues were removed, except for the tissues at the bone shaft, covering the nutrient foramina. Femur shafts were scanned using the micro-CT scanner at 20 µm resolution to detect foramen locations and numbers. Femora were then placed into Cal-Ex decalcifying solution for 3 weeks. After decalcification, tissues on the bone shaft were carefully removed to expose nutrient foramina. Femur shafts were separated from the whole bones and placed in 70% ethanol prior to histological embedding and sectioning. Femur shafts were embedded in paraffin and sectioned serially with 7 µm slice thickness through the whole cortical region, where the foramen is located (Figure 2), using a rotary microtome. Masson's trichrome stain was used to stain the tissues, to distinguish bones, vessel walls and nerves. A light microscope (Z2197, Olympus, Tokyo, Japan) connected to a 5MP digital imager (#44422, Celestron, USA) and a computer were used to take microphotographs of the foramen slices.
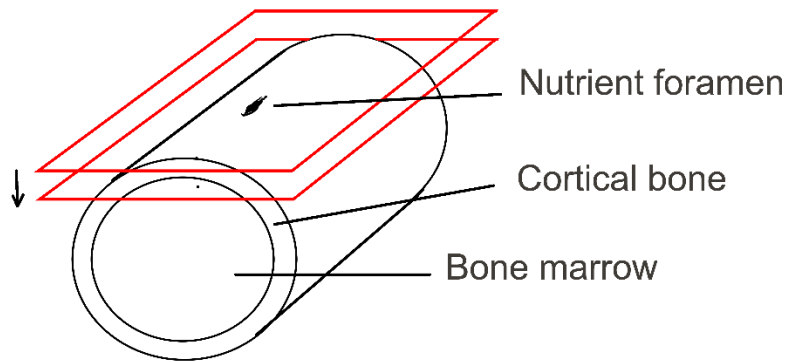
Figure 2. Schematic diagram of histological sectioning of femur shafts. The nutrient foramen faced upwards. Serial femur shaft slices were sectioned throughout the whole foramen passage in the cortical bone. Red squares represent histological cross-sections.

4.4. Statistical analysis

Most biological factors are related to body mass in non-linear ways. When comparing data such as foramen size, vessel size and blood flow data among chickens with different body mass, data need to have the effect of body mass removed (i.e. mass-independent data). The scaling of blood flow index (Q_i) in the femoral bone of cursorial birds on body mass has an exponent of 0.89 (Allan et al., 2014). As derived from Poiseuille's Law, $Q_i = r^4/L$, where Q_i (mm^3) is blood flow index, r (mm) is foramen radius substituting vessel radius, and L (mm) is an arbitrary length, assuming that femur length is geometrically similar to vessel length (Allan et al., 2014; Seymour et al., 2012). The units of Q_i are proportional to blood flow rate. Any length scales with body mass or volume to the 0.33 power, and area scales to the 0.67 power, if the shape is constant. Therefore, assuming that Q_i is proportional to body mass to the 0.89 power, L to the 0.33 power, then foramen radius should scale with body mass to the 0.305 power, and area to the ($0.305 \times 2 = 0.61$) in birds. Therefore, the raw data were converted to mass-independent nutrient artery radii (mm kg$^{-0.305}$) and areas (mm^2 kg$^{-0.61}$) for analysis.

If femora have more than one foramen or more than one perfused nutrient artery, foramen and nutrient artery radii for these femora were calculated from the summed

foramen and artery areas. Mass-independent areas of nutrient foramina were averaged from both legs and compared among three chicken groups using ANOVA in statistical software (Prism 6.0; GraphPad Software, La Jolla, CA, USA). Nutrient artery cross-sectional areas were collected only from femora with BriteVu successfully perfused in the artery lumina inside the foramina. If nutrient arteries of both femora were well-perfused, size data of the nutrient arteries were averaged from both femora, otherwise one femur's artery was a datum. Mass-independent areas and radii of nutrient arteries were compared among three chicken groups using ANOVA. If there was a significant difference, Tukey's multiple comparisons test was used for comparing means between any two groups. Lumen/foramen area ratio was calculated by dividing a nutrient artery lumen area by a foramen area for each properly perfused foramen. Error statistics are 95 % confidence intervals (CI).

4.5. Results

4.5.1 General observations of chicken femoral nutrient arteries and nutrient foramina

As the descending aorta passes into the abdominal region, it gives rise to external iliac and ischiatic arteries running into the legs, and the femoral arteries branch off the external iliac arteries (Midtgård, 1982; Xu et al., 2010). The femoral artery and ischiatic artery are the major arteries of the thigh, with the femoral artery often supporting the proximal muscles, and ischiatic artery providing the main blood supply of the hind limb. Femoral nutrient arteries of birds, including chickens, branch off the ischiatic arteries (Figure 3 and Figure 4A). After a single nutrient artery enters a femur shaft though a nutrient foramen, it bifurcates into ascending and descending arteries (Figure 4B, C). Most femora had only one nutrient foramen located at the mid-shaft region. Of 48 femora scanned in this study, 17 femora had two nutrient foramina, and three femora had three. Nutrient artery locations and foramen shapes were complex in femora with more than one nutrient foramen. Therefore, femora with more than one foramen are described separately below.
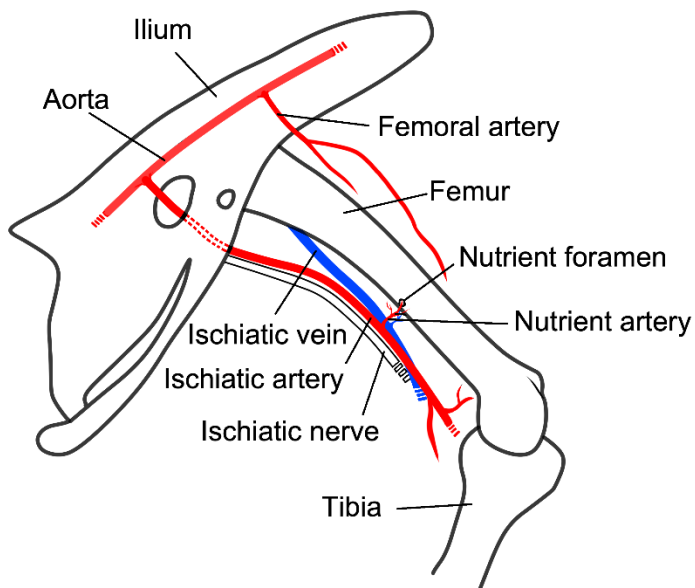
Figure 3. Schematic drawings of the vessel patterns surrounding the femur (medial view). The graph is drawn based on Midtgård (1982)'s descriptions and our own observations.
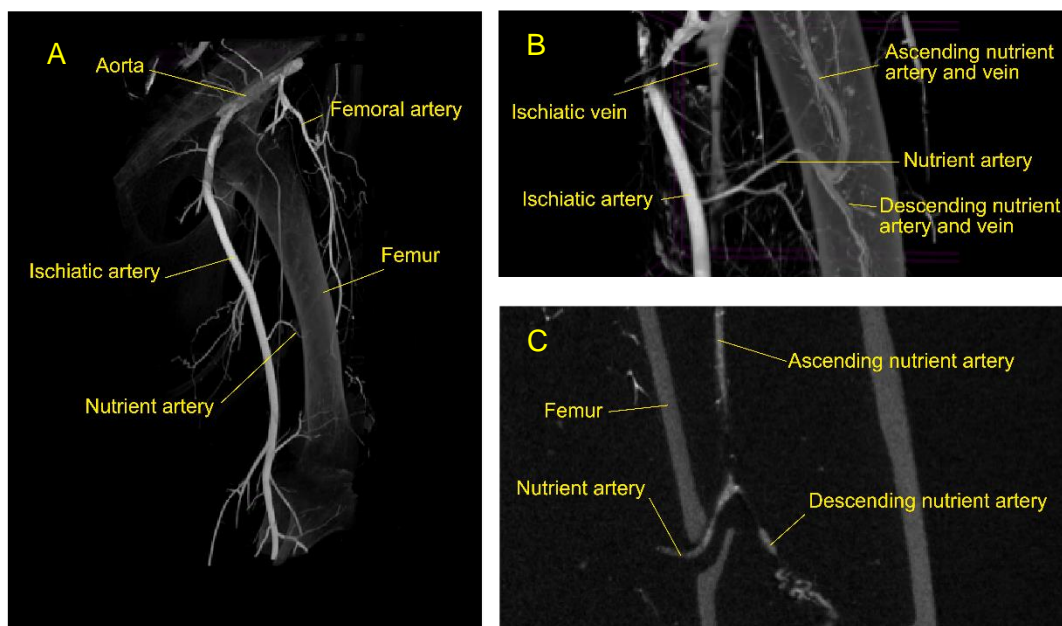

Figure 4. Micro-CT images of blood vessel distribution surrounding femora. A. Main arteries surrounding a femur. B. Ischiatic vein and ischiatic artery connected to the vein and nutrient artery inside a femur shaft. C. A cross-sectional image of a femur mid-shaft, with a nutrient foramen and a nutrient artery. Nutrient artery outside the foramen in image C does not appear due to sample orientation.

### 4.5.1.1 Femora with one nutrient foramen

A single nutrient foramen contained a nutrient artery, a vein and a nerve (Figure 4A). Most femora with only one nutrient foramen observed from histological sections did not reveal a vein inside the foramen, but exposed a large space between the artery and the foramen (Figure 5B). We believe veins in these foramina detached during processing because of their thin, fragile walls, as veins could be observed in some histological sections (Figure 5A) and on micro-CT images (Figure 4B). Cross-sectional areas of these nutrient foramina often appeared to be pear-shaped or elliptical, and the nutrient artery was located at the smaller end of the "pear" (Figure 6A, B & C). Nutrient foramen passages did not branch inside the cortical region in most cases. However, both femora of one chicken in this study revealed a passage that was single on the periosteal surface and branched into two passages within the cortical bone. One passage contained the nutrient artery and the other empty foramen probably contained the vein (Figure 7).
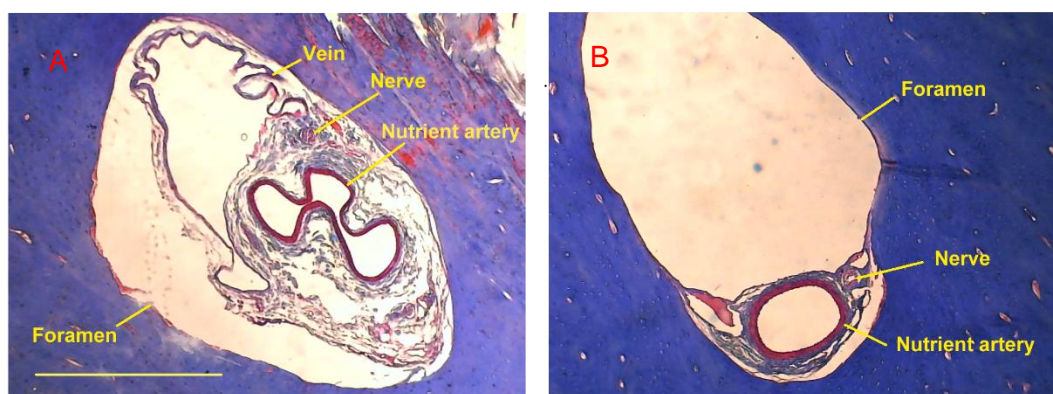
Figure 5. Microphotographs of histological nutrient foramen cross-sections with occupying tissues. A. A nutrient artery, a vein and a nerve occupy a nutrient foramen. B. A nutrient artery and a nerve occupy a nutrient foramen, leaving a large space between the foramen wall and the occupying tissues. (Note: 1. Histological foramen and vessel cross-sections were not sliced perpendicularly to either the foramen passage or the vessels; 2. All histological nutrient arteries were not pressurized properly.) The scale represents 0.5 mm.
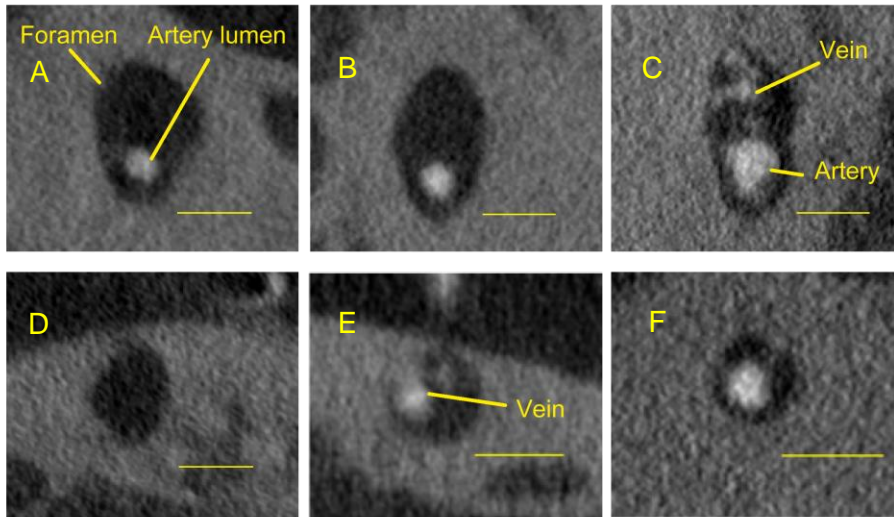
Figure 6. Different shapes of nutrient foramina with occupying vessel lumina filled with BriteVu observed from micro-CT images. A & B. Pear-shaped foramina with nutrient artery locating at the smaller area of the "pear". C. A pear-shaped foramen with both a nutrient artery and a vein partially filled with BriteVu. D. An "empty" round-shaped foramen. E. A round-shaped foramen with a vein. F. A round-shaped foramen with a nutrient artery. Scales represent 0.5 mm.
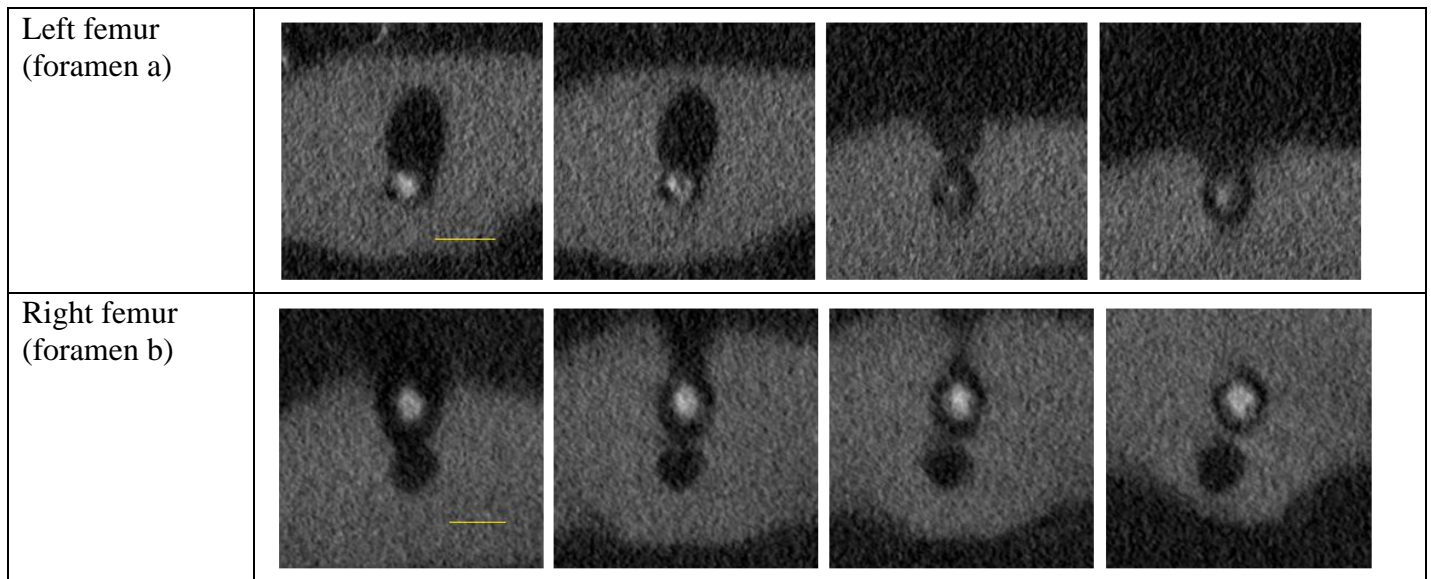
Figure 7. Tangential cross-sections of two nutrient foramen passages a and b on both femora of a chicken. From left to right, the cross-sections were collected from closer to the bone surface to the closer to the bone marrow. An invisible vein may be present in the "empty" space of each foramen. Scales represent 0.5 mm.

4.5.1.2 Femora with more than one foramen

In some cases when a femur had more than one foramen, only one foramen passed the nutrient artery branching off the ischiatic artery, as we often observed only one artery lumen filled with BriteVu inside one foramen. Other foramina appeared to be empty or have irregular-shaped lumen cross-sections (Figure 6D, E). This could be because the contrast medium failed to perfuse into the arteries inside these foramina or because these foramina may contain only a vein. Veins were not perfused intentionally with BriteVu in this study, but it entered veins in some cases, possibly through anastomoses or ruptures (e.g. Figure 4B). One femur, which had two nutrient foramina, showed an ischiatic vein partially perfused with BriteVu. We observed that one foramen of this femur contained a nutrient artery traced to the ischiatic artery and another foramen contained a vein traced to the ischiatic vein. Both of these foramen cross-sections were round-shaped. This sample indicated the possibility for a femur to have two nutrient foramina, with one occupied by an artery and other occupied by a vein. Another case showed a femur containing two foramina, each with a nutrient artery. In this specific example, the sizes of these two nutrient artery lumina were similar, but one foramen was round-shaped and the other one had a much larger pear-shaped cross-sectional area, suggesting that it also contained a vein (Figure 8). Both arteries branched off the ischiatic artery. After they ran into the femur shaft, one artery turned into an ascending artery and the other turned into a descending artery. No direct connections were observed between the two arteries inside the femur (Figure 8). A similar pattern occurred in the histological study of two femur shaft sections that contained two foramina (Figure 9). These images also suggested that femora with two nutrient foramina could both contain an artery. The nutrient artery sizes, foramen sizes, foramen shapes and the lumen/foramen size ratio between the two foramina of a femur may vary.
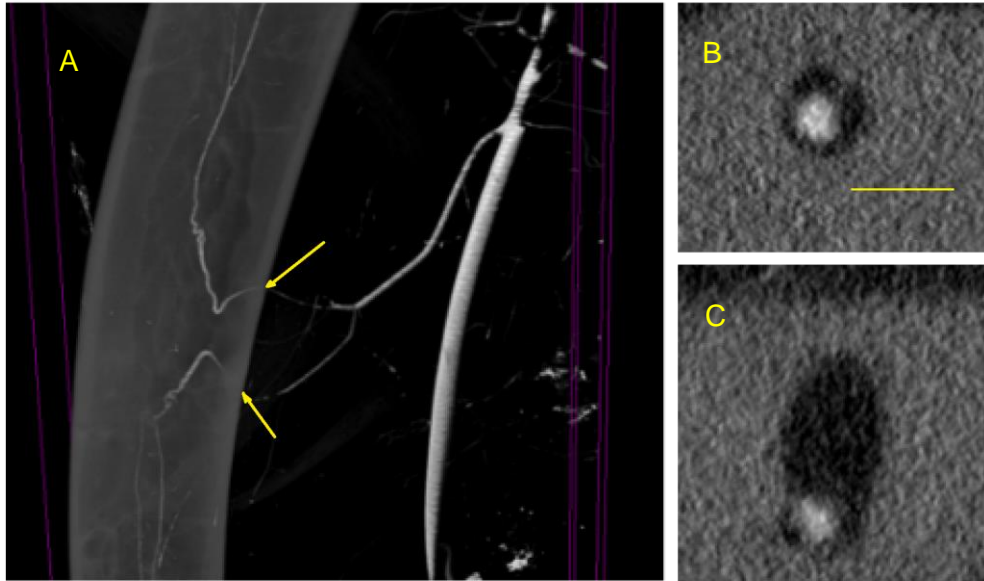
Figure 8. Micro-CT images of a femur with two nutrient arteries passing through two nutrient foramina. A. 3D image of a femur with two nutrient arteries. Arrows represent foramen locations. Arteries disappeared outside the bone because of vessel collapse. B & C. Two foramen cross sections with nutrient artery lumina filled will BriteVu are present in the right two images. A vein may locate in the foramen "empty" space of image C. The scale represents 0.5 mm for both foramen images B & C.
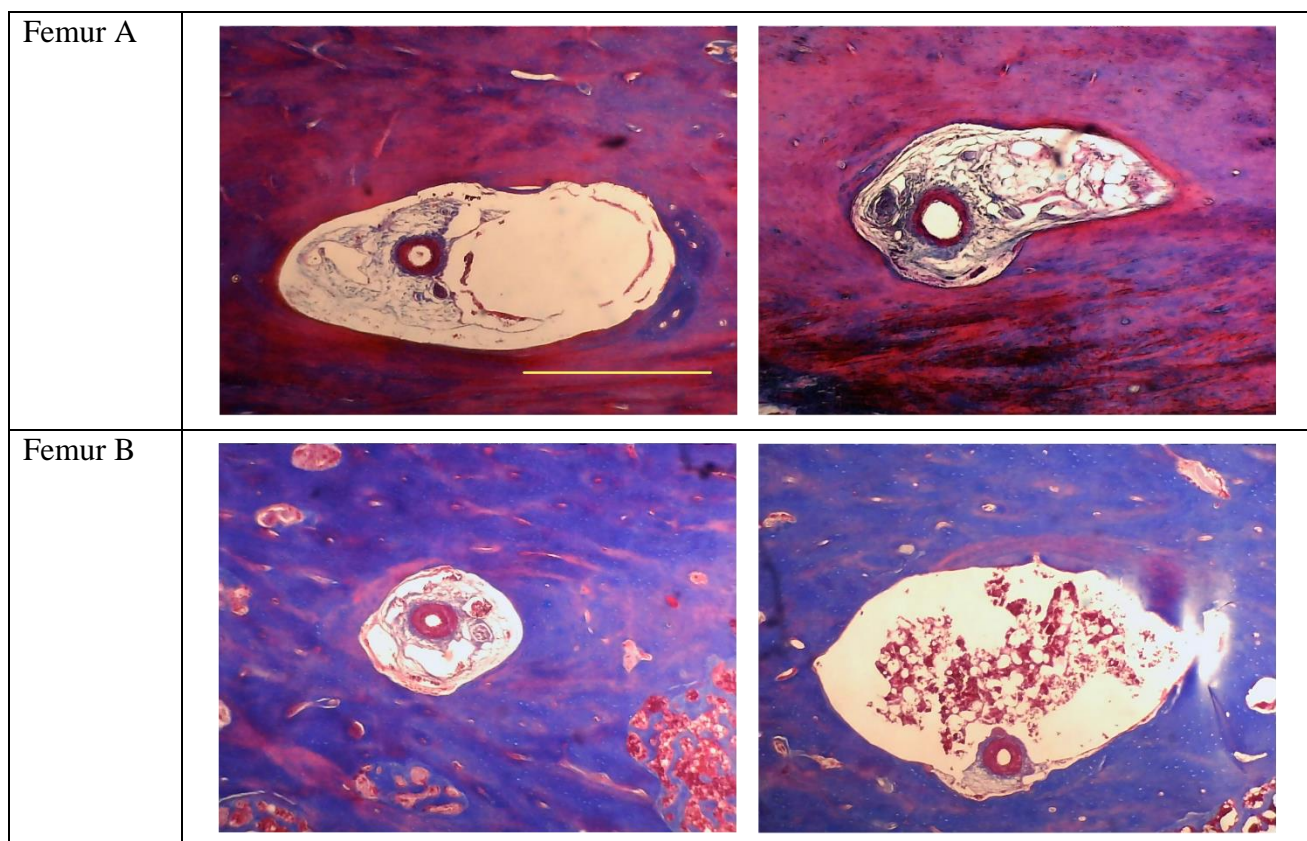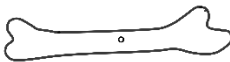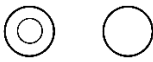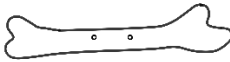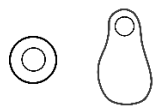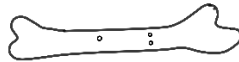
Femur A	
Femur B	

Figure 9. Microphotographs of histological cross-sections of femur A & B with two nutrient foramina. (Note: 1. Histological foramen and vessel cross-sections were not sliced perpendicularly to either the foramen passage or the vessels; 2. All histological nutrient arteries were not pressurized properly, apparent by the relatively thick arterial walls. 3. Femur A and B are from different chicken specimens) The scale represents 0.5 mm for all four images.
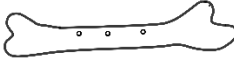
Foramen shapes and artery locations may be much more complex when a femur has more than two foramina. Foramen arrangements could vary among 3-foramen femora (Table 2). Femora with three foramina were rare and most of them failed to be completely filled with contrast medium. Only two 3-foramen femora were successfully perfused with BriteVu. Both femora had one foramen containing one nutrient artery and two other empty foramina. We are not certain about what vessels occupied the other two empty foramina. All observed foramen shapes, artery locations and foramen arrangements are summarized in Table 2.

Table 2. Observed nutrient foramen shapes, nutrient artery locations and foramen arrangements of femora with different foramen numbers based on this study. Foramen shapes are diagrammatic, not dimensionally accurate. Small circles represent nutrient artery lumen locations inside nutrient foramina. For foramen arrangements, smaller circles represent general foramen locations on the shafts of 48 femora scanned in this study. The observed numbers refer to femora with different foramen arrangements.

Foramen numbers on femur shaft	Foramen shapes and nutrient artery location	Foramen arrangements	Observed femur numbers
1			28
2			17
3			2
			1

We also examined another 50 femora analysed in the previous chapter (Chapter 3). Although femora were dissolved during the fluorescent microsphere experiment, we have the foramen number and foramen area data for those specimens. Of 98 femora analyzed in both studies, 30 femora had two nutrient foramina, and 4 femora had three foramina. To investigate whether foramen areas are the same between femora with different foramen numbers, 15 chickens were selected as they had one femur with one foramen, and the other femur with two foramina. Since either micro-CT scanning or a microscope was used to measure these foramen areas, total foramen areas between the left and right femora were compared using paired t-test in Graphpad, to exclude the impacts of method difference. No significant difference in summed areas existed between two femora with different foramen numbers ($P = 0.36$), and no significant

difference in radius calculated from summed areas existed between two femora (P = 0.29) (Figure 10A & B), suggesting the summed vessel area and nutrient blood supply may still be similar in femora with different foramen numbers. In addition, both the microsphere infusion experiment and this study found no significant differences in blood flow rates between left and right femora.
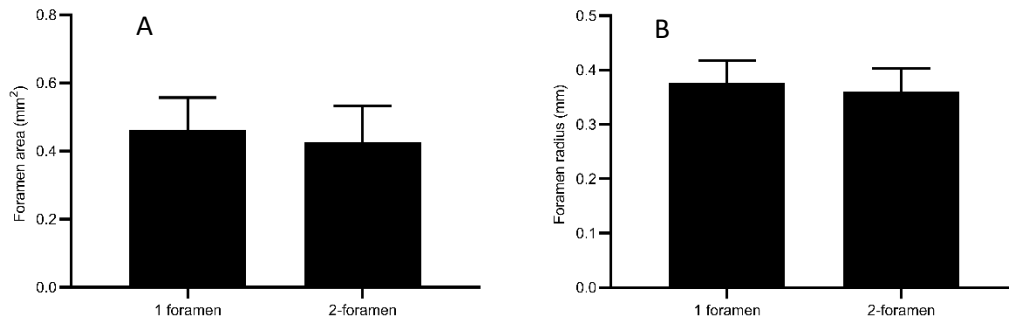
Figure 10. Nutrient foramen area (A) and radius (B) comparison between both femora of 15 chickens, with one femur containing one foramen and the other femur containing two foramina. Foramen areas of femora with two foramina are summed areas of the two foramina. Foramen radii were calculated from summed areas. Data collected are from both studies (Chapter 3 and 4). Error bars represent 95% confidence interval (CI) of the means.

4.5.2 Relationships between femoral nutrient foramen and nutrient artery sizes

Mean and 95% confidence intervals of body mass, nutrient foramen and nutrient artery sizes among three chicken groups are summarized in Table 3. Among the six chickens with one leg perfused with BriteVu with physiological pressure and the other with hand pressure, four of them had both femora with only one foramen on the femur shaft. Nutrient artery sizes between both legs of these four chickens are not significantly different from each other (P = 0.30), suggesting higher hand pressure does not affect lumen size measurements inside the nutrient foramina. Including the size data of the nutrient arteries collected from samples perfused under both physiological and hand pressure, average lumen/foramen area ratio of 45 foramina is 23.0 ± 3.8 %. Some femora have more than one foramen, and knowledge is incomplete about how nutrient arteries supply these bones. Therefore, lumen/foramen area ratios of femora with only one foramen were compared among three chicken

groups, to achieve direct ratio comparison. Only samples infused with BriteVu under physiological pressure were chosen for this ratio comparison, and 26 samples were analysed. Lumen/foramen area ratio of femora with only one nutrient foramen is 20.0 ± 3.2 %. This ratio of non-laying hens is 16.0 ± 4.0 %, which is significantly lower than laying hens (26.1 ± 7.3 %) ($P = 0.0097$), but not significantly different from roosters (19.4 ± 4.9 %) ($P = 0.55$) (Figure 11). Nutrient arteries of laying hens apparently occupy more area inside the nutrient foramina than the non-laying hens and roosters. There is lack of knowledge about how arteries occupy femora with multiple foramina. However, no significant difference in summed areas existed between two femora with different foramen numbers ($P = 0.36$), and no significant difference in radius calculated from summed areas existed between two femora ($P = 0.29$) (Figure 10A & B).

Table 3. Mean and 95% confidence intervals of body mass, nutrient foramen and nutrient artery sizes among non-laying hens, laying hens and roosters.

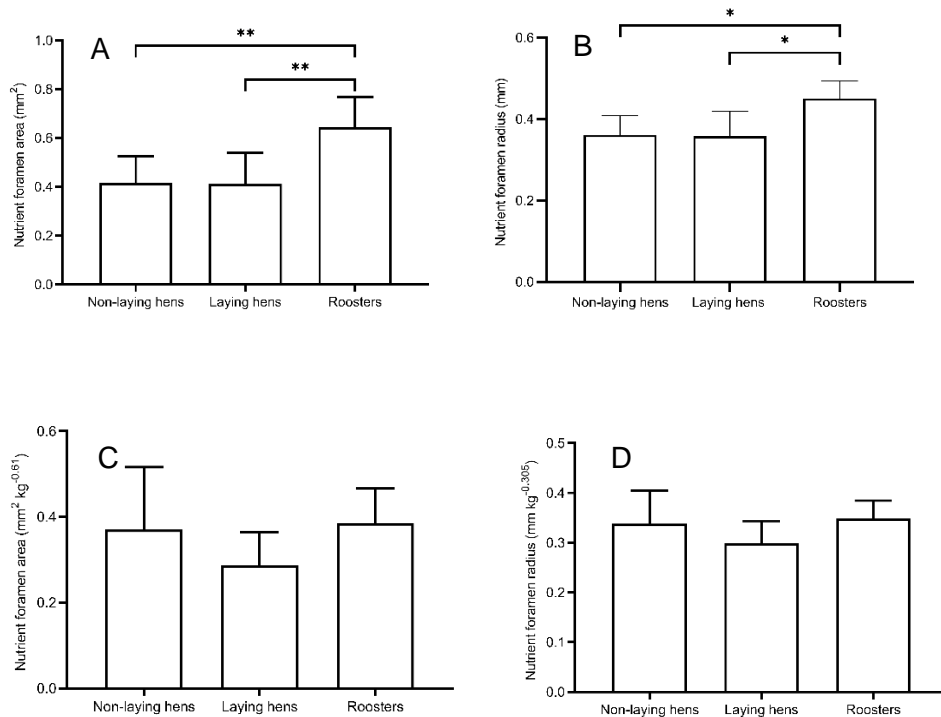| Groups	Nutrient foramen area (mm^2)	Nutrient foramen radius (mm)	Nutrient artery area (mm^2)	Nutrient artery radius (mm)	Body mass (kg)
Non-laying hens	0.42 ± 0.11	0.36 ± 0.048	0.056 ± 0.025	0.13 ± 0.029	1.3 ± 0.27
Laying hens	0.41 ± 0.13	0.36 ± 0.061	0.096 ± 0.030	0.17 ± 0.028	1.8 ± 0.19
Roosters	0.64 ± 0.12	0.45 ± 0.0019	0.10 ± 0.032	0.18 ± 0.026	2.3 ± 0.20
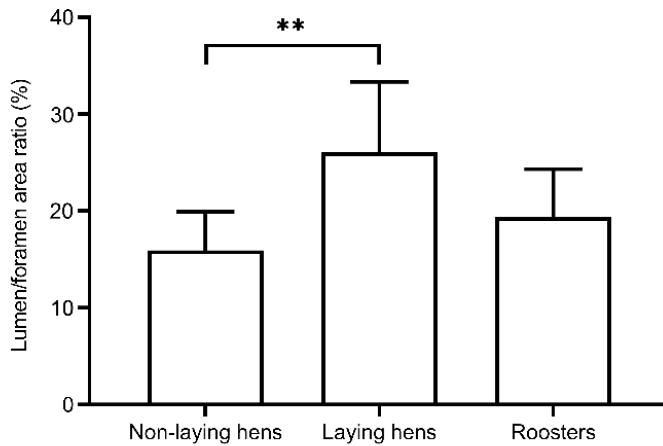
Figure 11. Lumen/foramen area ratio of femora with only one foramen among non-laying hens, laying hens and roosters. Error bars represent 95% confidence interval (CI) of the means. (**: $P \leq 0.01$).

Foramen size data were collected only from chickens with one or both successfully perfused femora with physiological levels of blood pressure. Absolute foramen areas (Non-laying hens: 0.42 ± 0.11 mm^2; Laying hens: 0.41 ± 0.13 mm^2) and radii (Non-laying hens: 0.36 ± 0.05 mm; Laying hens: 0.36 ± 0.06 mm) of two hen groups are not significantly different from each other (Area: $P = 1.00$ Radius: $P = 0.99$). Absolute foramen areas (0.64 ± 0.12 mm^2) and radii (0.45 ± 0.04 mm) of roosters were significantly higher than the non-laying hens (Area: $P = 0.0097$; Radius: $P = 0.014$) and laying hens (Area: $P = 0.0086$; Radius: $P = 0.011$) (Figure 12A & B).

The significant differences in absolute foramen size among the three chicken groups were apparently related to body mass. There were no significant differences in mass-independent areas ($P = 0.20$) and radii ($P = 0.19$) of nutrient foramina (Figure 12C & D). Average mass-independent area of nutrient foramina was 0.35 ± 0.052 mm^2 kg$^{-0.61}$, and radius was 0.33 ± 0.025 mm kg$^{-0.305}$, for the three chicken groups combined.

Figure 12. Absolute nutrient foramen areas (A) and radii (B), and mass-independent nutrient foramen areas (C) and radii (D) among non-laying hens, laying hens and roosters. Error bars represent 95% confidence interval (CI) of the means. (*: $P \leq 0.05$; **: $P \leq 0.01$).

Size data of nutrient arteries were also collected from femora perfused under physiological pressure. Absolute lumen areas were 0.06 ± 0.02, 0.10 ± 0.03 and 0.10 ± 0.03 mm^2 for non-laying hens, laying hens and roosters, respectively. Non-laying hens had significantly smaller lumen areas than the roosters ($P = 0.02$). Absolute lumen radii were 0.13 ± 0.03, 0.17 ± 0.03 and 0.18 ± 0.03 mm for non-laying hens, laying hens and roosters, respectively. Non-laying hens had significantly smaller lumen radii than the laying hens ($P = 0.04$) and roosters ($P = 0.01$) (Figure 13A &B). No significant differences were observed in mass-independent areas ($P = 0.26$) and radii ($P = 0.15$) of nutrient artery lumina among three chicken groups (Figure 13C & D). Average mass-independent area of the nutrient artery lumen was 0.060 ± 0.010 mm^2 $kg^{-0.61}$, and radius was 0.14 ± 0.012 mm $kg^{-0.305}$, for the three chicken groups.
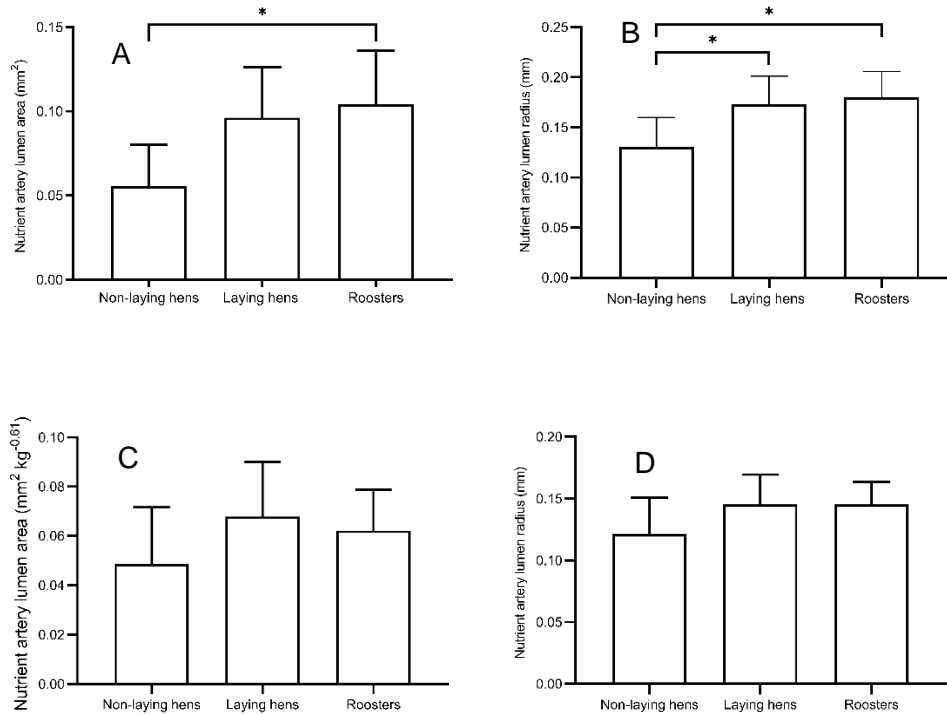
Figure 13. Absolute areas (A) and radii (B) of nutrient artery lumina, and mass-independent areas (C) and radii (D) of nutrient artery lumina among non-laying hens, laying hens and roosters. Error bars represent 95% confidence interval (CI) of the means. No significant differences occur among groups. (*: $P \leq 0.05$; **: $P \leq 0.01$).

4.6. Discussion

Previous studies on femoral nutrient foramina calculated femoral bone blood flow indices (Q_i) rather than absolute blood flow rates, because the artery lumen-foramen size relationship was unknown. To improve these studies, the ratio of wall thickness to nutrient artery lumen radius needs to be investigated. Apart from the lumen/foramen area ratio described in the results, the ratio of wall thickness to lumen radius is another ratio for estimating artery sizes from foramen sizes, and it was used in previous carotid foramen studies (Boyer and Harrington, 2018; Boyer and Harrington, 2019; Seymour et al., 2015; Seymour et al., 2016; Seymour et al., 2019a). Although artery walls cannot be observed directly in micro-CT images, we can estimate the wall thickness by measuring the distance between the lumen and foramen wall. If absolute nutrient artery blood flow rates can be estimated from nutrient artery lumen sizes, we can also improve the foramen technique on femoral bone blood flows. Absolute nutrient artery blood flow rates of three chicken groups in this study

can be compared and related to gender differences and other physiological processes such as calcium turnover intensity. Moreover, a study used fluorescent microsphere technique to estimate absolute regional blood flow rates of femoral bone (Chapter 3). By comparing blood flow rates estimated from both nutrient artery sizes and the microsphere study, we can examine whether both methods are capable of providing similar blood flow values. Since femur shaft can have multiple foramina, it is possible to miss some foramina to measure due to their locations or their small sizes. It is also vital to explore the impacts of this type of mismeasurement, in order to avoid and reduce measurement errors.

4.6.1 The size of the femoral nutrient artery

The 'foramen technique' uses the size of a foramen to evaluate the rate of blood flow in the artery that passes through it. In the case of the internal carotid artery that completely fills the carotid foramen in primates and marsupials, absolute blood flow rate ($\dot{Q}$) can be estimated from the artery lumen radius (r_i), assuming that the outer arterial radius (r_o) equals effective foramen radius and the ratio of wall thickness to lumen radius w = (r_o - r_i)/r_i is a constant (Seymour et al., 2015; Seymour et al., 2016; Seymour et al., 2019a). Fourteen studies of the sizes of the human carotid arteries and carotid foramen revealed that w averages 0.3 (Hu et al., 2020). In the case of the nutrient artery that does not fill the nutrient foramen, another approach is necessary. Birds are considered to have relatively thicker artery walls compared to mammals with similar lumen sizes, as birds in general have an approximately 30 % higher blood pressure than mammals (Seymour et al., 2004). Assuming that nutrient arteries are circular and fill a section of a noncircular foramen (Figure 14A) or a circular foramen (Figure 14B), the "outer circumference" of the nutrient artery cross-sections were measured subjectively using Fiji and converted into artery outer radius (r_o). Average wall thickness-lumen ratio estimated from 45 chicken femoral nutrient foramina was 0.57 ± 0.08. This value is significantly higher than 0.4, which is expected if, according to Law of Laplace, transmural pressure is directly proportional to wall thickness (Westerhof et al., 2019), and avian arteries have the same mechanical properties as mammalian arteries. Eight round-shaped foramina were almost entirely occupied by one artery, and the wall-lumen ratio of these specimens is 0.62 ± 0.26, which is not significantly different from the average wall-lumen ratio (0.57 ± 0.08). These estimates should be approached with caution. Measuring the artery "outer

circumference" is somewhat subjective, as it is difficult to clearly define the outer artery wall. Additionally, contrast medium might slightly shrink inside the vessel lumen during solidification. If this were the case, the nutrient artery blood flow rates would be also underestimated from artery lumen sizes. Moreover, wall thickness might be slightly different between mammals and birds because of their different artery wall components and structures. For example, fenestrated external elastic lamina, which has been illustrated in only a few mammalian species, is usually found in arteries with a great amount of elastic tissue persisting in the wall media and adventitia. However, this structure is found in bird vessels with only the internal elastic lamina (Pfister, 1927). Nutrient artery wall structures may not be the same in birds and mammals. The wall-lumen ratio of the avian femoral nutrient artery needs to be calibrated by considering more factors. Another point is that the pear-shaped foramen cross sections often occur at a certain depth of the cortical bone, whereas foramen shapes often appear elliptical on the bone surface. Therefore, the size of the artery cannot be reliably determined by optical instruments observing the bone surface.
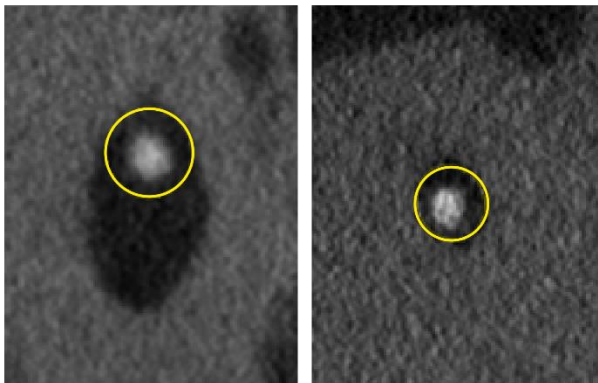
Figure 14. Outer circumferences of nutrient arteries. Estimated outer circumference of a nutrient artery in a pear-shaped nutrient foramen (A) and a round-shaped nutrient foramen (B). Yellow circles represent the outer circumferences.

4.6.2 Blood flow estimation from nutrient artery sizes

Blood flow rates ($\dot{Q}$, cm s^{-1}) can be estimated from artery lumen radius (r_i, cm) using theoretical and empirical approaches. The theoretical approach is through Poiseuille's "shear stress equation": $\dot{Q} = (\tau\pi r_i^3)/(4\,\eta)$, where τ (dyn cm^{-1}) is wall shear stress and η is blood viscosity (dyn s cm^{-2}) (Lehoux and Tedgui, 2003). Some previous foramen

studies used this equation to estimate human internal carotid artery blood flow rate
(Seymour et al., 2015; Seymour et al., 2016; Seymour et al., 2019a). $\dot{Q}$ can also be
estimated from artery sizes empirically. Seymour et al. (2019b) collected artery lumen
radii coupled with blood flow rates in 22 named arteries varying in radius from 3.65
µm to 1.12 cm in nine mammalian species. The empirical equation describes the
relationship between blood flow rate ($\dot{Q}$, cm s^{-1}) and artery lumen radius (r_i, cm):

$$\log \dot{Q} = -0.20\ (\log r_i)^2 + 1.91 \log r_i + 1.82 \tag{1}$$

Both approaches produce similar results for primate internal carotid artery blood flow
rates, if the scaling of wall shear stress is known (Seymour et al., 2019a).

This chapter relates nutrient artery blood flow rates with nutrient artery lumen sizes
according to the empirical equation (1), although the equation is based on blood
vessels of mammals. If a femur has multiple foramina, average blood flow rate of
nutrient artery in this femur was calculated by summing the blood flow values from
each foramen. The results of these calculations based on contrast imaging can be
compared to measurements of femur shaft perfusion using a fluorescent microsphere
technique among all three chicken groups (Chapter 3), as the nutrient arteries supply
mainly the femur shafts. There was no significant difference in absolute blood flow
rates derived from the two methods (Figure 15A), although the data between the two
studies necessarily involved different chicken individuals. Non-laying hens tended to
have lower blood flow compared to the laying hens. Although no significant
difference in blood flow between two hen groups was observed in this study (P =
0.19), a significant difference was found in the microsphere study (P = 0.02). The
microsphere study considered laying hens and roosters as adult chickens, as non-
laying hens still had a relatively higher growth rate, and the average femur shaft blood
flow of adults was 0.44 ml min^{-1} (Chapter 3). In this study, average femoral nutrient
artery lumen radius of laying hens and roosters was 0.175 mm. Shear stress in the
nutrient artery can be estimated according to the shear stress equation, assuming the
blood viscosity between mammals and birds is the same. The estimated shear stress is
69.7 dyn cm^{-2}. Wall shear stress can also be estimated from lumen radius only,
according an empirical equation: $\log\tau = -0.20 \times (\log r_i)^2 - 1.09\log r_i + 0.53$ (Seymour et

al., 2019b). The shear stress estimated this way is 67.3 dyn cm^{-2}, which is similar to 69.7 dyn cm^{-2}. This also suggest that the blood flow values collected from both microsphere infusion and vascular contrast technique match each other.

Both vascular contrast and fluorescent microsphere methods thus appear capable of providing similar estimates of absolute blood flow rates through femur shafts. However, this may be a fortuitous result of studying very small arteries. A companion study of the much larger chicken internal carotid artery (ICA) showed that blood flow rates estimated from contrast imaging was about five times lower than rates estimated by the fluorescent microsphere method (unpublished observations). We also compared chicken internal carotid artery lumen sizes collected from both vascular contrast and histological sectioning methods in this chapter. Measured artery sizes were affected by both methods to some extent (supplementary material). The results suggest that the vascular contrast method may not be applicable for correctly measuring large vessel lumen sizes. Larger arteries have thicker and more elastic vessel walls, which may compress contrast medium to a smaller volume before it solidifies. Choosing different casting materials may also affect cast vessel sizes. A number of studies used either the vascular corrosion casting method or contrast agent with micro-CT method to measure vessel size (Debbaut et al., 2010; Folarin et al., 2010; Junaid et al., 2017; Marxen et al., 2004; Vasquez et al., 2011), but few studies compared *in vivo* vessel sizes with cast vessel sizes. One study compared *in vivo* and cast vessel sizes using magnetic resonance imaging (MRI), corrosion casting and pressure fixation methods in rabbit aorto–iliac region, and the results indicated that lumen diameters of the pressurized-fixed samples were 18–29% shorter, and the cast vessel diameters were 5–17% shorter than ones collected from *in vivo* MR images (Moore et al., 1999). Therefore, more research is expected in the future to improve the vascular contrast method for regional blood flow estimation.
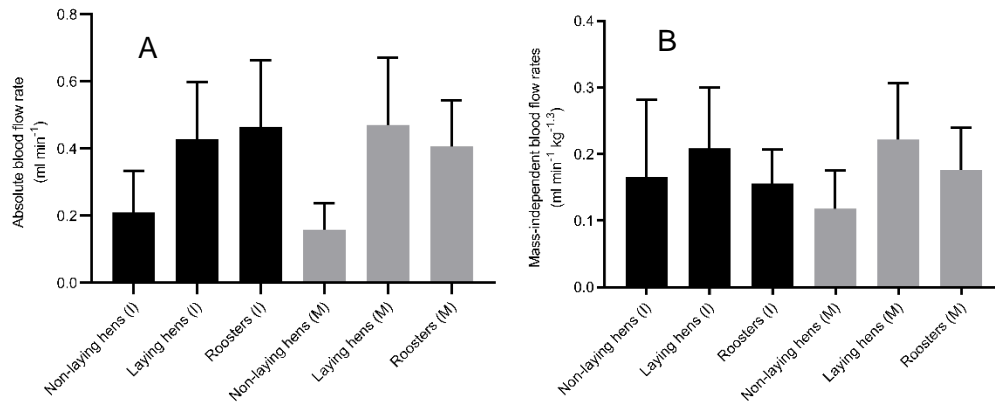
Figure 15. Nutrient artery blood flow rates estimated from artery lumina perfused by vascular contrast imaging (I) and absolute femur shaft blood flow rates determined with fluorescent microspheres (M) among non-laying hens, laying hens and roosters. Absolute flow rates are shown in panel A and mass-independent flow rates are shown in panel B. Error bars represent 95% CI of the means.
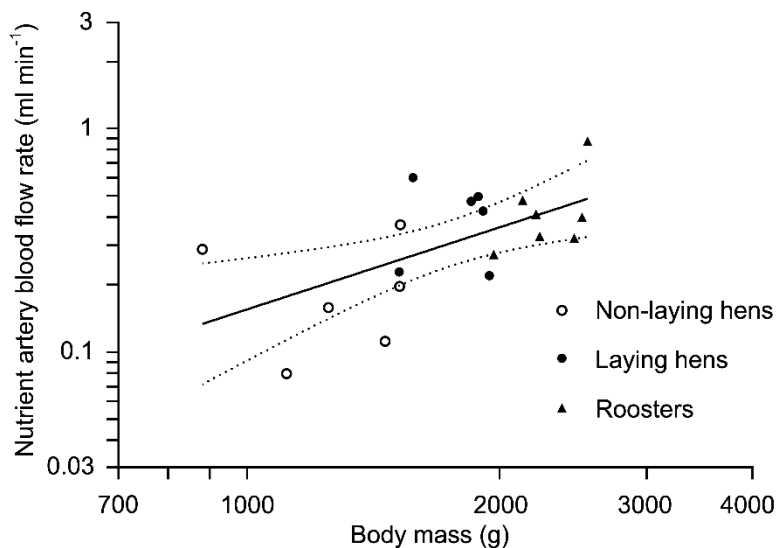
Figure 16. Relationship between nutrient artery blood flow rate ($\dot{Q}$, ml min^{-1}) and chicken body mass (M_b, g). Three different symbols represent three different chicken groups. The equation set to all groups is $\dot{Q} = 3.6 \times 10^{-5} \, M_b^{1.2 \pm 0.84}$. Dash lines represent 95% confident interval of the slope. Data are plotted on logarithmic scales.

To compare blood flow data more accurately among three chicken groups, nutrient artery blood flow rates need to be allometrically adjusted to account for body mass. Absolute nutrient artery blood flow rate on body mass across three chicken groups shows a positive correlation between these two variables, and the scaling exponent is 1.2 ± 0.84 (Figure 16), which is not significantly different from the 1.3 ± 0.93 scaling exponent calculated using microsphere infusion technique (Chapter 3). The 95% confidence interval of the scaling exponent is wide due to the small sample sizes and narrow body mass range, however the value of 1.3 was selected to compare mass-independent blood flow rates between the two studies. Mass-independent nutrient artery blood flow rates were calculated by dividing the estimated absolute blood flow rate by chicken body mass to the 1.3 power. Similar to absolute blood flow values, blood flow values in all chicken groups between two methods are not significantly different (Figure 15 B; Figure A8).

The fluorescent microsphere study showed that mass-independent blood flow in the femur shaft of laying hens was significantly higher than in non-laying hens ($P = 0.04$) (Chapter 3). The average mass-independent blood flow rate in the nutrient artery estimated by imaging showed a similar pattern in non-laying hens (0.12 ml min^{-1} kg$^{-1.3}$), laying hens (0.22 ml min^{-1} kg$^{-1.3}$) and roosters (0.18 ml min^{-1} kg$^{-1.3}$). However, the differences were not significantly different ($P = 0.67$) (Figure 15). Regional blood flow rates are associated with energy requirements of local tissues, as higher metabolism requires more oxygen and blood flow. Laying hens may require extra blood flow to carry calcium during eggshell formation. Medullary bone is a special bone type acting as calcium reserves in birds and crocodilians, and it replaces trabecular bone in chicken leg bones as they reach sexual maturity (Whitehead, 2004). Medullary bone is capable of being absorbed and renewed rapidly (Bain et al., 2016), in order to maintain calcium balance in bones of domestic chickens. Laying hens transport about 2.2 g of calcium into eggshell of each egg (Bouvarel et al., 2011) and about 20 – 40 % of this calcium passes through bone (Bar, 2009). Although nutrient artery blood flow rates estimated from the vascular imaging technique between the non-laying and laying hen groups are not significantly different from each other, the difference is significant when measured with microspheres (Figure 15B). Intense calcium turnover in laying hens explains the trend for greater bone perfusion in our ISA brown layers.

4.6.3 Nutrient foramen size and number

Nutrient artery lumen sizes of single foramen femora can be estimated from the foramen sizes using average lumen/foramen ratio of 20%, but it becomes complex in multiple-foramen femora. Both size and location of the nutrient artery and vein can vary among femora with more than one foramen, and the artery vessel size differences between femora with different foramen numbers are unclear at this stage. Therefore, the artery lumen sizes cannot be estimated from multiple-foramen femora using a simple ratio at this stage. Without knowing the artery lumen sizes, we cannot estimate absolute nutrient artery blood flow rates using equation (1). However, femoral regional bone blood flow rates are not significantly different between left and right femora (Chapter 3). In addition, the summed foramen areas of paired-femora with single and two foramina are not significantly different (Figure 10A &B). These suggests that nutrient artery blood flow rates between left and right femora should be similar, even when they have different foramen numbers. Therefore, although we cannot estimate vessel lumen sizes from multiple-foramen femora, we can still estimate absolute nutrient artery blood flow rates by assuming summed foramen areas as single foramen area, and artery lumen sizes of these femora can also be estimated using the lumen/foramen ratio of 20%. It should be pointed out that these estimated artery lumen sizes are not real lumen sizes, and they are only used for estimating absolute nutrient artery perfusion rates of femora with more than one foramen.

In practice, it may be impractical to measure some foramina. For example, foramina may be fused with rocks on fossil bones. Blood flow estimation is affected if a fossil femur contains more than one foramen, and only the largest one can be observed. To investigate how much errors can be introduced if only the largest foramen areas are measured in femora with more than one foramen, 34 multiple-foramen femora were selected. Among these samples, 30 femora had two nutrient foramina, and four femora had three. On average, the largest foramen accounted for 68 ± 4.5 % of the summed foramen area of individual femur, ranging from 44–90 %. Considering only femora with two foramina, their largest foramen accounted for 70 ± 4.5 % of the summed foramen area (n = 30), and it was significantly higher than the 53 ± 9.9 % estimated from femora with three foramina (n = 4). To compare differences between blood flow estimated from summed foramen areas and from the largest foramen areas, we use the average lumen/foramen ratio of 20% and equation (1) described above, to

estimate blood flow. Assuming blood flow estimated from the summed areas as 100 % blood supply, blood flow estimated from the largest foramen contribute 63 ± 5.3% of the blood flow, ranging from 34–87 %. If only femora with two foramina are considered in the calculation, the value is 63 ± 5.3 %, which is significantly higher than the 43 ± 10 % found in femurs with three foramina. Therefore, foramina which have been missed during measurement can lead to severe underestimation of femoral bone blood flow. The impact increases as the missing foramen number increases. In addition, the lumen/foramen ratio of 20% was used to estimate blood flow rates in the largest foramen, as we assume the largest foramen as the only foramen on the femur shaft. However, the lumen/foramen ratio in the largest foramen of a multiple-foramen femur can vary, and it would introduce more errors into the blood flow estimation. To obtain accurate femoral bone blood flow, foramen numbers need to be carefully identified for each bone specimen.

In conclusion, lumen/foramen ratio of nutrient foramina and nutrient artery is 23.0 ± 3.8 % for all foramina containing arteries. For femora with one nutrient foramen, the ratio is 20.0 ± 3.2 %. The vascular contrast technique seems capable of estimating flow rates by imaging nutrient arteries, as estimated blood flow rates are not significantly different from flow rates collected from the fluorescent microsphere technique. Blood flow rates in the nutrient arteries tend to be higher in laying hens than in non-laying hens, albeit not significantly, but consistent with significant differences in rates measured with microspheres. This may be related to extra calcium mobilization during laying periods. Nutrient artery locations and nutrient foramen shapes across chicken individuals can vary, therefore the size relationship between the foramen and occupying vessels requires further investigation. Nutrient foramen numbers and sizes need to be carefully determined for each bone specimen to avoid underestimation of blood flow.

4.7. Acknowledgements

4.8. Supplementary material

4.8.1 Comparison of arterial size measurements from CT scanning with contrast medium and histological sectioning

It is impractical to harvest and cannulate femoral nutrient arteries from chickens due to their small sizes. Therefore, we were not able to compare the femoral nutrient artery sizes collected from both micro-CT scanning and histological sectioning. To compare vessel size difference between vascular contrast and histological sectioning methods, common carotid artery bifurcations of 9 non-laying hens, 10 laying hens and 6 roosters were harvested within 30 min after sacrificing the chickens during the fluorescent microsphere experiments (Nelson, 2021). The external carotid artery (ECA) and internal carotid artery (ICA) of the bifurcation were both ligated using suture (Figure S1). Vinyl tubing (internal diameter: 0.5 mm; external diameter: 0.9 mm) was inserted via the common carotid artery up to the bifurcation, sutured and glued in place. Saline solution flushed any remaining blood out of the bifurcation via the tubing. The bifurcations were placed into a 4 ml vial with 10 % formalin, while 10 % formalin was instilled into the bifurcation via the tubing under physiological pressure, using the same set up as described before in Chapter 4. Under these conditions, the arteries expanded to a size similar to that in the living animal. After fixation, the tubing was removed, and the bifurcations were preserved in 10 % formalin. 1–2 days before histological study, the ICAs were sectioned from the bifurcations and placed into 70% ethanol. Artery sections were place vertically with cross-sections facing upwards. Appropriate sizes of vinyl tubing were placed into the artery lumina to maintain shape of the arteries and avoid vessel collapse. External diameters of the vinyl tubing were slightly shorter than the internal diameter of the vessels, so that the tubing could not touch the vessel inner wall. During embedding, vessels were removed from the tubing and embedded in paraffin. Three, 7 µm thick, serial sections at three levels along an artery with 50 µm increase were sectioned out using a rotary microtome (Figure S1). A cold water bath was used to reduce vessel wall layer separation. Masson's trichrome was used to stain the arteries, to distinguish different artery wall layers. Photos of ICAs were taken using a stereo microscope (VMZ 1x-4x, Olympus, Japan) connected to a 5MP digital imager (#44422, Celestron, USA) and a computer. Inner perimeters of the arteries were measured using Fiji and were converted into vessel inner radii and areas. Lamellar unit layer number

114

in each ICA wall media was counted using a light microscope (Z2197, Olympus, Tokyo, Japan) connected to a 5MP digital imager (#44422, Celestron, USA) and a computer.

Common carotid artery and brain vasculature of 6 non-laying hens, 7 laying hens and 6 roosters were perfused using BriteVu under physiological pressure. The surgical procedures involved are similar to the procedures described in Chapter 4.
The bifurcation was identified and the same ICA region (Figure S1 and Figure S5) was collected using both DataViewer and Fiji, and the areas were converted to lumen radii.
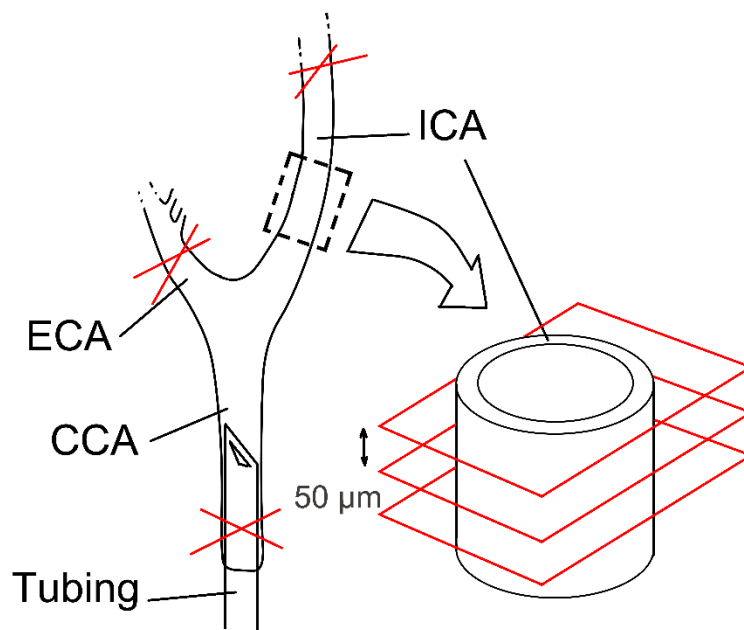
Figure S1. Schematic diagram of common carotid bifurcation cannulation and histological sectioning of an internal carotid artery. Red crosses represent locations that require ligations. Black dotted-lined square represents the location of collected ICA sections. Red squares represent histological cross sections.

Mass-independent areas of ICA lumina at common carotid artery bifurcation were compared among three chicken groups using ANOVA and between vascular contrast and histological sectioning technique using t-test in a statistical software (Prism6.0; GraphPad Software, La Jolla, CA, USA). The way to calculate mass-independent areas and radii is described in Chapter 4. Numbers of ICA Lamellar unit were

averaged from both left and right arteries and compared among three chicken groups using ANOVA test. Error statistics are 95 % confidence intervals (CI).

There is no significant differences in both internal carotid artery (ICA) areas and radii among three chicken groups using either technique (Figure S2 & S3).
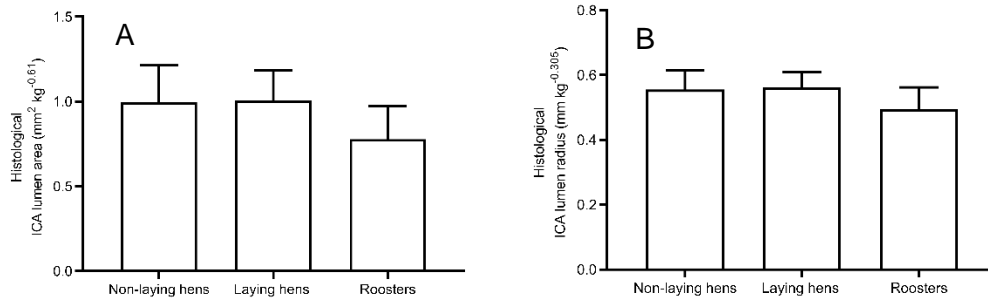
Figure S2. Mass-independent areas (A) and radii (B) of ICA lumina measured from histological artery sections among three chicken groups. Error bars represent 95 % CI of the means.
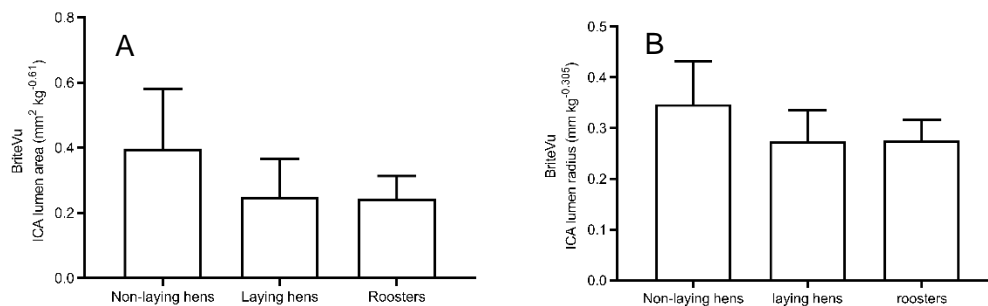
Figure S3. Mass-independent areas (A) and radii (B) of ICA lumina measured from artery lumens filled with BriteVu among three chicken groups. Error bars represent 95 % CI of the means.

However, ICA cross-sections of the histological chicken at common carotid bifurcation have significantly larger mass-independent lumen areas (0.95 ± 0.11 mm^2 kg$^{-0.61}$) and radii (0.54 ± 0.030 mm^2 kg$^{-0.61}$) compared to the areas (0.29 ± 0.069 mm^2 kg$^{-0.61}$) and radii (0.30 ± 0.034 mm^2 kg$^{-0.61}$) measured from ICA lumens filled with BriteVu (Area: $P < 0.0001$; Radius: $P < 0.0001$) (Figure S3). Average histological

116

ICA lumen radius at the bifurcation is 0.63 mm, which refers to 10.4 ml min^{-1} of blood flow, according to a empirical equation that describes the relationship between the artery lumen radii and absolute blood flow rates (Seymour et al., 2019b). The average BriteVu ICA lumen radius is 0.35 mm, which only represents 2.5 ml min^{-1} of blood flow. The predicted blood flow rates represent an approximate five times difference between the two methods (Figure S4). Since there are no in *vivo* chicken ICA lumen size or blood flow data at carotid bifurcation available to compare with, no conclusion can be made in regard to the data accuracy.
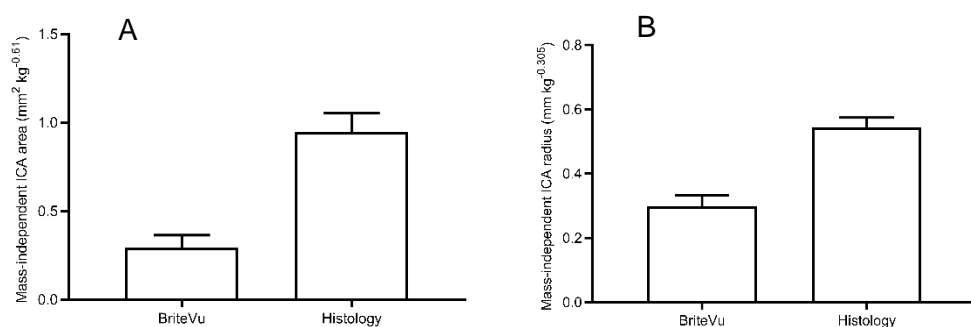
Figure S4. Chicken mass-independent ICA areas (A) and radii (B) collected using vascular contrast (BriteVu) and histological sectioning. Error bars represent 95% CI of the means. Data collected by the two methods necessarily involved different chicken individuals.

However, we are certain that the BriteVu ICA lumen size data collected are not precise, as some ICA at the bifurcation have non-circular cross sections, suggesting they were not pressurized properly. A study measured ICA lumen sizes in the internal carotid foramina from the same chicken individuals (Nelson, 2021). As an ICA runs from the bifurcation and through the internal carotid foramen, three arteries branch off the ICA (Figure S5). Despite a large ICA size variation at carotid bifurcation (mean area with 95% CI: 0.4 ± 0.085 mm^2), size variation in internal carotid foramina is small (mean area with 95% CI: 0.18 ± 0.022 mm^2) collected from the same individuals (Nelson, 2021). This provides another piece of evidence related to Chapter 4 that large arteries were not properly pressurized with BriteVu, and it might cause vessel constriction. Same phenomenon can also be observed in chicken ischiadic arteries. Nine ischiadic artery lumen areas from five laying hens were measured, and

the areas vary from 0.76–3.1 mm^2. Average area is 2.0 ± 0.58 mm^2, showing a large size variation

Histological ICA lumen sizes collected in this study do not refer to actual lumen sizes as the walls seem overly stretched (Figure S6). Total ICA wall thickness was not able to be measured because a great proportion of vessels had wall separation problem during histological embedding and sectioning processes. The average number of ICA medial lamellar unit layers of all three chicken groups is 11.0 ± 0.34. There is no significant difference in layer numbers among three chicken groups. The lamellar units in our specimens were overly stretched, and there are overlay of units and broken units persist in the samples (Figure S7). These issues affect the counted numbers to some extent. However, even with these issues, the layer number variation for all ICA specimens is small. Despite of species body mass, lamellar unit number in mammalian aorta can be seen as proportional to the aorta lumen diameter (Wolinsky and Glagov, 1967). Our histological ICA has consistent number of lamellar units, but larger lumen size variation, therefore the histological ICA sizes collected in our study do not represent accurate artery sizes.
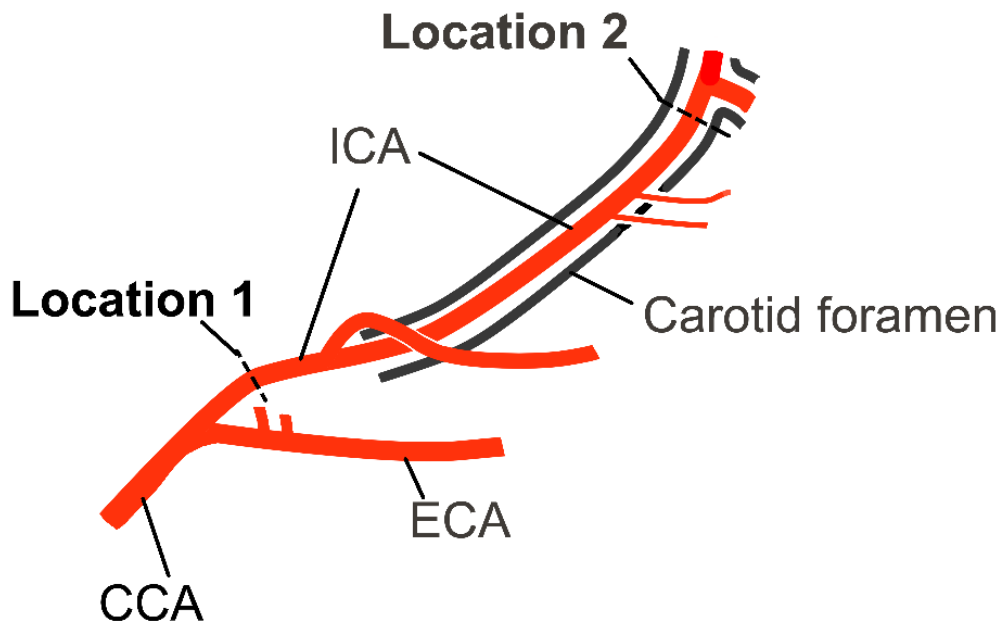
Figure S5. Diagram of internal carotid artery (ICA) pathway from the common carotid artery bifurcation to the carotid foramen. Location 1 represents the location of ICA sections collected for histological ICA lumen area analysis. Location 2 represents the location of ICA sections measured using vascular contrast method. (CCA: common carotid artery, ECA: external carotid artery).

Figure S6. Varied sizes of histological internal carotid artery cross-sections at the common carotid artery bifurcation. The scale represents 0.5 mm.
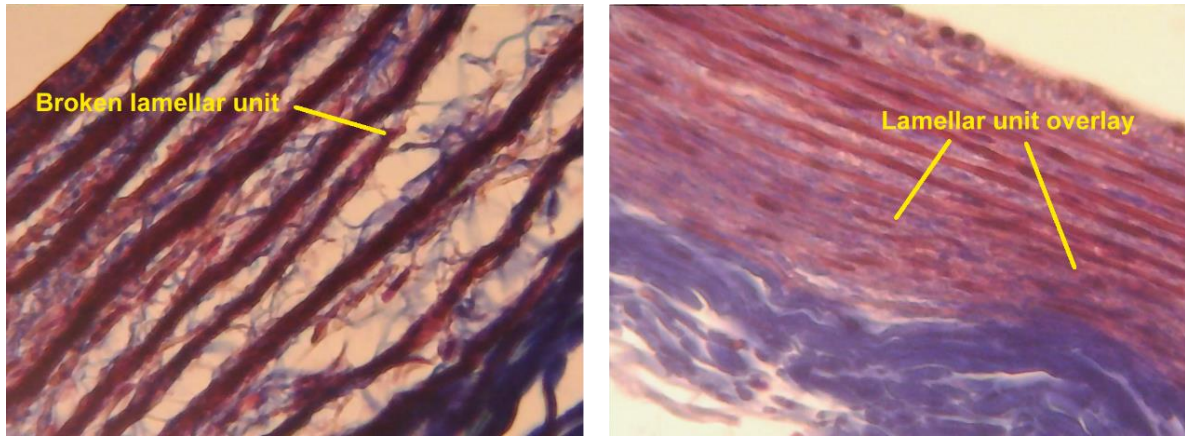
Figure S7. Microphotographs of lamellar unit in internal carotid artery media of chickens.

4.8.2 Femoral shaft blood flow rate comparison between vascular contrast and microsphere infusion methods

Figure S8A & B show another way of comparing the blood flows collected from both vascular contrast and fluorescent microsphere technique on a graph. This way of comparison gives a more direct visual and intuitive comparison between the two methods. Nutrient artery blood flow rates were collected using a vascular contrast method, and femur shaft blood flow rates were collected using a microsphere infusion method. Absolute or mass-independent blood flows in the nutrient artery and femur shaft were plotted on both axes. Blood flows estimated from both methods among three chicken groups locate close to the line of identity. Both vascular contrast and fluorescent microsphere method thus seems capable of providing similar results in regards to measuring absolute blood flow rates through femur shafts.
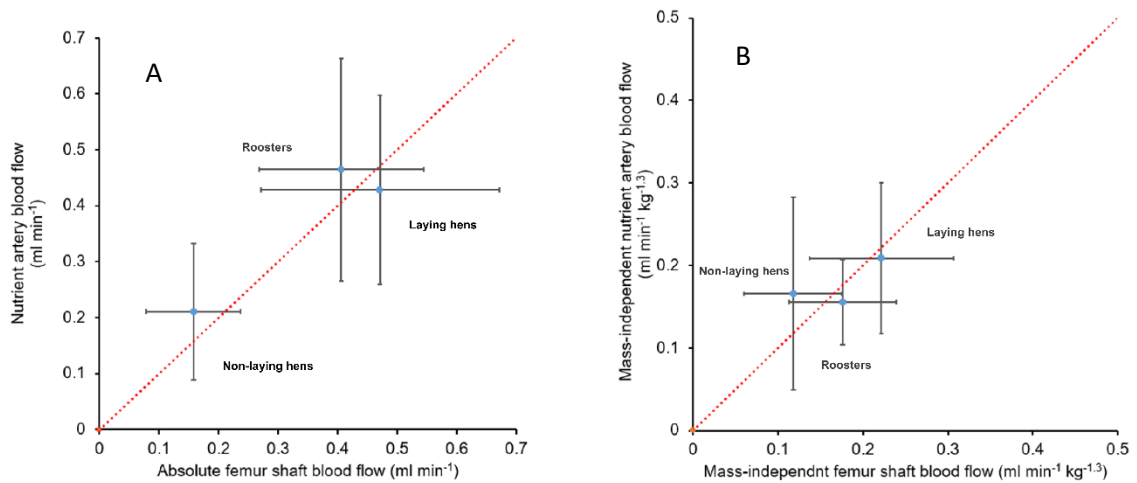
Figure S8. Comparison of nutrient artery blood flows and femur shaft blood flows among non-laying hens, laying hens and roosters between vascular contrast and fluorescent microsphere technique. Absolute flow rates are shown in panel A and mass-independent flow rates are shown in panel B. Red dotted line represents the line of identity (Y = X). Error bars represent 95% CI of the means.

Chapter Five: Femoral bone blood flow in extant and extinct cursorial birds

Statement of Authorship

Title of Paper	Femoral bone blood flow in extant and extinct cursorial birds
Publication Status	Unpublished and Unsubmitted work written in manuscript style
Publication Details	

Principal Author

Name of Principal Author (Candidate)	Qiaohui Hu		
Contribution to the Paper	Analysed data, wrote the initial manuscript draft, and reviewed and edited subsequent drafts.		
Overall percentage (%)	60%		
Certification:	This paper reports on original research I conducted during the period of my Higher Degree by Research candidature and is not subject to any obligations or contractual agreements with a third party that would constrain its inclusion in this thesis. I am the primary author of this paper.		
Signature		Date	10/11/2020

Co-Author Contributions

By signing the Statement of Authorship, each author certifies that:

i. the candidate's stated contribution to the publication is accurate (as detailed above);

ii. permission is granted for the candidate in include the publication in the thesis; and

iii. the sum of all co-author contributions is equal to 100% less the candidate's stated contribution.

Name of Co-Author	Miller, C. V		
Contribution to the Paper 25%	Data collection		
Signature		Date	17/11/2020

Name of Co-Author	Roger S. Seymour		
Contribution to the Paper 15%	Provided advice, reviewed and edited manuscript drafts.		
Signature		Date	20/11/2020

5.1. Abstract

A recent regional blood flow estimation method called the 'foramen technique' measures foramen sizes in bones to estimate vessel sizes, as blood flow rates determine blood vessel and foramen sizes. This technique is a useful tool to examine blood flow rates of extinct animals without knowing the blood vessel sizes. However, it is often difficult to measure the foramen sizes on fossilized bones, as the foramina can be filled with mineral matrix. This study estimated femoral bone blood flow of 17 extinct cursorial bird species by measuring femoral nutrient foramen openings of 22 femora in fossil bones. The blood flow values are combined and compared with a previous foramen study on extant and extinct cursorial birds. The results revealed that the scaling of femoral bone blood flow relative to body mass of extinct cursorial birds has a higher scaling exponent than extant cursorial birds. This difference may relate to flightlessness and total reliance on cursorial exercise, resulting in larger femora and larger foramina. This study provides an example of the 'foramen technique' being applied to fossil femora to estimate femoral bone blood flow, and in turn metabolic activity, of extinct animals.

5.2. Introduction

Studying physiologies of extinct animals allows us to hypothesize how they lived, behaved and evolved. It builds up the knowledge of the old, unfamiliar world. However, physiological function can only be inferred from fossil bones, as not many other tissues of extinct animals are well preserved, especially in vertebrates. Fossil bones can indicate the size and weight of the animal, and surface features such as muscle insertions can provide abundant information about functional morphology and behaviour. A recent method, called the 'foramen technique', is able to relate animal physiologies to regional blood flow through observing bone samples. This technique estimates a bone perfusion rate by simply measuring bone foramen size. The theory behind this technique is that the energy requirements of regional tissues determine the blood flow rates to them (Wolff, 2008). Blood flow rates in turn determine the sizes of the arteries (Seymour et al., 2019b). Where arteries pass through bone, the size of the foramen can be used to evaluate blood flow rate, thus a larger foramen indicates a higher blood flow rate and inferred higher metabolic rate. This technique was first described to relate femoral nutrient foramen sizes to locomotor activity levels of animals (Seymour et al., 2012). Since then, additional studies have used the foramen technique to investigate the relationship among regional blood flow rate, local tissue metabolism and foramen size (Allan et al., 2014; Boyer and Harrington, 2018; Boyer and Harrington, 2019; Seymour et al., 2015; Seymour et al., 2016).

The 'foramen technique' provides us an opportunity to look into extinct animals' blood flow rates without preservation of any soft tissues such as blood vessels. Moreover, the estimated regional blood flow rates can be associated with extinct animals' metabolism, lifestyles and habitat. It is often difficult to apply the 'foramen technique' to fossil bones, because their foramen passage may be filled with mineral matrix, and only the external openings of the nutrient foramina can be observed. In addition, the dense matrix makes it difficult for micro-CT scanning to distinguish foramen passages within fossilized bones due to low imaging contrast. Seymour et al. (2012) was the first study to apply the 'foramen technique' to extinct dinosaurs, which had relatively larger femoral nutrient foramina compared to extant mammals, revealing that they probably had a higher femoral bone blood flow rate, and consequently were probably very active animals. If the rate of blood flow is unchanged, a larger foramen or artery size may refer to a lower arterial blood

pressure. However, Seymour (2016) showed that some dinosaurs had high blood pressure and high oxygen demand. Allan et al. (2014) followed with a study of living birds and recently extinct moa, finding that the foramina indicated bone perfusion rates largely overlapping data from mammals. Allan's study also indicated that the estimated femoral bone blood flow was 1.9 times higher in bipedal cursorial birds than in quadrupedal mammals, supporting the theory that blood flow is related to locomotory stresses and bone repair (Lieberman et al., 2003; Robling et al., 2006).

To investigate levels of femoral bone blood flow in extinct cursorial birds, and to apply the 'foramen technique' on foramen samples with viewing difficulties, this study estimated femoral bone blood flow from 25 femora of 19 extinct cursorial bird species. Allan et al. (2014) reported femoral bone blood flow values of both extant and extinct cursorial birds. To examine if there are differences in femoral bone blood flow between extinct and extant cursorial birds, estimated values of extinct cursorial birds between our and Allan's study were compared with values from the extant cursorial bird species.

5.3. Methods

Extinct cursorial bird species were selected from the Smithsonian National Museum of Natural History. All species were cursorial birds living in period between the Upper Cretaceous and Quaternary (Table S1). Five extinct bird species had femur pairs, while the others had only one femur preserved. Mid-shaft circumferences (C_f, mm) of the femora were measured using a measuring tape. Femur lengths (L, mm) were measured using electronic callipers for specimens up to 150 mm and a tape measure for those larger. Photos of the foramen external openings with a scale next to and level with them were taken using a macro lens. Best-fit ellipses were drawn to outline the external opening areas of the foramina in Fiji (Open Source, www.fiji.sc), and the foramen dimensions including major diameter, minor diameter and foramen area were recorded (Figure 1).
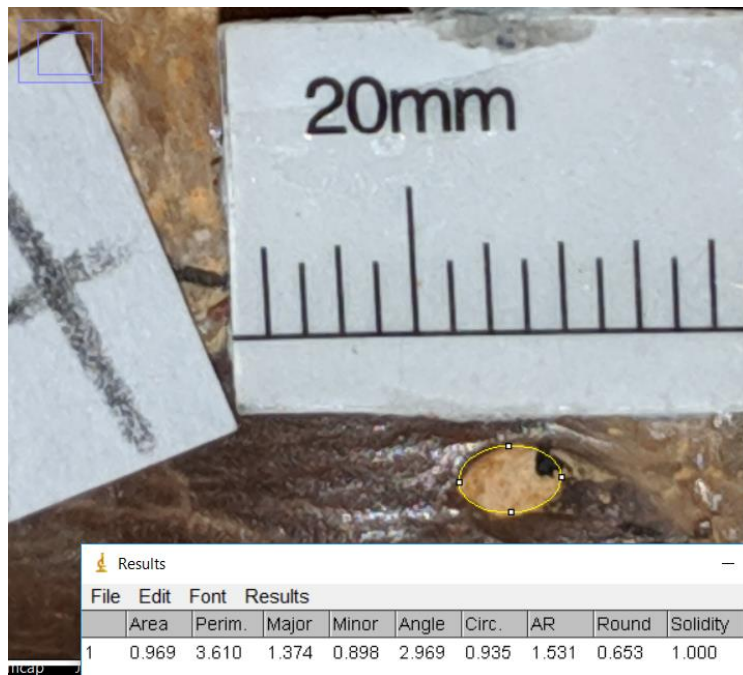
Figure 1. A scaled image of a foramen external opening of a *Hesperornis regalis* femur. The best-fit ellipse of the foramen external opening area was measured in Fiji. Values including area, major and minor diameters of this ellipses were recorded. The smallest scale increment represents 0.5 mm.

5.4. Statistical analysis

As in Allan et al. (2014), body mass (M_b, g) of our extinct cursorial birds was estimated by averaging the values calculated from three body mass estimation equations based on femur length (Prange et al., 1979) and circumference (Campbell and Marcus, 1992; Dickison, 2007). Foramen radii were calculated from minor diameters of the foramen external openings (see Discussion for rationale). If an individual bird had both femora, foramen radii and body masses were estimated and averaged from both femora. Femoral bone blood flow index indices (Q_i, mm^3) were calculated based on femur lengths (L, mm) and foramen radii (r_o, mm) according to a blood flow index equation ($Q_i = r_o{}^4/L$). The equation is based on Poiseuille's Law and provides a value that is proportional to actual blood flow rate, according to scaling assumptions presented earlier (Seymour et al., 2012).

If a femur had more than one foramen, the Q_i value of this femur is calculated by summing the Q_i value of each foramen. Among our extinct cursorial birds, seven species are moa, with two species (*Pachyornis elephantopus* and *Emeus crassus*) also

127

involved in Allan et al.'s study. Q_i values for the eight moa species reported by Allan et al. (2014) were combined with our extinct cursorial dataset. Body mass and Q_i values of *Pachyornis elephantopus* and *Emeus crassus* were averaged from twoAllan's and our studies. The scaling relationship of Q_i on M_b of all 25 extinct cursorial birds and the 13 extant cursorial birds reported by Allan et al. (2014) were plotted onto a double log axes graph in statistical software (Prism 6.0; GraphPad Software, La Jolla, CA, USA). The scaling of Q_i on M_b between extant and extinct cursorial bird species were compared using Analysis of Covariance (ANCOVA) statistical test (Zar, 1998). Most extinct birds in this study were flightless birds. Although the flying ability of some extinct birds such as Lithornithids and Hesperornithids is still in debate (Altimiras et al., 2017; Bell and Chiappe, 2020), here we classified Lithornithids including *Lithornis* and *Paracathartes* as flighted birds and Hesperornithids as flightless birds. The classification of flighted and flightless birds is presented in Table S1 and S2. Among the 13 extant bird species, 10 of them have the ability to fly. ANCOVA was also used to compare the Q_i difference between flighted and flightless cursorial birds. If ANCOVA revealed significantly different scaling exponents between two datasets, the ranges over which the data were significantly different between the two datasets were tested using the Johnson-Neyman test (White, 2003). A polynomial equation was also used to indicate the relationship between log Q_i and log M_b of all 37 cursorial birds. 95% confidence interval bands were plotted onto all figures with GraphPad software.

5.5. Results

The estimated body masses of the extinct cursorial bird range from 0.7 kg to 411 kg, which represents a 586-fold range. Body masses of the extant cursorial birds range from 67.5 g to 40.6 kg, which represents a 601-fold range. Femoral bone blood flow index (Q_i) of extinct cursorial birds scales with body mass to the 1.11 ± 0.37 power, which is significantly higher than the scaling of Q_i of extant cursorial birds (0.53 ± 0.43) ($F_{1, 34} = 4.74$; $P = 0.04$) (Figure 2). The Johnson-Neyman test found that extinct cursorial birds with body masses lighter than 5.5 kg have Q_i that are not significantly different from the extant cursorial birds. Above 5.5 kg, Q_i in extinct species is significantly higher.
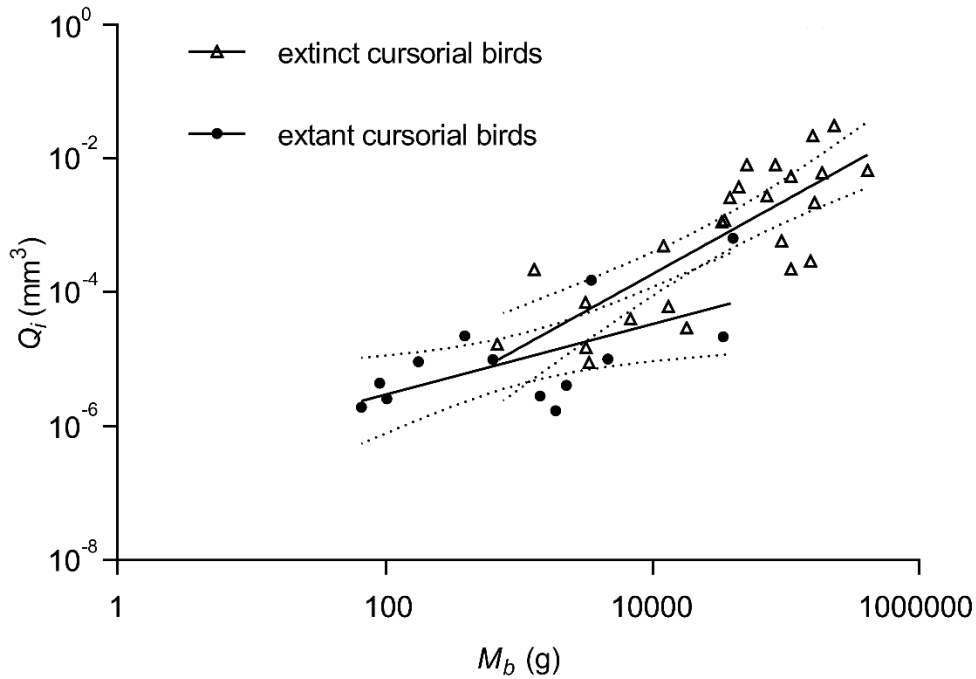
Figure 2. Relationships between femoral bone blood flow index (Q_i) and body mass (M_b) in extant and extinct cursorial birds. Extant cursorial birds are represented by black dots ($Q_i = 2.55 \times 10^{-7} M_b^{0.53 \pm 0.43}$) and extinct cursorial birds are represented by hollow triangles ($Q_i = 6.66 \times 10^{-9} M_b^{1.11 \pm 0.37}$). The dotted lines refer to 95% confidence intervals for each regression mean.

Q_i of flightless cursorial birds scales with body mass to the 1.41 ± 0.45 power, which is also significantly higher than the scaling of Q_i of flighted cursorial birds (0.45 ± 0.60) ($F_{1, 34} = 7.10$; $P = 0.01$) (Figure 3). The Johnson-Neyman test revealed that flightless cursorial birds with body masses range from 316 g to 106 kg have Q_i values that are not significantly different from values of the flighted cursorial birds.
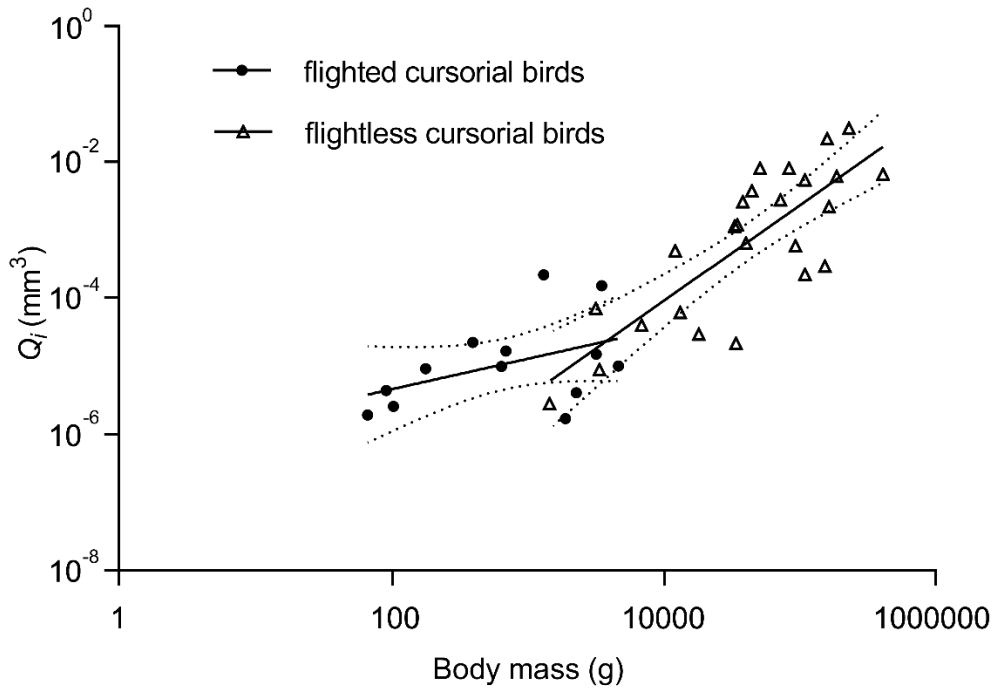
Figure 3. Relationships between femoral bone blood flow index (Q_i) and body mass (M_b) in extant flighted and flightless cursorial birds. Flighted birds are represented by black dots ($Q_i = 5.71 \times 10^{-7} M_b^{0.45 \pm 0.60}$) and flightless birds are represented by hollow triangles ($Q_i = 2.13 \times 10^{-10} M_b^{1.41 \pm 0.45}$). The dotted lines refer to 95% confidence intervals for each regression mean.

If we consider all cursorial bird data as a whole dataset and plot onto double-logged scales (Figure 4), a second-order polynomial equation fits the data slightly better ($R^2 = 0.75$) than a linear regression (log $Q_i = 1.03$ log M_b - 7.91) ($R^2 = 0.72$).

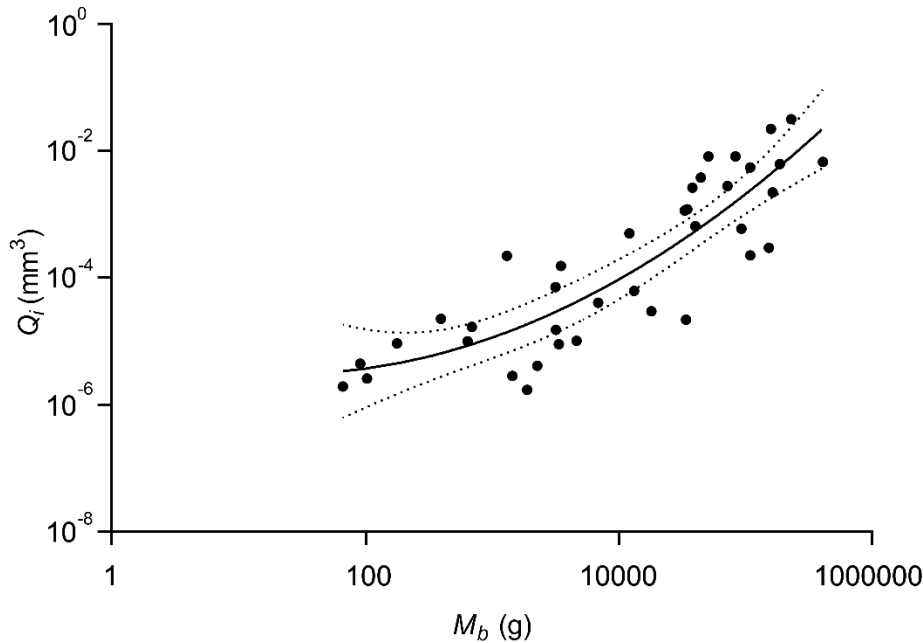**Figure 4. Relationships between femoral bone blood flow index (Q_i) and body mass (M_b) in extant and extinct cursorial birds.** Extant and extinct species are represented with black dots (log Q_i = 0.21 (log M_b)^2 - 0.59 log M_b -5.12). The dotted lines refer to 95% confidence intervals for the regression mean.

5.6. Discussion

The scaling of femoral bone blood flow index (Q_i) on body mass (M_b) in extinct cursorial birds yields an exponent of 1.35 ± 0.44, which is significantly steeper than in extant cursorial birds (0.53 ± 0.43) (Figure 2). In other words, as body mass increases, the increase in femoral blood flow rate in extinct cursorial birds is higher than predicted by extant cursorial birds. The comparison between the scaling of Q_i on M_b of flighted and flightless cursorial birds also shows similar results, with the flighted birds having a low exponent of 0.37 ± 0.61, and the flightless birds having a significantly higher exponent of 1.43 ± 0.41 (Figure 3). The scaling of Q_i in flighted birds has a wide 95% confidence interval band due to small sample size and narrow range of M_b. The higher exponent of the studied extinct cursorial birds could be related to the obligate cursoriality in larger species. In this study, the larger cursorial birds are mostly flightless birds. Most extant cursorial birds analysed in this study have smaller body masses and have the ability to fly (Table S2). Because the power required for flight scales with a higher exponent than the metabolic power available

131

for flight (Pennycuick, 1972; Tobalske, 2016), there is a upper limit to body mass seen in extant flying birds (12 –20 kg) (Calder, 1996). Specialized gliding flight, which extracts energy from the atmosphere, is believed to be the only way extinct birds larger than this could fly (Chatterjee et al., 2007; Ksepka, 2014). No extinct taxa included in this study display adaptations for gliding flight. The Johnson-Neyman test found that flighted and flightless cursorial birds with body mass range ranging from 316 g to 106 kg not having significantly different Q_i values. This broad body mass range may be due to small number of data points and narrow body mass range of the extant flighted, but predominantly cursorial birds. Extant birds such as ratites have lost their ability to fly and have evolved heavy body masses. Therefore, larger cursorial birds may rely more on femora during daily activities than smaller species, and consequently their femora would be expected to be larger in cross-sectional area. To test this, we estimated femur cross-sectional area from mid-shaft circumference of 17 extinct cursorial bird species, and compared the results to expected isometric scaling. Isometrically, any length scales with M_b to the 0.33 power, thus any area scales with M_b to the 0.67 power. The scaling of cross-sectional area on M_b has an exponent of 0.80 ± 0.04, which is significantly higher than 0.67 (Figure 5). Therefore, apart from flying ability, larger cursorial birds may also require stronger and larger femora not only to support their body masses to against gravity but also to deal with dynamic stresses during locomotion. A larger femur will require a higher blood perfusion to support and maintain bone health. In addition, lack of flying ability causes more loading stresses to be applied in femora of larger cursorial birds. This will lead to a higher frequency of microfractures on bones, which will result in a higher femoral bone blood flow to repair the damage. As the increase in Q_i in larger cursorial birds is higher than smaller species, a second-order polynomial equation, rather than a linear equation is more suitable to describe the relationship between log Q_i and log M_b, with the tangent (equivalent to the scaling exponent) being steeper as the body mass increases (Figure 4).
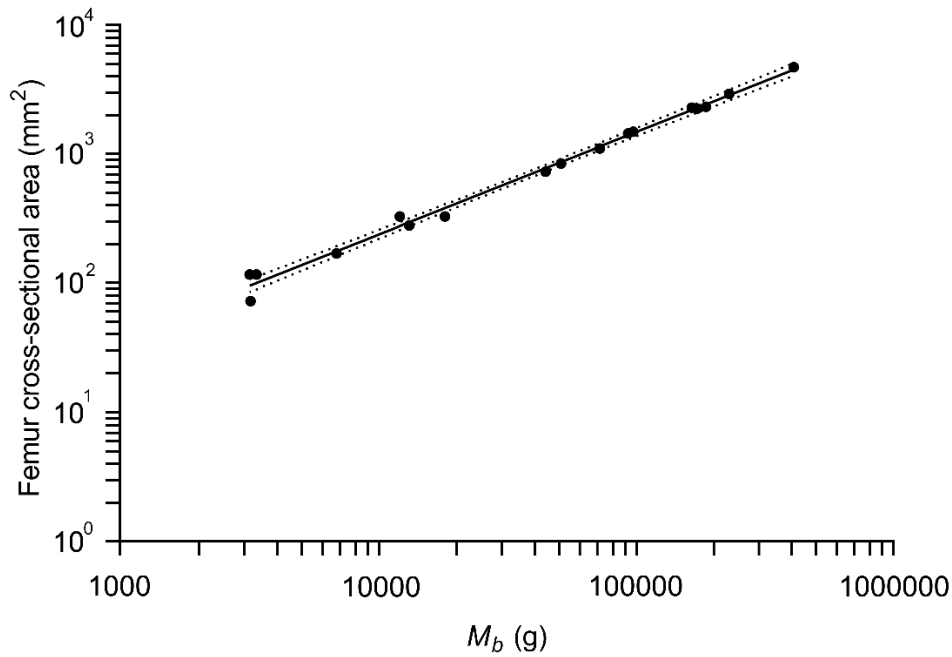
Figure 5. Relationships between femoral cross-sectional area and body mass (M_b) in extinct cursorial birds. Trend line equation is $Q_i = 0.15 M_b^{0.80 \pm 0.04}$. The dotted lines are 95% confidence intervals for the regression mean.

The present analysis necessarily uses measurement approaches that are the same as in previous studies for comparative purposes. However, we now understand the errors that earlier simplifications and assumptions might produce, investigated by Hu et al. (2020). Arteries and veins usually pass through bones at an angle and are often curved inside the cortical bone. A foramen passage, then, is not a perfect cylinder, and the cross-sectional areas along a foramen passage are not constant. The minimum area along a foramen passage is thought to be the most accurate way to predict the sizes of occupying vessels. However, this study could only measure foramen dimensions from the external openings. Measuring minor radius of the external opening of fossilized foramina is better than major radius or area to represent occupying vessel sizes, because it represents an imaginary cylindrical tube entering the bone at an angle. We assume the radii estimated from the external foramen opening are similar to the radii estimated from the minimum cross-sectional area along a foramen passage in femoral nutrient foramina. This is because the minimum cross-sectional area of a femoral nutrient foramen is often located very close to the external foramen opening, based on our previous observations. Therefore, we consider the 'foramen technique' to be

133

applicable to fossil femora. The relationship between log Q_i and log M_b of all cursorial birds (Figure 4) can thus be used for comparing Q_i values of other cursorial birds, no matter if they are extinct or not.

In summary, the increase in femoral bone blood flow of extinct cursorial birds is more sensitive to the increases in body mass than extant cursorial birds, likely due to many of the extinct birds included in this study having large body masses, which limit their flight ability and result in more stresses applied to their femora during locomotion. Larger extinct cursorial birds also require a higher femoral bone perfusion to support their enormous femora. This study also indicates that the 'foramen technique' is capable of estimating femoral bone blood flow indices from fossil femoral bones. The scaling relationship between estimated femoral blood flow indices and body masses in both the extinct and extant birds can be described using a single equation.

5.7. Acknowledgements

5.8. Supplementary material

Table S1. Femur and femoral nutrient foramen size values, femoral bone blood flow indices (Q_i), flying ability and museum accession numbers of 19 extinct cursorial birds collected from Smithsonian National Museum of Natural History.

Species	Foramen area (mm²)	Major radius (mm)	Minor radius (mm)	Midshaft circumference (mm)	Femur length (mm)	Q_i (mm³ × 10⁻⁶)	Flighted or not	Museum accession number
*Aepyornis maximus**	9.00; 1.83	2.41; 0.91	1.19; 0.64	242	332	6524	No	490397
Aepyornis sp.	11.71	2.10	1.77	191	316	31095	No	3013
Anomalopteryx fortis	5.92	1.97	0.96	95	230	3702	No	6618
Anthropornis nordenskjoeldi	0.24	0.29	0.26	46	120	39.6	No	402669
Baptornis advenus	0.13	0.27	0.16	38	69	8.81	No	244155
Diatryma sp.	5.03	1.33	1.20	170	348	6049	No	15118
Dinornis gracilis	2.40	1.24	0.61	134	244	583	No	7142
Dinornis ingens	4.91	1.78	0.88	169	274	2159	No	7187
*Emeus crassus**	6.63; 4.22	1.83; 1.35	1.16; 1.00	136	252	11035	No	2290
Hesperornis regalis	1.09	0.76	0.46	64	88	490	No	13580
Hesperornis sp.	0.28	0.36	0.25	38	56	70.2	No	244158
Lithornis plebius	0.20	0.37	0.18	18	58	16.4	Yes	336534
Lithornis promiscuus	0.72	0.70	0.33	26	52	216	Yes	336535
Megalapteryx huttonii	5.81	1.58	1.17	103	232	8045	No	6610
Meionornis casuarinus	4.25	1.51	0.89	117	255	2728	No	2279, 7140
Pachyornis elephantopus	15.49	2.64	1.88	168	320	39122	No	2278, 6590
Paracathartes howardae	0.13	0.21	0.20	30	109	14.7	Yes	361412
Pezophaps solitaria	0.31	0.36	0.27	64	184	29.3	No	7122
Raphus cucullatus	0.53	0.54	0.31	59	152	60.4	No	22554

Species with * refer to femur samples having two foramina. Foramen area, major and minor radius of each foramen of the femur are listed in the table.

Table S2. Body masses and femoral bone blood flow indices (Q_i) and flying ability of 13 extant cursorial birds and 8 extinct moa species (Allan et al., 2014).

Extant species	Body mass (g)	Q_i (mm^3 × 10^{-6})	Flighted or not
Alectura lathami	2300	4.03	Yes
Ardeotis australis	4683	9.97	Yes
Burhinus grallarius	648	9.79	Yes
Casuarius casuarius	40600	637	No
Coturnix pectoralis	105	2.52	Yes
Dromaius novaehollandiae	34233	21.3	No
Eudyptula minor	1467	2.79	No
Gallinula ventralis	400	22.1	Yes
Gallirallus philippensis	180	9.01	Yes
Leipoa ocellata	1917	1.66	Yes
Meleagris gallopavo	3525	151	Yes
Pedionomus torquatus	68	1.89	Yes
Turnix varius	93	4.35	Yes
Extinct species			
Anomalopteryx didiformis	34963	1184	No
Dinornis robustus	154140	289	No
Dinornis struthoides	110289	221	No
Emeus crassus	70419	5008	No
Euryapteryx curtus	33544	1128	No
Euryapteryx gravis	109946	5371	No
Megalapteryx didinus	34962	1184	No
Pachyornis elephantopus	146610	4610	No

Chapter Six: Conclusion

Significance and contribution

Regional blood supply is associated with regional tissue oxygen requirement, thus by studying animal regional blood flow, we are able to get insight into their regional metabolic demands in relation to physiological processes. It can also improve the understanding of how animals interact with their environment. Measuring regional blood flow is challenging, especially in small vessels. The foramen technique can estimate regional blood flow rate of arteries passing through foramina. It allows us to estimate blood flow from foramen sizes without knowing the actual blood vessel sizes. In addition, this technique does not require more complex work on blood flow of living animals. However, foramen size is not the same as the size of the occupying vessels. Prior to estimating absolute blood flow rates using the foramen technique, the knowledge of foramen and vessel morphologies and sizes are required. The major aims of the experiments conducted in this thesis are to investigate how foramen size relates to vessels size and regional blood flow rate, and to improve this foramen technique for further regional blood flow studies. This goal was achieved with a combination of methods involving microphotography, micro-CT scanning, impression material casting, fluorescent microsphere infusions and vascular contrast imaging.

In Chapter 2, I measured sizes of kangaroo femoral nutrient foramina, kangaroo vertebral foramina, human carotid foramina and artificial foramina using microphotography, micro-CT scanning and a newly invented method called impression material casting. Choosing which method to use depends on specimen conditions and the availability of tools, time and funding. The size values were compared among all three methods to determine specific advantages and disadvantages of each method. The results showed that all three methods are capable of accurately measuring foramen sizes. Microphotography is chosen to be the most preferable method, but its limitations and measurement errors need to be carefully addressed and minimized. Chapter 2 also developed a model based on the shear stress equation, to explore how radius, shear stress, wall thickness and blood viscosity affect estimated blood flow rates. The results indicated that radius has the largest impact on estimated blood flow rates, and this also highlights the importance of an accurate method for measuring foramen size.

Chapter 3 focused on the relationship between femoral nutrient foramen sizes and absolute rate of blood flow in the femoral bone of chickens. By using a fluorescent microsphere infusion technique along with reference blood withdrawal, the absolute femoral bone blood flow of chickens could be measured and compared with literature values. This study allowed me to compare the absolute bone blood flow rates with the blood flow indices obtained from the nutrient foramen sizes for the first time. This relationship in chickens was further compared with the femoral bone blood flow indices of other cursorial birds obtained from a previous foramen study. The absolute rate of blood flow in the femoral bone of cursorial birds match their maximum metabolic rates, which refer to their aerobic activity levels. Moreover, the chicken femoral bones were divided into three parts during the experiments to investigate blood flow distribution between the epiphyses and the shaft. The distributions in chickens was similar to that in rats, with higher blood flow supporting two femur ends compared to the shaft. The measurements of chapter 3 also compared femoral bone blood flow rates among non-laying hens, laying hens and roosters, to investigate the impacts of life stage and gender on femoral bone blood flow. The results revealed that extra calcium required for eggshell formation during the egg laying period may contribute to the extra blood flow demand of laying hens. Gender itself does not affect chicken femoral bone blood flow around sexual maturity.

The experiments conducted in Chapter 4 aimed to investigate femoral nutrient foramen shapes, morphologies and nutrient artery locations within the foramina. Both vascular contrast imaging and histological embedding and sectioning techniques were utilised in this chapter to achieve the goal. Using both vascular contrast and micro-CT scanning techniques allowed me to visualize and measure nutrient artery lumen sizes inside the nutrient foramina for the first time, despite their small sizes. More importantly, the lumen sizes are also useful for estimating the absolute nutrient artery blood flow rates, which can then be compared with the femur shaft blood flow rates collected from chapter 3. The two techniques resulted in similar values for blood flow rate. Micro-CT images of blood vessels filled with contrast media provide information about the blood vessel distribution surrounding a chicken femur. A chicken femur shaft can have more than one nutrient foramen and nutrient artery. Both the micro-CT images and histological sectioning of the nutrient foramen cross-sections indicated that the foramen cross-sectional areas and the passing vessels can vary among

individual femora. These observations showed that the size relationship between the femoral nutrient foramen and occupying vessels is much more complex than we thought. The percentage area of a nutrient artery within a nutrient foramen was estimated from femora with only one nutrient foramen, and this size ratio may able to apply to femora of other species. In addition, although the artery wall cannot be observed directly in micro-CT images, the inflated artery lumen is circular, so that wall thickness could be estimated from the minimum distance between the lumen and the foramen wall such that the entire "outer circumference" could be visualized.

Chapter 5 examined whether the 'foramen technique' can be applied to fossil bones and whether extinct and extant cursorial birds have different femoral blood flow rates. The results showed that the scaling of femoral bone blood flow on body mass in extinct cursorial birds has a higher exponent than in extant cursorial birds. The difference may be explained by total reliance on cursorial exercise and flightlessness in extinct cursorial birds. The study showed that the 'foramen technique' is able to estimate femoral bone blood flow values from fossilized femora.

Challenges during the studies
Although microphotography was selected to be the standard method for measurement foramen size, its limitations and measurement errors are more difficult to address, compared to the other methods. Unlike micro-CT or impression material casting, microphotography cannot "slice" a foramen passage into different sections. Numerous factors such as foramen shape, light angle, viewing angle and viewing distance can all affect the measured values. Despite the microphotographic method seeming to be the easiest foramen measurement method, skills are required to minimize the errors.

The microsphere technique requires withdrawing blood from the animal at a constant, known rate to calibrate the blood flow rates to perfused tissues. We decided to withdraw blood from the chickens' brachial arteries. However, without knowing the normal chicken brachial artery blood flow rate, it was difficult to set the withdrawal rate. Besides, cardiac output and blood flow distribution in chickens can be altered by surgical operations such as opening the chests and injecting anaesthetics (Fermoso et al., 1964; Raffe et al., 1993). Withdrawing a slightly higher rate of blood flow can lead to vessel collapse, which results in an inaccurate number of fluorescent

microspheres in the withdrawal blood. This problem led several times to experimental failures during the study. Blood flow rates of the same region among different sized animals can also be different. We struggled to find the suitable withdrawal blood flow rate and we ended up using two different rates. This is because one withdrawal rate, which was successfully applied to chickens with relatively larger body sizes, were not applicable for some smaller-sized chickens. Therefore, we set up another lower withdrawal blood flow rate for some of the smaller chickens.

Wall thickness to lumen radius ratio for the human internal carotid artery (ICA) was determined to be 0.3 in our previous studies (Hu et al., 2020; Seymour et al., 2020), but this ratio may differ in other species, even in other mammals, because of differences in arterial blood pressure and structure of the vessel wall. Although birds and mammals are both endothermic animals with similar 4-chamber hearts, their vascular systems are slightly different. To this stage, we only know that birds have a higher blood pressure compared to mammals (Seymour et al., 2004), and their vessel wall tissues are only slightly different (Pfister, 1927). According to Law of Laplace, pressure is directly proportional to wall thickness, and birds have generally 30 % higher blood pressure. Therefore, the wall thickness of bird ICA was estimated to be 30 % thicker than mammals, giving a wall-lumen ratio of 0.4. However, the assumption that the vessel wall responds exactly the same to lumen size changes between birds and mammals needs to be tested empirically.

Vascular casting methods have not been widely used to estimate vessel size, and no previous studies investigated chicken nutrient artery sizes. Therefore, we do not know whether the sizes of the nutrient artery lumina estimated using BriteVu (Chapter 4) represent correct *in vivo* lumen sizes. We tried to use 10 % formalin to fix chicken legs and even tried to fix a whole chicken under physiological pressure, hoping the nutrient arteries can be fixed in their normal shapes. However, after histological embedding and sectioning of the femoral nutrient foramina, the arteries inside did not seem to be fixed properly. Example images are shown in Chapter 4. We therefore could not compare the BriteVu nutrient artery lumen sizes with histologically fixed nutrient artery lumen sizes. Furthermore, our methods also proved incapable of fixing larger arteries, such as internal carotid arteries. For example, most internal carotid arteries removed from the chicken body and fixed under physiological pressure

showed overly-stretched artery walls with separated layers. Details are described in the supplementary material of Chapter 4.

Future directions

This thesis mainly focuses on the relationships among femoral nutrient foramen size, nutrient artery size and femoral bone blood flow. Only one species (i.e. chicken) was used to determine these relationships. Chapter 3 estimated absolute femoral bone blood flow of other cursorial birds based only on chicken femoral bone blood flow values. However, the relationship between absolute blood flow rate and blood flow index may not be linear among cursorial bird species, and more data points would be necessary to confirm the relationship. More cursorial bird species need to be involved in the study to improve the understanding of this relationship, so that a better blood flow prediction model can be created. Birds are living dinosaurs, therefore they may have similar physiologies. There is the potential for investigating absolute rate of blood flow in the femoral bone of dinosaurs based on the known relationships we found in chickens. Since femoral bone blood flow seems to correlate to animal maximum aerobic metabolic rate, which refers to their activity levels (Allan et al., 2014; Seymour et al., 2012), we might be able to estimate dinosaur metabolic rate in the future nutrient foramen studies. The question of whether dinosaurs were endothermic or ectothermic has been debated for centuries. Because no blood vessels of dinosaurs have been preserved, investigating dinosaur femoral bone blood flow from femoral nutrient foramina may provide a piece of evidence to answer this question.

The standard foramen measurement method described in Chapter 2 needs to be improved for measuring fossil foramina in the future, as fossilized bones are often replaced by minerals and encased in dense matrix. We may not able to use micro-CT to observe the whole foramen passages within fossilized bones, because of their small size and lack of imaging contrast. However, fossils removed from the matrix show the external openings of nutrient foramina clearly, and they can be measured with calipers, microphotography or impression casting (Seymour et al., 2015; Seymour et al., 2016; Seymour et al., 2012). Chapter 5 provided an example of the technique being applied to fossil femora to estimate femoral bone blood flow. Femoral nutrient foramina have relatively simple structures, as their passages do not curve dramatically

in cortical bones. In addition, according to our observations, the minimum cross-sectional area of a femoral nutrient foramen often locates close to the external opening. However, when applying the 'foramen technique' to foramina with complex structures (e.g. carotid foramina), the size difference between the external opening area and minimum cross-sectional area of these foramina need to be investigated and calibrated, to reduce measurement errors.

In Chapter 4, we found that the femoral nutrient foramen morphologies are much more complex compared to carotid foramina. Nutrient artery numbers and locations can vary among specimens. But since not enough samples were used to investigate all the possibilities of foramen shapes and vessel arrangements, we are not able to describe all possibilities in depth. The vascular trees surrounding and inside the chicken femora in this study were poorly infused with BriteVu due to the fact that we ligated two ends of the ischiatic artery. In addition, since BriteVu has a higher viscosity than blood, it could not be infused under physiological pressure into small arteries farther way from the infusion point. To answer the questions about how vessels distribute, supply and leave the femoral bone, a clearer mapping of the vascular trees inside and surrounding a femur is necessary. A femur is not only supported by the nutrient foramen, but also supported by other arteries such as periosteal, epiphysial and metaphyseal arteries. A clear mapping can also provide information about the connections between different arteries and may result in a fuller understanding of regional blood vessel distribution and regional bone tissue metabolism.

References:

Abou-Madi, N. (2001). Avian anesthesia. *Veterinary Clinics of North America: Exotic Animal Practice* **4**, 147-167.

Aird, W. C. (2011). Discovery of the cardiovascular system: from Galen to William Harvey. *Journal of Thrombosis and Haemostasis* **9**, 118-129.

Allan, G. H., Cassey, P., Snelling, E. P., Maloney, S. K. and Seymour, R. S. (2014). Blood flow for bone remodelling correlates with locomotion in living and extinct birds. *Journal of Experimental Biology* **217**, 2956-2962.

Altimiras, J., Lindgren, I., Giraldo-Deck, L. M., Matthei, A. and Garitano-Zavala, Á. (2017). Aerobic performance in tinamous is limited by their small heart. A novel hypothesis in the evolution of avian flight. *Scientific Reports* **7**, 1-15.

Amin, T. M. and Sirs, J. A. (1985). The blood rheology of man and various animal species. *Quarterly Journal of Experimental Physiology and Cognate Medical Sciences* **70**, 37-49.

Anetzberger, H. and Birkenmaier, C. (2016). The microsphere method for investigating bone blood flow. In *Skeletal Circulation in Clinical Practice*, (ed. R. K. Aaron), pp. 53-84. New Jersey: World Scientific.

Anetzberger, H., Thein, E., Becker, M., Zwissler, B. and Messmer, K. (2004a). Microspheres accurately predict regional bone blood flow. *Clinical Orthopaedics and Related Research* **424**, 253-265.

Anetzberger, H., Thein, E., Loffler, G. and Messmer, K. (2004b). Fluorescent microsphere method is suitable for chronic bone blood flow measurement: a long-term study after meniscectomy in rabbits. *Journal of Applied Physiology* **96**, 1928-1936.

Anetzberger, H., Thein, E., Maier, M., Birkenmaier, C. and Messmer, K. (2004c). Fluorescent microspheres are reliable for serial bone blood flow measurements. *Clinical Orthopaedics and Related Research* **427**, 241-248.

Aoun, M. A., Nasr, A. Y. and Aziz, A. M. A. (2013). Morphometric study of the carotid canal. *Life Science Journal* **10**, 2559-2562.

Aref, M. W., Akans, E. and Allen, M. R. (2017). Assessment of regional bone tissue perfusion in rats using fluorescent microspheres. *Bone Reports* **6**, 140-144.

Bain, M. M., Nys, Y. and Dunn, I. C. (2016). Increasing persistency in lay and stabilising egg quality in longer laying cycles. What are the challenges? *British Poultry Science* **57**, 330-338.

Bar, A. (2009). Calcium transport in strongly calcifying laying birds: mechanisms and regulation. *Comparative Biochemistry and Physiology Part A: Molecular and Integrative Physiology* **152**, 447-469.

Barbee, R. W., Perry, B. D., Re, R. N. and Murgo, J. P. (1992). Microsphere and dilution techniques for the determination of blood flows and volumes in conscious mice. *American Journal of Physiology* **263**, R728-R733.

Bell, A. and Chiappe, L. M. (2020). Anatomy of Parahesperornis: Evolutionary Mosaicism in the Cretaceous Hesperornithiformes (Aves). *Life* **10**, 62.

Berlis, A., Putz, R. and Schumacher, M. (1992). Direct and CT measurements of canals and foramina of the skull base. *The British Journal of Radiology* **65**, 653-661.

Black, A. J., Topping, J., Durham, B., Farquharson, R. G. and Fraser, W. D. (2000). A detailed assessment of alterations in bone turnover, calcium

homeostasis, and bone density in normal pregnancy. *Journal of Bone and Mineral Research* **15**, 557-563.

Boelkins, J. N., Mueller, W. J. and Hall, K. L. (1973). Cardiac output distribution in the laying hen during shell formation. *Comparative Biochemistry and Physiology Part A: Physiology* **46**, 735-743.

Boussel, L., Serusclat, A., Skilton, M. R., Vincent, F., Bernard, S., Moulin, P., Saloner, D. and Douek, P. C. (2007). The reliability of high resolution MRI in the measurement of early stage carotid wall thickening. *Journal of Cardiovascular Magnetic Resonance* **9**, 771-776.

Bouvarel, I., Nys, Y. and Lescoat, P. (2011). Hen nutrition for sustained egg quality. In *Improving the safety and quality of eggs and egg products*, eds. Y. Nys M. Bain and F. Vanimmerseel), pp. 261-299. Cambridge: Woodhead Publishing.

Boyer, D. M. and Harrington, A. R. (2018). Scaling of bony canals for encephalic vessels in euarchontans: implications for the role of the vertebral artery and brain metabolism. *Journal of Human Evolution* **114**, 85-101.

Boyer, D. M. and Harrington, A. R. (2019). New estimates of blood flow rates in the vertebral artery of euarchontans and their implications for encephalic blood flow scaling: A response to Seymour and Snelling (2018). *Journal of Human Evolution* **128**, 93-98.

Boyer, D. M., Kirk, E. C., Silcox, M. T., Gunnell, G. F., Gilbert, C. C., Yapuncich, G. S., Allen, K. L., Welch, E., Bloch, J. I. and Gonzales, L. A. (2016). Internal carotid arterial canal size and scaling in Euarchonta: Re-assessing implications for arterial patency and phylogenetic relationships in early fossil primates. *Journal of Human Evolution* **97**, 123-144.

Brookes, M. and Revell, W. J. (1998). Blood Supply of Bone: Scientific Aspects. London, UK: Springer.

Brubaker, R. L. and Mueller, W. J. (1971). Blood flow, blood volume and carbonic anhydrase activity of the avian femur during bone resorption and accretion. *Federation of American Societies for Experimental Biology* **30**, 346.

Brummer, A. B., Savage, V. M. and Enquist, B. J. (2017). A general model for metabolic scaling in self-similar asymmetric networks. *PLoS Computational Biology* **13**, e1005394.

Burton, A. C. (1965). Physiology and Biophysics of the Circulation. Chicago: Year Book Medical Publishers.

Calder, W. A. (1996). Size, function, and life history. New York: Dover Publications.

Çalgüner, E., Turgut, H., Gözil, R., Tunç, E., Sevim, A. and Keskil, S. (1997). Measurements of the carotid canal in skulls from Anatolia. *Cells Tissues Organs* **158**, 130-132.

Campbell, K. E. and Marcus, L. (1992). The relationship of hindlimb bone dimensions to body weight in birds. *Natural History Museum of Los Angeles County Science Series* **36**, 395-412.

Carmeliet, P. (2003). Angiogenesis in health and disease. *Nature Medicine* **9**, 653-660.

Caro, C. G., Pedley, T., Schroter, R. and Seed, W. (2012). The Mechanics of the Circulation. Cambridge: Cambridge University Press.

Chatterjee, S., Templin, R. J. and Campbell, K. E. (2007). The aerodynamics of *Argentavis*, the world's largest flying bird from the Miocene of Argentina. *Proceedings of the National Academy of Sciences* **104**, 12398-12403.

Chien, G. L., Anselone, C. G., Davis, R. F. and Van Winkle, D. M. (1995). Fluorescent vs. radioactive microsphere measurement of regional myocardial blood flow. *Cardiovascular Research* **30**, 405-412.

Cibis, M., Potters, W. V., Selwaness, M., Gijsen, F. J., Franco, O. H., Lorza, A. M. A., de Bruijne, M., Hofman, A., van der Lugt, A. and Nederveen, A. J. (2016). Relation between wall shear stress and carotid artery wall thickening MRI versus CFD. *Journal of Biomechanics* **49**, 735-741.

Cohen, M. M. (2006). The new bone biology: Pathologic, molecular, and clinical correlates. *American Journal of Medical Genetics Part A* **140a**, 2646-2706.

Colleran, P. N., Wilkerson, M. K., Bloomfield, S. A., Suva, L. J., Turner, R. T. and Delp, M. D. (2000). Alterations in skeletal perfusion with simulated microgravity: a possible mechanism for bone remodeling. *Journal of Applied Physiology* **89**, 1046-1054.

Currey, J. D. (2002). Bones: structure and mechanics. the United Kingdom: Princeton University Press.

Debbaut, C., Monbaliu, D., Casteleyn, C., Cornillie, P., Van Loo, D., Masschaele, B., Pirenne, J., Simoens, P., Van Hoorebeke, L. and Segers, P. (2010). From vascular corrosion cast to electrical analog model for the study of human liver hemodynamics and perfusion. *IEEE Transactions on Biomedical Engineering* **58**, 25-35.

Deveci, D. and Egginton, S. (1999). Development of the fluorescent microsphere technique for quantifying regional blood flow in small mammals. *Experimental Physiology* **84**, 615-630.

Dickison, M. R. (2007). The allometry of giant flightless birds, pp. 20-57. USA: Duke University Durham, North Carolina.

Elagib, H. and Ahmed, A. (2011). Comparative study on haematological values of blood of indigenous chickens in Sudan. *Asian Journal of Poultry Science* **5**, 41-45.

Etches, R. J. (1987). Calcium logistics in the laying hen. *The Journal of Nutrition* **117**, 619-628.

Fermoso, J. D., Richardson, T. Q. and Guyton, A. C. (1964). Mechanism of decrease in cardiac output caused by opening the chest. *American Journal of Physiology-Legacy Content* **207**, 1112-1116.

Ferrell, W. R., Khoshbaten, A. and Angerson, W. J. (1990). Responses of bone and joint blood vessels in cats and rabbits to electrical stimulation of nerves supplying the knee. *The Journal of Physiology* **431**, 677-687.

Folarin, A., Konerding, M., Timonen, J., Nagl, S. and Pedley, R. (2010). Three-dimensional analysis of tumour vascular corrosion casts using stereoimaging and micro-computed tomography. *Microvascular Research* **80**, 89-98.

Glagov, S., Zarins, C., Giddens, D. P. and Ku, D. N. (1988). Hemodynamics and atherosclerosis - insights and perspectives gained from studies of human arteries. *Archives of Pathology and Laboratory Medicine* **112**, 1018-1031.

Glenny, R., Bernard, S. and Brinkley, M. (1993). Validation of fluorescent-labeled microspheres for measurement of regional organ perfusion. *Journal of Applied Physiology* **74**, 2585-2597.

Greve, J. M., Les, A. S., Tang, B. T., Draney Blomme, M. T., Wilson, N. M., Dalman, R. L., Pelc, N. J. and Taylor, C. A. (2006). Allometric scaling of wall shear stress from mice to humans: quantification using cine phase-contrast MRI and computational fluid dynamics. *American Journal of Physiology-Heart and Circulatory Physiology* **291**, H1700-H1708.

Grubb, B. R. (1983). Allometric relations of cardiovascular function in birds. *American Journal of Physiology-Heart and Circulatory Physiology* **245**, H567-H572.

Grundnes, O. and Reikeras, O. (1991). Effect of physical activity on muscle and bone blood flow after fracture. Exercise and tenotomy studied in rats. *Acta Orthopaedica Scandinavica* **62**, 67-69.

Guyton, J. R. and Hartley, C. J. (1985). Flow restriction of one carotid artery in juvenile rats inhibits growth of arterial diameter. *American Journal of Physiology-Heart and Circulatory Physiology* **248**, H540-H546.

Harrington, A. R., Kuzawa, C. W. and Boyer, D. M. (2019). Carotid foramen size in the human skull tracks developmental changes in cerebral blood flow and brain metabolism. *American Journal of Physical Anthropology* **169**, 161-169.

Heil, M., Eitenmüller, I., Schmitz-Rixen, T. and Schaper, W. (2006). Arteriogenesis versus angiogenesis: similarities and differences. *Journal of Cellular and Molecular Medicine* **10**, 45-55.

Heinonen, I., Kemppainen, J., Kaskinoro, K., Langberg, H., Knuuti, J., Boushel, R., Kjaer, M. and Kalliokoski, K. K. (2013). Bone blood flow and metabolism in humans: effect of muscular exercise and other physiological perturbations. *Journal of Bone and Mineral Research* **28**, 1068-1074.

Hu, Q., Nelson, T. J. and Seymour, R. S. (2020). Bone foramen dimensions and blood flow calculation: best practices. *Journal of Anatomy* **236**, 357-369.

Hu, Q., Nelson, T. J., Snelling, E. P. and Seymour, R. S. (2018). Femoral bone perfusion through the nutrient foramen during growth and locomotor development of western grey kangaroos (*Macropus fuliginosus*). *Journal of Experimental Biology* **221**, 1-6.

Hunt, D. and Savage, V. M. (2016). Asymmetries arising from the space-filling nature of vascular networks. *Physical Review E* **93**, 062305.

Huo, Y. and Kassab, G. S. (2012). Intraspecific scaling laws of vascular trees. *Journal of the Royal Society Interface* **9**, 190-200.

Huo, Y. and Kassab, G. S. (2016). Scaling laws of coronary circulation in health and disease. *Journal of Biomechanics* **49**, 2531-2539.

Hurwitz, S. (1965). Calcium turnover in different bone segments of laying fowl. *American Journal of Physiology-Legacy Content* **208**, 203-207.

Jones, E. A., le Noble, F. and Eichmann, A. (2006). What determines blood vessel structure? Genetic prespecification vs. hemodynamics. *Physiology* **21**, 388-395.

Junaid, T. O., Bradley, R. S., Lewis, R. M., Aplin, J. D. and Johnstone, E. D. (2017). Whole organ vascular casting and microCT examination of the human placental vascular tree reveals novel alterations associated with pregnancy disease. *Scientific Reports* **7**, 1-10.

Kaihara, S., Van Heerden, P. D., Migita, T. and Wagner, H. N. J. (1968). Measurement of distribution of cardiac output. *Journal of Applied Physiology* **25**, 696-700.

Kassab, G. S. (2006). Scaling laws of vascular trees: of form and function. *American Journal of Physiology-Heart and Circulatory Physiology* **290**, H894-H903.

Kerschnitzki, M., Zander, T., Zaslansky, P., Fratzl, P., Shahar, R. and Wagermaier, W. (2014). Rapid alterations of avian medullary bone material during the daily egg-laying cycle. *Bone* **69**, 109-117.

Kobayashi, S., Takahashi, H. E., Ito, A., Saito, N., Nawata, M., Horiuchi, H., Ohta, H., Ito, A., Yamamoto, N. and Takaoka, K. (2003). Trabecular minimodeling in human iliac bone. *Bone* **32**, 163-169.

Koike, M. and Nomura, S. (1966). Time serial change in normal physiological values accompanying with growth of chick. *Japanese Journal of Zootechnical Science* **37**, 89-93.

Ksepka, D. T. (2014). Flight performance of the largest volant bird. *Proceedings of the National Academy of Sciences* **111**, 10624-10629.

Ku, D. N. (1997). Blood flow in arteries. *Annual Review of Fluid Mechanics* **29**, 399-434.

Langille, B. L. and O'Donnell, F. (1986). Reductions in arterial diameter produced by chronic decreases in blood flow are endothelium-dependent. *Science* **231**, 405-407.

Lehoux, S. and Tedgui, A. (2003). Cellular mechanics and gene expression in blood vessels. *Journal of Biomechanics* **36**, 631-643.

Lehoux, S., Tronc, F. and Tedgui, A. (2002). Mechanisms of blood flow-induced vascular enlargement. *Biorheology* **39**, 319-324.

Lieberman, D. E., Pearson, O. M., Polk, J. D., Demes, B. and Crompton, A. W. (2003). Optimization of bone growth and remodeling in response to loading in tapered mammalian limbs. *Journal of Experimental Biology* **206**, 3125-3138.

Lu, D. and Kassab, G. S. (2011). Role of shear stress and stretch in vascular mechanobiology. *Journal of the Royal Society Interface* **8**, 1379-1385.

Makowski, E. L., Meschia, G., Droegemueller, W. and Battaglia, F. C. (1968). Measurement of umbilical arterial blood flow to the sheep placenta and fetus in utero. Distribution to cotyledons and the intercotyledonary chorion. *Circulation Research* **23**, 623-631.

Marxen, M., Thornton, M. M., Chiarot, C. B., Klement, G., Koprivnikar, J., Sled, J. G. and Henkelman, R. M. (2004). MicroCT scanner performance and considerations for vascular specimen imaging. *Medical Physics* **31**, 305-313.

Merrill, G. F., Russo, R. E. and Halper, J. M. (1981). Cardiac output distribution before and after endotoxin challenge in the rooster. *American Journal of Physiology-Regulatory, Integrative and Comparative Physiology* **241**, R67-R71.

Midtgård, U. (1982). Patterns in the blood vascular system in the pelvic limb of birds. *Journal of Zoology* **196**, 545-567.

Moore, J. A., Rutt, B. K., Karlik, S. J., Yin, K. and Ethier, C. R. (1999). Computational blood flow modeling based on *in vivo* measurements. *Annals of Biomedical Engineering* **27**, 627-640.

Murray, C. D. (1926). The physiological principle of minimum work: I. The vascular system and the cost of blood volume. *Proceedings of the National Academy of Sciences of the United States of America* **12**, 207-214.

Naidoo, N., Lazarus, L., Ajayi, N. O. and Satyapal, K. (2017). An anatomical investigation of the carotid canal. *Folia Morphologica* **76**, 289-294.

Nakano, T., Thompson, J. R., Christopherson, R. J. and Aherne, F. X. (1986). Blood flow distribution in hindlimb bones and joint cartilage from young growing-pigs. *Canadian Journal of Veterinary Research* **50**, 96-100.

Nelson, T. J. (2021). Dimensions of bony foramina as an indirect measure of blood flow rate: Inferences across phylogenetic and ontogenetic sequences. In *Biological Sciences*, vol. Doctor of Philosophy: The University of Adelaide.

Neutze, J. M., Wyler, F. and Rudolph, A. M. (1968). Use of radioactive microspheres to assess distribution of cardiac output in rabbits. *Journal of Physiology* **2**, 486-495.

Newberry, M. G., Ennis, D. B. and Savage, V. M. (2015). Testing foundations of biological scaling theory using automated measurements of vascular networks. *PLoS Computational Biology* **11**, e1004455.

Nys, Y. and Le Roy, N. (2018). Calcium homeostasis and eggshell biomineralization in female chicken. In *Vitamin D*, (ed. D. Feldman), pp. 361-382. London, UK: Academic Press.

Orsi, A. M., Domeniconi, R. F., Artoni, S. M. B. and Joffre Filho, G. (2006). Carotid arteries in the dog: structure and histophysiology. *International Journal of Morphology* **24**, 239-244.

Overbeeke, J. J., Dujovny, M., Dragovic, L. and Ausman, J. I. (1991). Anatomy of the sympathetic pathways in the carotid canal. *Neurosurgery* **29**, 838-844.

Packard, G. C. and Boardman, T. J. (1999). The use of percentages and size-specific indices to normalize physiological data for variation in body size: wasted time, wasted effort? *Comparative Biochemistry and Physiology Part A: Molecular & Integrative Physiology* **122**, 37-44.

Pasternak, H. S., Kelly, P. J. and Owen, J. C. A. (1966). Estimation of oxygen consumption, and carbon dioxide production and blood flow of bone in growing and mature dogs. *Mayo Clinic Proceedings* **41**, 831-835.

Paullus, W. S., Pait, T. G. and Rhoton Jr, A. L. (1977). Microsurgical exposure of the petrous portion of the carotid artery. *Journal of Neurosurgery* **47**, 713-726.

Pees, M. and Krautwald-Junghanns, M. E. (2009). Cardiovascular physiology and diseases of pet birds. *Veterinary Clinics of North America: Exotic Animal Practice* **12**, 81-97.

Pennycuick, C. J. (1972). Animal Flight. London: Edward Arnold.

Pfister, H. I. C. (1927). On the distribution of the elastic tissue in the blood vessels of birds. *Journal of Anatomy* **61**, 213-222.

Prange, H. D., Anderson, J. F. and Rahn, H. (1979). Scaling of skeletal mass to body mass in birds and mammals. *The American Naturalist* **113**, 103-122.

Qiao, Y., Guallar, E., Suri, F. K., Liu, L., Zhang, Y., Anwar, Z., Mirbagheri, S., Xie, Y. J., Nezami, N. and Intrapiromkul, J. (2016). MR imaging measures of intracranial atherosclerosis in a population-based study. *Radiology* **280**, 860-868.

Raffe, M. R., Mammel, M., Gordon, M., Duke, G., Redig, P. and Boros, S. (1993). Cardiorespiratory effects of ketamine-xylazine in the great horned owl. *Raptor Biomedicine. University of Minnesota, Minneapolis, USA*, 150-153.

Richter, J. P. (1970). The notebooks of Leonardo da Vinci. New York: Dover Publications.

Risau, W. and Flamme, I. (1995). Vasculogenesis. *Annual Review of Cell and Developmental Biology* **11**, 73-91.

Robling, A. G., Castillo, A. B. and Turner, C. H. (2006). Biomechanical and molecular regulation of bone remodeling. *Annual Review of Biomedical Engineering* **8**, 455-498.

Rucci, N. (2008). Molecular biology of bone remodelling. *Clinical Cases in Mineral and Bone Metabolism* **5**, 49-56.

Saam, T., Raya, J. G., Cyran, C. C., Bochmann, K., Meimarakis, G., Dietrich, O., Clevert, D. A., Frey, U., Yuan, C. and Hatsukami, T. S. (2009). High resolution carotid black-blood 3T MR with parallel imaging and dedicated 4-channel surface coils. *Journal of Cardiovascular Magnetic Resonance* **11**, 41.

Saba, L., Sanfilippo, R., Montisci, R. and Mallarini, G. (2010). Carotid artery wall thickness: comparison between sonography and multi-detector row CT angiography. *Neuroradiology* **52**, 75-82.

Saba, L., Sanfilippo, R., Montisci, R., Suri, J. S. and Mallarini, G. (2013). Carotid artery wall thickness measured using CT: inter-and intraobserver agreement analysis. *American Journal of Neuroradiology* **34**, E13-E18.

Saba, L., Sanfilippo, R., Pascalis, L., Montisci, R., Caddeo, G. and Mallarini, G. (2008). Carotid artery wall thickness and ischemic symptoms: evaluation using multi-detector-row CT angiography. *European Radiology* **18**, 1962-1971.

Salles, J. P. (2016). Bone metabolism during pregnancy. *Annales d'endocrinologie* **77**, 163-168.

Sapirstein, L. A. and Hartman, F. A. (1959). Cardiac output and its distribution in the chicken. *American Journal of Physiology-Legacy Content* **196**, 751-752.

Schirrmacher, K., Lauterbach, S. and Bingmann, D. (1997). Oxygen consumption of calvarial bone cells *in vitro*. *Journal of Orthopaedic Research* **15**, 558-562.

Schmid-Schönbein, H., Wells, R. and Goldstone, J. (1969). Influence of deformability of human red cells upon blood viscosity. *Circulation Research* **25**, 131-143.

Schwartz, N., Patel, B., Garland Jr, T. and Horner, A. (2018). Effects of selective breeding for high voluntary wheel-running behavior on femoral nutrient canal size and abundance in house mice. *Journal of Anatomy* **233**, 193-203.

Sedlmayr, J. C. and Witmer, L. M. (2002). Rapid technique for imaging the blood vascular system using stereoangiography. *The Anatomical Record* **267**, 330-336.

Semenza, G. L. (2007). Vasculogenesis, angiogenesis, and arteriogenesis: mechanisms of blood vessel formation and remodeling. *Journal of Cellular Biochemistry* **102**, 840-847.

Serrat, M. A. (2009). Measuring bone blood supply in mice using fluorescent microspheres. *Nature Protocols* **4**, 1749-1758.

Seymour, R. S. (2016). Cardiovascular physiology of dinosaurs. *Physiology* **31**, 430-441.

Seymour, R. S., Angove, S. E., Snelling, E. P. and Cassey, P. (2015). Scaling of cerebral blood perfusion in primates and marsupials. *Journal of Experimental Biology* **218**, 2631-2640.

Seymour, R. S., Bennett-Stamper, C. L., Johnston, S. D., Carrier, D. R. and Grigg, G. C. (2004). Evidence for endothermic ancestors of crocodiles at the stem of archosaur evolution. *Physiological and Biochemical Zoology* **77**, 1051-1067.

Seymour, R. S., Bosiocic, V. and Snelling, E. P. (2016). Fossil skulls reveal that blood flow rate to the brain increased faster than brain volume during human evolution. *Royal Society Open Science* **3**, 160305.

Seymour, R. S., Bosiocic, V. and Snelling, E. P. (2017). Correction to 'Fossil skulls reveal that blood flow rate to the brain increased faster than brain volume during human evolution'. *Royal Society Open Science* **4**, 170846.

Seymour, R. S., Bosiocic, V., Snelling, E. P., Chikezie, P. C., Hu, Q., Nelson, T. J., Zipfel, B. and Miller, C. V. (2019a). Cerebral blood flow rates in recent great apes are greater than in *Australopithecus* species that had equal or larger brains. *Proceedings of the Royal Society B* **286**, 20192208.

Seymour, R. S., Hu, Q. and Snelling, E. P. (2020). Blood flow rate and wall shear stress in seven major cephalic arteries of humans. *Journal of Anatomy* **236**, 522-530.

Seymour, R. S., Hu, Q., Snelling, E. P. and White, C. R. (2019b). Interspecific scaling of blood flow rates and arterial sizes in mammals. *Journal of Experimental Biology* **222**, jeb199554.

Seymour, R. S., Smith, S. L., White, C. R., Henderson, D. M. and Schwarz-Wings, D. (2012). Blood flow to long bones indicates activity metabolism in mammals, reptiles and dinosaurs. *Proceedings of the Royal Society B-Biological Sciences* **279**, 451-456.

Singh, I. J., Sandhu, H. S. and Herskovits, M. S. (1991). Bone vascularity. In *Bone*, vol. 3 (ed. B. K. Hall), pp. 141-164. Boca Raton, Florida: CRC press.

Sirsat, S. K., Sirsat, T. S., Faber, A., Duquaine, A., Winnick, S., Sotherland, P. R. and Dzialowski, E. M. (2016). Development of endothermy and concomitant increases in cardiac and skeletal muscle mitochondrial respiration in the precocial Pekin duck (*Anas platyrhynchos domestica*). *Journal of Experimental Biology* **219**, 1214-1223.

Skilton, M. R., Boussel, L., Bonnet, F., Bernard, S., Douek, P. C., Moulin, P. and Serusclat, A. (2011). Carotid intima–media and adventitial thickening: comparison of new and established ultrasound and magnetic resonance imaging techniques. *Atherosclerosis* **215**, 405-410.

Somesh, M. S., Sridevi, H. B., Murlimanju, B. V. and Pai, S. R. (2014). Morphological and morphometric study of carotid canal in Indian population. *International Journal of Biomedical Research* **5**, 455-460.

Sommer, G., Regitnig, P., Költringer, L. and Holzapfel, G. A. (2009). Biaxial mechanical properties of intact and layer-dissected human carotid arteries at physiological and supraphysiological loadings. *American Journal of Physiology-Heart and Circulatory Physiology* **298**, H898-H912.

Sturkie, P. (1986). Heart and circulation: anatomy, hemodynamics, blood pressure, blood flow. In *Avian Physiology*, (ed. P. Sturkie), pp. 130-166. New York: Springer.

Tobalske, B. W. (2016). Evolution of avian flight: muscles and constraints on performance. *Philosophical Transactions of the Royal Society B: Biological Sciences* **371**, 20150383.

Tronc, F., Mallat, Z., Lehoux, S., Wassef, M., Esposito, B. and Tedgui, A. (2000). Role of Matrix Metalloproteinases in Blood Flow–Induced Arterial Enlargement: Interaction With NO. *Arteriosclerosis, Thrombosis, and Vascular Biology* **20**, e120-e126.

Tronc, F. o., Wassef, M., Esposito, B., Henrion, D., Glagov, S. and Tedgui, A. (1996). Role of NO in flow-induced remodeling of the rabbit common carotid artery. *Arteriosclerosis, Thrombosis, and Vascular Biology* **16**, 1256-1262.

Trueta, J. (1963). The role of the vessels in osteogenesis. *Journal of Bone and Joint Surgery* **45B**, 402-418.

Van Oosterhout, M., Willigers, H., Reneman, R. and Prinzen, F. (1995). Validation of fluorescent microsphere technique for measurement of organ perfusion with improved sample processing method. *American Journal of Physiology* **269**, H725-H733.

Varner, J., Clifton, K. R., Poulos, S., Broderson, J. R. and Wyatt, R. D. (2004). Lack of efficacy of injectable ketamine with xylazine or diazepam for anesthesia in chickens. *Lab Animal* **33**, 36-39.

Vasquez, S. X., Gao, F., Su, F., Grijalva, V., Pope, J., Martin, B., Stinstra, J., Masner, M., Shah, N. and Weinstein, D. M. (2011). Optimization of microCT imaging and blood vessel diameter quantitation of preclinical specimen vasculature with radiopaque polymer injection medium. *Plos One* **6**.

Vijaywargiya, M., Deopujari, R. and Athavale, S. A. (2017). Anatomical study of petrous and cavernous parts of internal carotid artery. *Anatomy and Cell Biology* **50**, 163-170.

Watase, H., Sun, J., Hippe, D. S., Balu, N., Li, F., Zhao, X., Mani, V., Fayad, Z. A., Fuster, V. and Hatsukami, T. S. (2018). Carotid artery remodeling is segment specific: an in vivo study by vessel wall magnetic resonance imaging. *Arteriosclerosis, Thrombosis, and Vascular Biology* **38**, 927-934.

Weinberg, P. D. and Ethier, C. R. (2007). Twenty-fold difference in hemodynamic wall shear stress between murine and human aortas. *Journal of Biomechanics* **40**, 1594-1598.

Westerhof, N., Stergiopulos, N. and Noble, M. I. (2010). Snapshots of hemodynamics: an aid for clinical research and graduate education. New York: Springer.

Westerhof, N., Stergiopulos, N., Noble, M. I. and Westerhof, B. E. (2019). Law of laplace. In *Snapshots of Hemodynamics*, pp. 51-55. Boston: Springer.

White, C. R. (2003). Allometric analysis beyond heterogeneous regression slopes: use of the Johnson-Neyman technique in comparative biology. *Physiological and Biochemical Zoology* **76**, 135-140.

White, C. R. and Seymour, R. S. (2014). The role of gravity in the evolution of mammalian blood pressure. *Evolution* **68**, 901-908.

Whitehead, C. (2004). Overview of bone biology in the egg-laying hen. *Poultry Science* **83**, 193-199.

Whiteside, L. A., Simmons, D. J. and Lesker, P. A. (1977). Comparison of regional bone blood flow in areas with differing osteoblastic activity in the rabbit tibia. *Clinical Orthopaedics and Related Research* **124**, 267-270.

Wideman, R. F., Jr. (1999). Cardiac output in four-, five-, and six-week-old broilers, and hemodynamic responses to intravenous injections of epinephrine. *Poultry Science* **78**, 392-403.

Windberger, U., Bartholovitsch, A., Plasenzotti, R., Korak, K. J. and Heinze, G. (2003). Whole blood viscosity, plasma viscosity and erythrocyte aggregation in nine mammalian species: reference values and comparison of data. *Experimental Physiology* **88**, 431-440.

Wolff, C. B. (2008). Normal cardiac output, oxygen delivery and oxygen extraction. *Advances in Experimental Medicine and Biology* **599**, 169-182.

Wolinsky, H. and Glagov, S. (1967). A lamellar unit of aortic medial structure and function in mammals. *Circulation Research* **20**, 99-111.

Xu, J., Wang, X., Toney, C. B., Seamon, J. and Cui, Q. (2010). Blood supply to the chicken femoral head. *Comparative Medicine* **60**, 295-299.

Zar, J. H. (1998). Biostatistical Analysis. New Jersey: Prentice-Hall, Inc.